STRUCTURAL AND FUNCTIONAL STUDIES OF *SALMONELLA* TYPHIMURIUM EFFECTORS GTGE AND SPVB

A Thesis Submitted to the College of

Graduate Studies and Research

In Partial Fulfillment of the Requirements

For the Degree of Master of Science

In the Department of Biochemistry

University of Saskatchewan

Saskatoon

By

CAISHUANG XU

Permission to Use

In presenting this thesis in partial fulfillment of the requirements for a Postgraduate degree from the University of Saskatchewan, I agree that the Libraries of this University may make it freely available for inspection. I further agree that permission for copying of this thesis in any manner, in whole or in part, for scholarly purposes may be granted by the professor or professors who supervised my thesis work or, in their absence, by the Head of the Department or the Dean of the College in which my thesis work was done. It is understood that any copying or publication or use of this thesis or parts thereof for financial gain shall not be allowed without my written permission. It is also understood that due recognition shall be given to me and to the University of Saskatchewan in any scholarly use which may be made of any material in my thesis.

Requests for permission to copy or to make other use of material in this thesis in whole or part should be addressed to:

Head of the Department of Biochemistry

University of Saskatchewan

Saskatoon, Saskatchewan, S7N 5E5

ABSTRACT

Salmonella is a genus of Gram-negative bacteria, which is a major cause of foodborne disease. To create a safe intracellular environment for the pathogen within the host cells, *Salmonella* secretes a large number of effectors into the host cytosol. My research concentrates on a structural and functional characterization of two *Salmonella* effectors, GtgE and SpvB. GtgE is a cysteine protease that specifically cleaves closely related GTPases, Rab29, Rab32 and Rab38. The full-length GtgE and several truncated constructs were cloned, expressed and purified. Extensive crystallization trials were performed with these constructs. In addition, several crystallization rescue strategies have been employed, including introducing entropy-reducing surface mutations, chemical modification to the protein surface, and co-crystallization of inactive GtgE variants with substrate peptide. Despite these extensive efforts, no crystals were obtained. However, new information about GtgE was discovered such as low protease activity *in vitro* against GST-Rab32 and identification of the N-terminal ~30 residues of GtgE as required for the full function.

SpvB is a mono-ADP-ribosyltransferase that modifies G-actin. SpvB is composed of two structural domains. The C-terminal domain of SpvB (SpvB-C) possesses the mono-ADP-ribosyltransferase activity and its structure has been determined. This study provides the first structural determination of the N-terminal domain of SpvB (SpvB-N) at 2.4 Å resolution. This domain is made primarily of β-strands and shows similarity to the N-terminal segment of YenB, an ABC toxin component. A long groove on the protein surface suggests that it functions as a recognition domain. The hypothesis that SpvB-N guides the localization of SpvB and targets the protein to actin was tested, but a co-immunoprecipitation assay excluded strong interaction between SpvB-N and actin. Moreover, SpvB-N expressed as a GFP fusion localized to the

nucleus while SpvB and SpvB-C localized to the cytosol. I have shown further that SpvB-C was sufficient to disrupt the actin cytoskeleton and induce cell apoptosis. The similarity of SpvB-N to YenB prompted us to investigate its cytotoxicity but only a marginal effect on the host cells was noted. Experiments to study the function of the SpvB-N were able to exclude some possibilities and narrowed down the spectrum of potential functions.

ACKNOWLEDGMENTS

Foremost, I would like to express my sincere gratitude to my supervisor, Professor Miroslaw Cygler, for his invaluable supervision and support during my research, study and writing. I greatly appreciate his helpful guidance. Besides my supervisor, I would like to thank my committee members, Dr. Yu Luo, Dr. Jeremy Lee and Dr. Scot Stone, for their comments, suggestions, tough questions and encouragement. I also would like to thank my dearest lab mates for sharing experience and for stimulating discussions.

My sincere thanks also go to Dr. Wolfgang Koester for his help, advice and for allowing me to perform some of the experiments in his lab, to Drs. Guennadi Kozlov, Oleg Dmitriev and Mr. Corey Yu for their help in GtgE NMR experiments, to Drs. Maia Cherney and Michal Boniecki for their help in SpvB crystallization, to Drs. Lei Li, Zhaojia Wu and Mr. Li Qin for their help in working with mammalian cells, to Ms. Elisabet Jakova for her help with the nanopore study, to Drs. Aron White and Bill Roesler for providing the pFLAG-CTC and pEGFP-N1 vector respectively, to Dr. John Brumell for providing pCFP-Rab32 plasmid, to CLS CMCF beamline stuff for their help in collecting diffraction data, to the College of Medicine Protein Characterization and Crystallization Facility (PCCF) for access to the instruments required for my research and to Dr. Michal Boniecki for his help in accessing PCCF instruments and in data analysis, and to CIHR-THRUST for providing scholarship and opportunities to discuss my research with other THRUSTees.

Last but not least, I would like to thank my family and my friends for their continuous support in my life.

TABLE OF CONTENTS

LIST OF TABLES

LIST OF FIGURES

LIST OF ABBREVIATIONS

Abbreviation	
Amp^r	$Ampcillin^{resistant}$
APS	Ammonium persulfate
ART	ADP-ribosyltransferase
ASU	Assymetric unit
BNT/BCIP	Nitroblue tetrazolium/ 5-bromo-4-chloro-indolyl phosphate
CI	Competition index
Co-IP	Co-immunoprecipitation
CTR	C-terminal region
DAPI	4',6-diamidino-2-phenylindole
DSS	4,4-dimethyl-4-silapentane-1sulfonic acid
DTT	Dithiothreitol
EDTA	Ethylenediaminetetraacetic acid
EM	electric-microscopy
FBS	Fetal Bovine Serum
GAP	GTPase activating protein
GDI	Guanine dissociation inhibitor
GEF	Guanine exchange factor
GSH	Glutathione
HEPES	4-(2-hydroxyethyl)-1-piperazineethanesulfonic acid
HRP	Horseradish peroxidase
HSQC	Heteronuclear Single Quantum Correlation
IM	Inner membrane
IPTG	Isopropyl β-D-1-thiogalactopyranoside
$Kana^r$	$Kanamycin^{resistant}$
LB	Luria broth
LDH	Lactate dehydrogenase
LIC	Ligase independent cloning
MAPK	mitogen-activated protein kinase
Ni-NTA	Nickel-nitrilotriacetic acid
NMR	Nuclear magnetic resonance
NP40	Nonidet P40
NTR	N terminal region
OD_{600}	Optical density at 600 nm
OM	Outer membrane
PAGE	Polyacrylamide gel electrophoresis
PBS	Phosphate buffered saline
PBST	0.1% (v/v) Tween-20 in PBS
PCR	polymerase chain reaction
PES	Polyethersulfone
PI3P	Phosphatidylinositol 3-phosphate
PVDF	Polyvinylidene fluoride
RILP	Rab-interacting lysosomal protein
S. bongori	*Salmonella bongori*

S. enterica	*Salmonella enterica*
S. Enteritidis	*Salmonella enterica* serovar Enteritidis
S. Typhi	*Salmonella enterica* serovar Typhi
S. Typhimurium	*Salmonella enterica* serovar Typhimurium
SCV	*Salmonella*-containing vacuole
SDS	Sodium dodecyl sulfate
Sifs	*Salmonella* induced filaments
SPI	*Salmonella* pathogenicity island
TAE	Tris-acetate EDTA buffer
TB	Terrific broth
TcA	A component of Tc toxin (ABC toxin)
TCA	Trichloroacetic acid
TcB	B component of Tc toxin (ABC toxin)
TcC	C component of Tc toxin (ABC toxin)
TEMED	*N*,*N*,*N*,*N*′ -Tetramethylethane-1,2-diamine
TTSS	Type III secretion systems

1. Introduction

1.1 *Salmonella* infection

Salmonella is a genus of Gram-negative bacteria, which causes diseases ranging from gastroenteritis to typhoid fever in humans (Ho *et al.*, 2002). The major transmission pathway of *Salmonella* in humans is through the consumption of contaminated food or water. *Salmonella* infection is the second most frequently reported foodborne disease and is relatively common in Canada (Favrin *et al.*, 2003). According to the Public Health Agency of Canada about 4 million Canadians suffer from food-related illnesses each year. *Salmonella* infection is also a global burden. It was reported that ~95 million cases of gastroenteritis occur each year due to *Salmonella* poisoning and 80 million of these are foodborne (Majowicz *et al.*, 2010). The systemic disease typhoid fever affects yearly an estimated 20 million people worldwide and causes ~200,000 deaths (Crump *et al.*, 2004; Crump and Mintz, 2010). *Salmonella* species are intracellular pathogens (Jantsch *et al.*, 2011). Antibiotic therapy is commonly used for curing *Salmonella* infection. However, bacteria develop different strategies to survive antibiotic treatment. The bacterial resistance challenges the treatments for bacterial infection. As a result, more and more research has been directed to address these pathogenic diseases.

1.2 *Salmonella* nomenclature

The genus *Salmonella* comprises two species, *Salmonella bongori* (*S. bongori*) and *Salmonella enterica* (*S. enterica*) (Fig. 1-1). The *S. enterica* has six subspecies, namely: *enterica* (I), *salamae* (II), *ariozonae* (III), *diarizonae* (IV), *houtenae* (V) and *indica* (VI) (Reeves *et al.*, 1989). The subspecie *S. enterica* (I) has more than 2400 serovars (Faucher *et al.*, 2005). The serovars are classified into two groups according to the syndromes they cause, non-typhoidal serovars and typhoidal serovars. Non-typhoidal serovars, like *S. enterica* serovars Typhimurium and Enteritidis, are major causes of gastroenteritis (Spanò and Galán, 2012). These serovars account for ~65% of the most frequently isolated serotypes (Ishola and Holt, 2008). Most non-typhoidal serovars have a broad range of animal hosts. Typhoidal *Salmonella* serovars, including *Salmonella* Typhi (*S.* Typhi) and *Salmonella* Paratyphi A-C, are specifically adapted to humans or higher primates and cause typhoid fever or paratyphoid fever (Spanò and Galán, 2012).

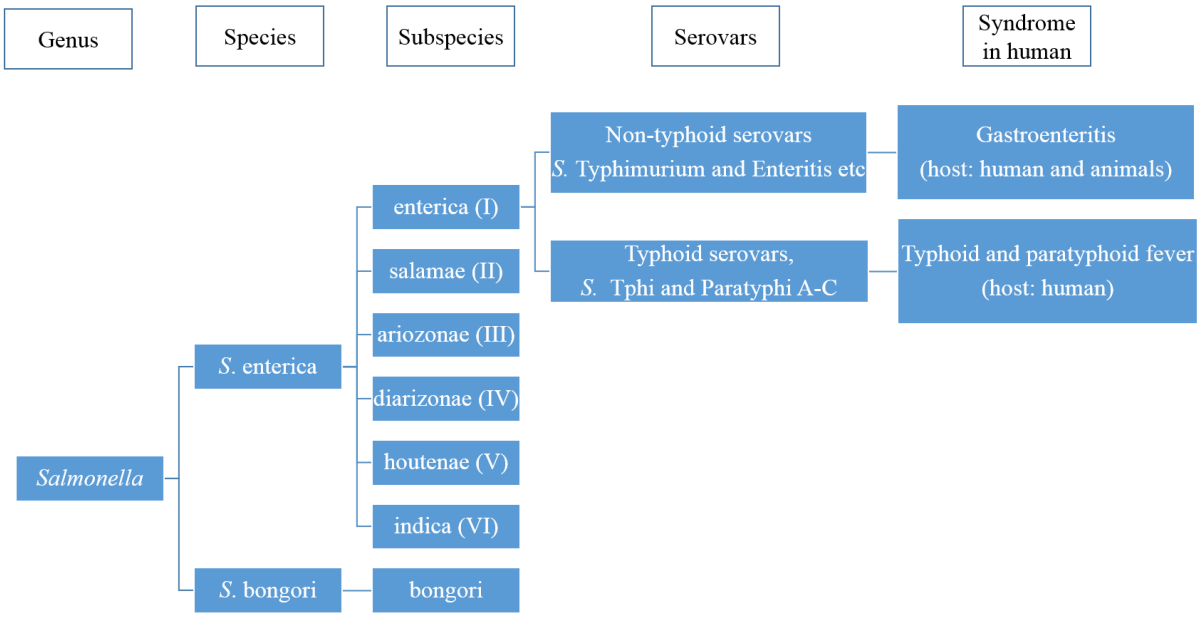

Fig. 1-1. Classification of *Salmonella* species and subspecies. The last column indicates the human syndrome caused by *Salmonella* serovars. The permissible host types are shown in brackets. *S.* Typhi and Paratyphi are human-specific and other serovars have a broad range of hosts.

1.3 *Salmonella* type three secretion systems (TTSS)

Like the human multilayer defense systems, bacteria evolved various strategies to overcome the host's defense mechanisms in order to colonize, to persist and to spread. These strategies include structural, biochemical, and genetic modification of bacteria. Understanding how *Salmonella* survives the immune response is of great importance to fully understand *Salmonella* pathogenicity.

The genome of *S.* Typhimurium consists of a ~4,800 Mb chromosome and an additional ~95 kb virulence plasmid (Fig. 1-2.A) (Sabbagh *et al.*, 2010). It was estimated that about 4% of the *Salmonella* genome is required for bacterial virulence (Bowe *et al.*, 1998). Most of the virulence genes are located within the *Salmonella*-pathogenicity islands (SPIs). The SPIs are large cassettes composed of a series of genes and operons (Marcus *et al.*, 2000). Five SPIs have been identified in *S.* Typhiumurium. SPI-1 and SPI-2 are of greatest importance for bacterial virulence because each encodes a type III secretion system (TTSS), which are used to deliver virulent proteins, called effectors, directly from the bacterial cytoplasm to the host cytosol. SPI-1 and SPI-2 not only encode TTSS but also the proteins that are secreted through these two secretion systems, proteins that regulate the expression of SPI-1 and SPI-2, as well as other

proteins that help bacterial survival (Fig. 1-2.B) (Moest and Méresse, 2013). Effectors are injected into the host cells through TTSS to create a pathogen-favorable environment (Wilson *et al.*, 2011; Galán *et al.*, 2014).

TTSS is a multi-mega Dalton complex, formed by more than 20 proteins. TTSS has a complex architecture with four main parts: the basal body, the needle, the needle tip and the translocon (Fig. 1-3) (Galán and Wolf-Watz, 2006; Galán *et al.*, 2014). The basal body is formed by proteins that oligomerize into ring structures, which are embedded in the bacterial inner and outer membrane (Bergeron *et al.*, 2013). The basal body structure associates with chaperons and ATPase on the cytoplasmic side of the inner membrane (Diepold and Wagner, 2014). A needle-like ~50 nm channel, called the needle filament, adapts to the basal structure and protrudes outside the bacterial membrane (Kubori *et al.*, 2000). At the end of the needle filament is a tip complex that detects and contacts the host cell and regulates the secretion of effectors. The tip complex also facilitates the insertion of a translocon complex into the host membrane. The translocon complex opens a pore in the host membrane to allow the effectors to enter the host cytosol (Burkinshaw and Strynadka, 2014).

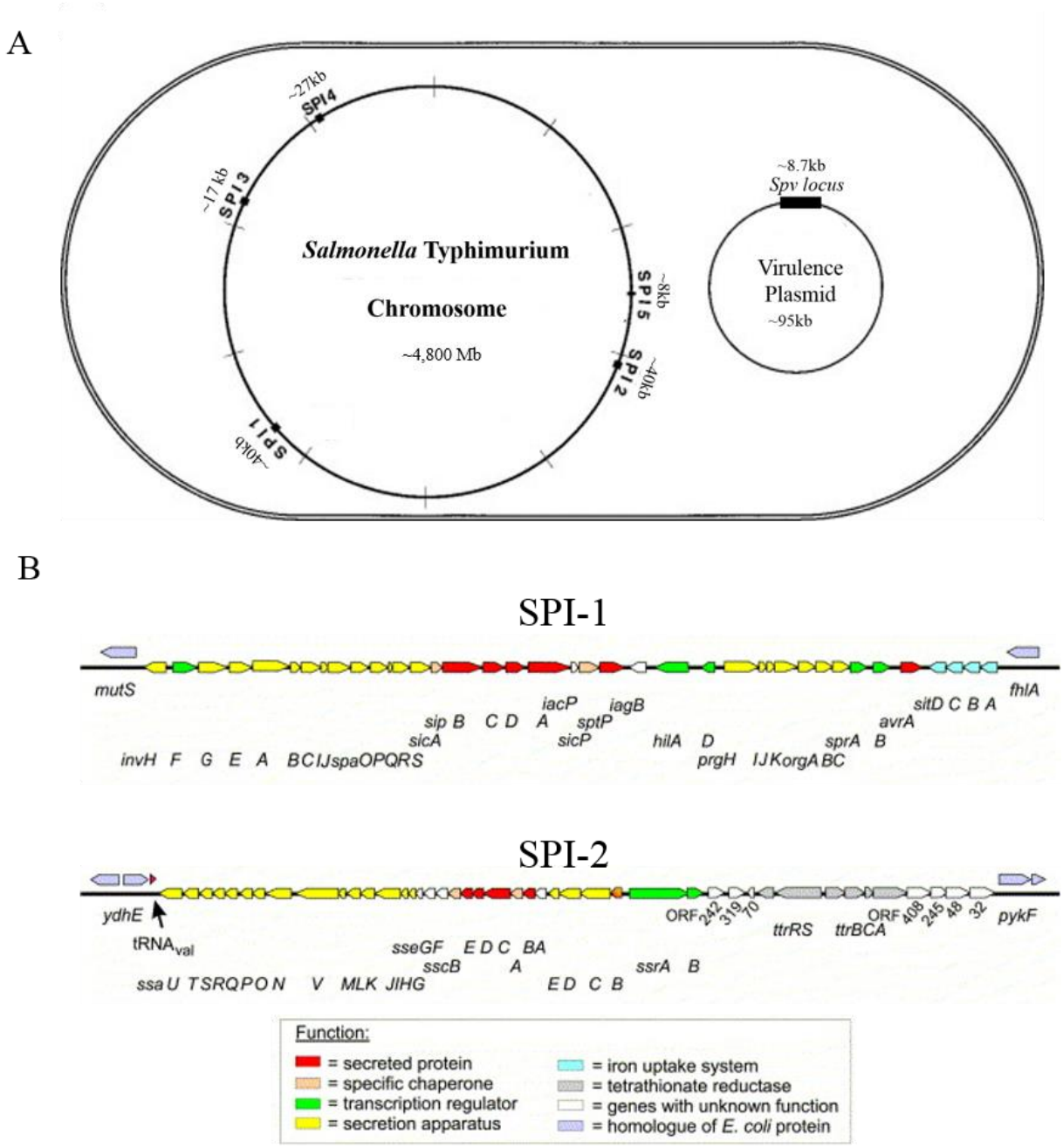

Fig. 1-2. Representation of the *S.* Typhimurium genome and SPI-1 and SPI-2. **A**. Schematic representation of *S.* Typhimurium genome. The figure is modified from (Marcus *et al.*, 2000). *S.* Typhimurium genome is comprised of a chromosome and a separate virulence plasmid. The essential SPIs and the *spv* locus are labeled in the chromosome and on the plasmid. The respective sizes of SPIs and the virulence plasmid are labeled (Marcus *et al.*, 2000). **B**. Distribution of genes on SPI-1 and SPI-2. The figure is adapted from (Hansen-Wester and Hensel, 2001) with permission. The functional classes of SPI-1 and SPI-2 genes are represented by different colors.

A

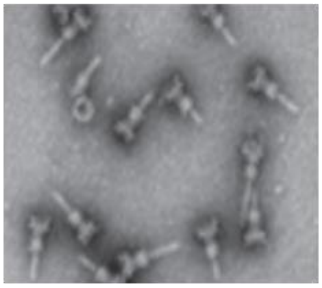

B

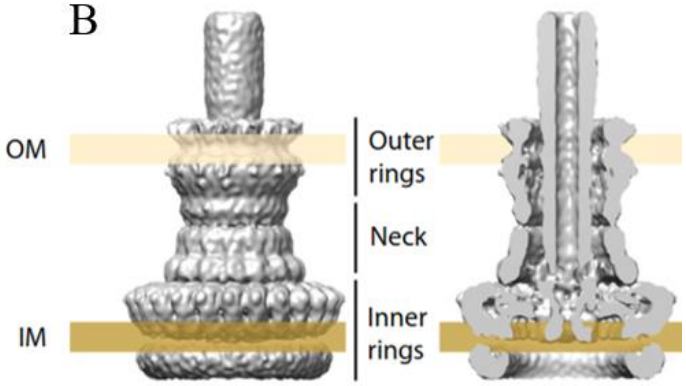

C

(a) Schema	(b) Structural elements	(c) SPI-1 T3SS	(d) SPI-2 T3SS
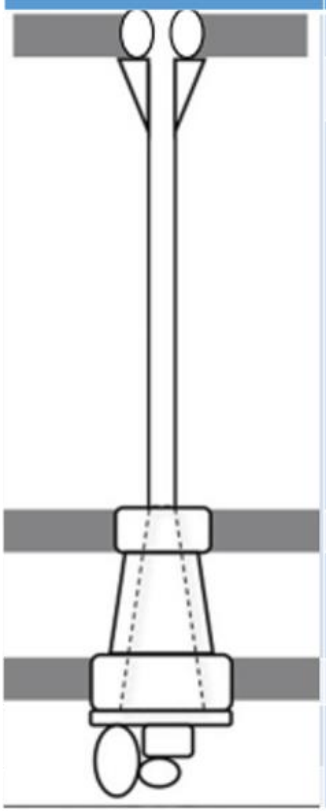	Translocon	SipB, SipC	SseB, SseC
	Needle tip	SipD	SseD
	Needle	PrgI	SseB, SsG
	Outer membrane ring	InvG, InvH	SsaC
	Neck	InvG, PrgH, PrgK	SsaJ
	Inner membrane ring	SpaO, SpaP,SpaR,SpaS	SsaD, SsaR-V
	chaperons	InvB, SicA, SigE,SicP	SrcA, SscB,SsaE

Fig. 1-3. The structure and composition of *Salmonella* TTSS. **A**. Cryo EM image of *Salmonella* TTSS, adapted from (Kosarewicz *et al.*, 2012) with permission. **B**. Surface representation of a 3-D reconstruction of TTSS based on cryo-EM data. This figure is adapted from (Diepold and Wagner, 2014) with permission. The complex consists of the basal structure and the needle filament. OM indicates the outer membrane and IM the inner membrane. Neck indicates the region connecting the outer and inner membrane ring structures. **C**. *Salmonella* TTSS components. (a) schematic representation of TTSS structure, (b) structural elements of TTSS, (c) and (d) protein components according to structural elements for TTSS-1 and TTSS-2. The figure is modified from (Moest and Méresse, 2013) with permission.

1.4 Overview of the functions of *Salmonella* effectors

Although the two *Salmonella* TTSS are similar in their overall structures, effectors secreted through these two systems are different and they perform different functions. More than 30 effectors secreted through both TTSS have been identified (Bakowski *et al.*, 2008). Generally, TTSS-1 and its substrates are more likely to affect the invasion of bacteria while TTSS-2 and its substrates promote intracellular survival (Paesold *et al.*, 2002).

The expression of *Salmonella* TTSS-1 and TTSS-2 and the delivery of effectors during infection of intestinal epithelial cells are summarized in a schematic flow diagram (Fig. 1-4). *Salmonella* pre-assembled TTSS-1 senses and adheres to the host cells (Schlumberger *et al.*, 2005). The adherence triggers the full assembly of TTSS-1 and the injection of effectors that rearrange the actin cytoskeleton (Zierler and Galán, 1995; Schlumberger *et al.*, 2005; Bakowski *et al.*, 2007). This actin rearrangement causes ruffling of the host cell membrane and the engulfment of bacterium (Hardt *et al.*, 1998; Jepson *et al.*, 2001; Buchwald *et al.*, 2002; Williams *et al.*, 2004). The engulfed bacterium remains in a separated compartment, called the *Salmonella*-containing vacuole (SCV) (Steele-Mortimer, 2008). Meanwhile, more TTSS-1 are assembled and more TTSS-1 effectors are expressed and secreted into the host cytoplasm to help stabilize the SCV and to alter the host cell signaling pathways (Schlumberger and Hardt, 2006). Once inside the host cells, the expression of TTSS-1 and its substrates is downregulated. The TTSS-1 effectors are degraded by the host proteasome pathways at different rates (Schlumberger and Hardt, 2006). When TTSS-1 is downregulated, the expression of SPI-2 and its effectors is upregulated in the acid vacuole (Fierer *et al.*, 1993; Chen *et al.*, 1996). TTSS-2 effectors are further secreted to manipulate the host cytoskeleton and to direct SCV maturation (Figueira and Holden, 2012). Bacterium replicates inside the mature SCV (Bakowski *et al.*, 2008).

The expression of TTSS-1 and TTSS-2 effectors is strictly regulated by the bacterium, both temporally and spatially, (Schlumberger and Hardt, 2006). This is particularly evident when the two effectors have opposite functions. The functions of effectors can be classified into four groups: (1) acting as translocon components to be inserted into the host membranes, (2) interfering with host cytoskeleton dynamics, (3) directing SCV dynamics and (4) mediating host signaling pathways (Table 1-1). TTSS effectors are not limited to the effectors listed in Table 1-1. For several effectors their functions are still unknown.

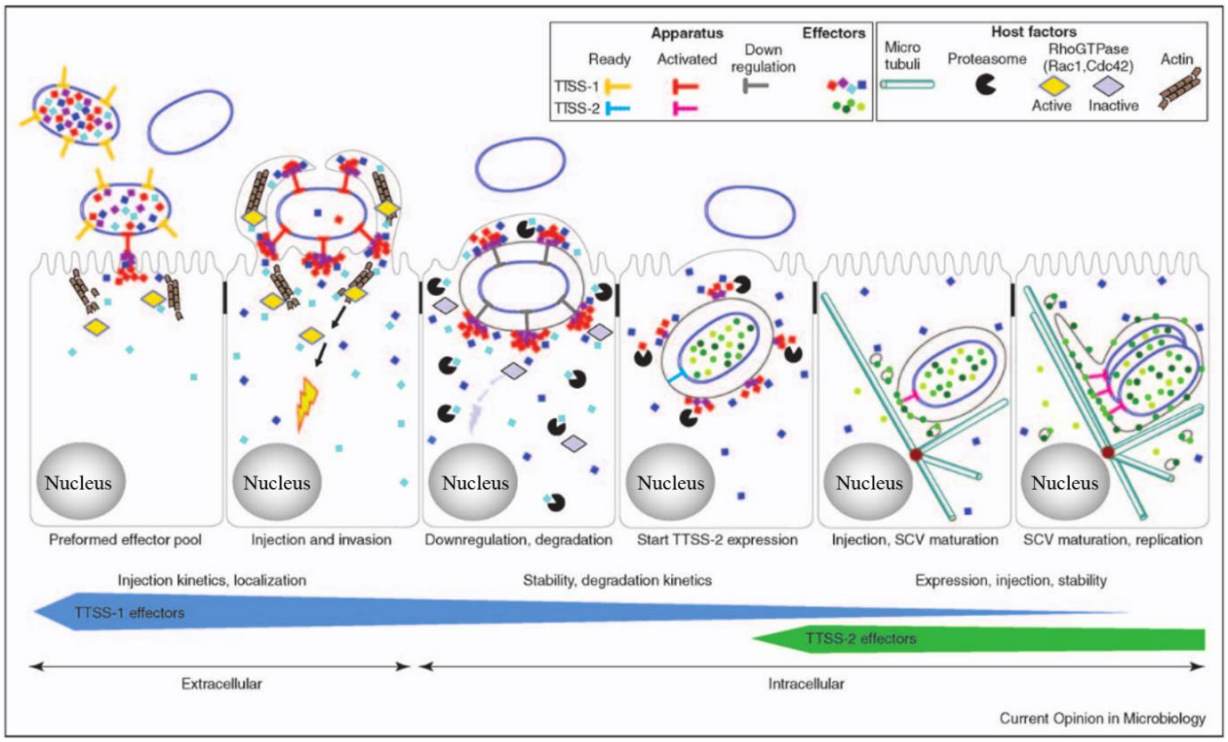

Fig. 1-4. Schematic overview of the expression of *Salmonella* TTSS-1 and TTSS-2 and the delivery of effectors during infection of intestinal epithelial cells. The contact between bacterium, pre-loaded with TTSS-1 apparatus (yellow) and effectors (squares), and the host cell initiates the translocation of effectors that cause host cytoskeleton rearrangement resulting in bacterial engulfment. The engulfed bacterium remains within the SCV, a replication niche. Once inside the host cell, the expression of TTSS-1 and its effectors is downregulated, while expression of TTSS-2 (blue) and its substrates (circles) is upregulated. The secreted TTSS-2 effectors guide the maturation of SCV. Bacterium replicates inside the mature SCV. The figure is adapted from (Schlumberger and Hardt, 2006) with permission.

Table 1-1. Overview of functions of *Salmonella* effectors secreted though TTSSs.

Effectors	**Function**	**Host cell targets**	**Reference**
TTSS-1 substrates			
Translocon components			
SipB(SspC)	1. A TTSS Translocon; 2. Activates pro-apoptotic enzyme caspase 1.	cytokeratin 8; caspase 1	(Scherer *et al.*, 2000; Barta *et al.*, 2012)
SipD	TTSS Translocon	?	(Collazo and Galán, 1997)
Cytoskeleton dynamic			
SptP	1. A tyrosine phosphate; 2. A GTPase activating protein (GAP) that disrupts of actin cytoskeleton.	Cdc42, Rac1	(Stebbins and Galán, 2000)

SopE	Mimics eukaryotic guanine exchange factors (GEFs)	Cdc42, Rac1, Rab5	(Buchwald *et al.*, 2002)
SopE2	Mimics GEFs	Cdc42	(Williams *et al.*, 2004)
SipA	Polymerizes actin	actin	(Lilic *et al.*, 2003)
SipC	1. Direct binds to actin; 2. Nucleates actin polymerization; 3. Condensates actin filaments into cables.	actin	(Hayward and Koronakis, 1999)
SCV membrane dynamic			
SopB	1. A phosphoinositide phosphatase; 2. Mimic host guanine dissociation inhibitor (GDI).	Membrane phospholipid, Cdc42	(Burkinshaw *et al.*, 2012)
SopD*	1. Plays a role in membrane fission and macropinosome formation; 2. Acts cooperatively with SopB to promote host cytoskeleton rearrangement.	?	(Bakowski *et al.*, 2007)
SopD2*	1. Mediates SCV trafficking; 2. Promotes the formation of *Salmonella*-induced filaments.	Rab7	(Jiang *et al.*, 2004)
GtgE	A cysteine protease	Rab29, Rab32 and Rab38	(Spano *et al.*, 2011; Spanò and Galán, 2012)
Cell immune signaling			
AvrA	1. An acetyltransferase; 2. Inhibits JNK, MAPKs activity.	MKK7	(Du and Galán, 2009; Wu *et al.*, 2012)
SopA	E3 ubiquitin-protein ligase	Ubiquitin pathway E2 enzymes: UbcH5a, UbcH5c and UbcH7.	(Higashide and Zhou, 2006; Zhang *et al.*, 2006; Diao *et al.*, 2008)
SspH1*	1. An E3 ubiquitin-protein ligase; 2. Polyubiquitinates host PKN1.	Ubiquitin pathway E2 enzymes; PKN1	(Haraga and Miller, 2006)
GtgE	A cysteine protease	Rab29, Rab32 and Rab38	(Spano *et al.*, 2011; Spanò and Galán, 2012)
TTSS-2 substrates			
Cell immune signaling			
SseL	A deubiquitinase	Ubiquitin, ubiquitin	(Rytkönen *et al.*, 2007)

		conjugated proteins	
SspH2	An E3 ubiquitin ligase	Ubiquitin pathway E2 enzymes	(Quezada *et al.*, 2009)
SCV membrane dynamic			
SsaB (SpiC)	Interferes with intracellular trafficking	Potentially HOOK3 protein	(Uchiya *et al.*, 1999)
SifA	1. Promotes the formation of *Salmonella* induced filaments (Sifs); 2. Mimic GEFs.	SKIP and RhoA-family GTPases: RhoA, RhoB and RhoC	(Brumell *et al.*, 2002; Boucrot *et al.*, 2005; Ohlson *et al.*, 2008)
PipB2	1. Links kinesin-1 onto SCV membrane; 2. Required for centrifugal extension of Sifs.	kinesin-1	(Henry *et al.*, 2006)
SseJ	1. Negatively regulates the formation of Sifs; 2. A deacylase; 3. A cholesterol esterification protein.	cholesterol	(Ohlson *et al.*, 2005; Nawabi *et al.*, 2008)
Effectors with unknown delivery pathways			
SpvB	An actin mono-ADP-ribosyltransferase	actin	(Hochmann *et al.*, 2006; Margarit *et al.*, 2006)
SpvC	A phosphothreonine lyase that irreversibly inactivates host MAP kinases	MAPK2/ERK2, MAPK3/ERK1, and p38	(Li *et al.*, 2007; Chen *et al.*, 2008; Mazurkiewicz *et al.*, 2008)

The * indicates that effectors are also secreted though SPI-2 TTSS.

1.5 GtgE is a virulence protein cleaving Rab29, Rab32 and Rab38

1.5.1 Overview of the biogenesis of *Salmonella*-containing vacuole

Phagocytosis is an important defense mechanism for the host cells in fighting against bacterial infection (Steele-Mortimer, 2008). Rab GTPases are important for mediating the phagosome dynamic (Smith *et al.*, 2007) and it is not surprising that they are targeted by effectors. Rab (Ras-related in brain) proteins belong to the Ras superfamily of small GTPases (Touchot *et al.*, 1987). Four Rabs, Rab1-4, were first identified when using oligonucleotide strategy to clone YPT (a Ras member in yeast) related cDNAs from the mice brain library (Touchot *et al.*, 1987).

Rab GTPases play essential role in the regulation of membrane identity, vesicle formation, vesicle and organelle motility and vesicular trafficking (Stenmark and Olkkonen, 2001; Zerial and McBride, 2001; Pfeffer, 2013). Protein markers Rabs (Rab8B, Rab13 and Rab35) are translocated into the classic phagosome membrane, which contains non-invasive bacteria. These proteins are shown to promote the fusion of phagosome to lysosome (Fig. 1.5) (Bakowski *et al.*, 2008). The phagosome is also quickly acidified through the action of vacuolar ATPase in the phagosome membrane, which pumps H^+ into the phagosome. The acidified and matured phagosome is directed to fuse with the lysosome, which releases anti-microbial proteins to destroy the invader (Bakowski *et al.*, 2008; Steele-Mortimer, 2008).

Unlike the classic phagosome, SCV matures differently to avoid the fusion with lysosome (Brumell and Grinstein, 2004). The maturation of SCV depends on the recruitment of lipids and different endocytic protein markers, such as small GTPases Rab5, Rab7 and Rab11 (Fig. 1-5) (Knodler and Steele-Mortimer, 2003). Upon formation of SCV, a TTSS-1 effector SopB is secreted to acquire Rab5, which directs vesicular trafficking, onto the SCV membrane (Mallo *et al.*, 2008). Subsequently, Rab5 attracts a phosphatidylinositol 3-kinase Vsp40 which generates phosphatidylinositol 3-phosphate (PI3P) and blocks phago-lysosome fusion (Mallo *et al.*, 2008). PI3P in turn attracts early endosome-associated protein EEA1, which also binds to Rab5 (Mallo *et al.*, 2008; Steele-Mortimer, 2008). Bacteria also use SopB to recruit sorting nexin1 protein, which removes the late-endosomal marker mannose 6-phosphate receptor from the membrane (Bujny *et al.*, 2008). Moreover, SopB is also involved in the activation of Rab14, which delays the SCV-lysosome fusion and facilitates bacterial replication inside the SCV (Kuijl *et al.*, 2007).

The maturation of SCV also requires SopD2, which interacts with a late endosome protein marker Rab7, although bacteria try to limit the interaction between SCV and the late endosome (Brumell *et al.*, 2003). Rab7 attracts Rab-interacting lysosomal protein (RILP), which bridges the Rab7-containing membrane with the microtubule dynein motor complex (Cantalupo *et al.*, 2001; Ramsden *et al.*, 2007). With the help of Rab7 and RILP, SCV traffics along the microtubules. Effector SseJ is also found to mediate SCV dynamics by esterifying cholesterol in the SCV membrane (Ruiz-Albert *et al.*, 2002). Several effectors, such as SifA, SopA, SopD2, SspH2, and SsaB, are involved in mediating the SCV-associated actin dynamics and the formation of *Salmonella* induced filaments (SIFs), which are essential for SCV trafficking (Brumell and Grinstein, 2004; Ramsden *et al.*, 2007; Bakowski *et al.*, 2008; McGhie *et al.*, 2009).

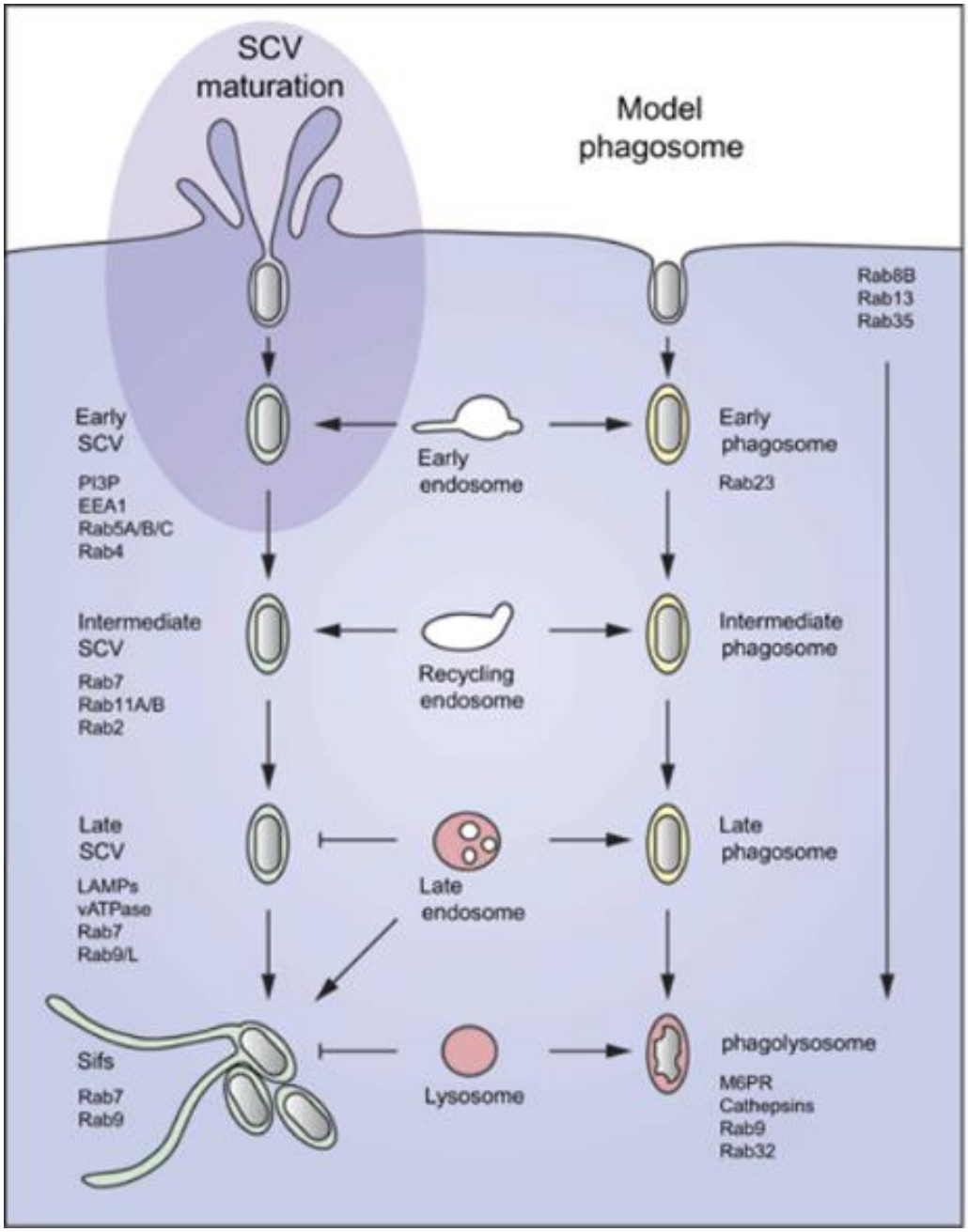

Fig. 1-5. Biogenesis of SCV. Endosomal markers on the pathogenic SCV (left) compared with markers (right) acquired by a model phagosome containing the *ΔinvA/inv* strain of *S.* Typhimurium, which is non-invasive. The figure is adapted from (Steele-Mortimer, 2008) with permission.

1.5.2 GtgE is an important virulence effector for *S*. Typhimurium

In *S.* Typhimurium, GtgE is a protein encoded within the Gifsy-2 lambdoid prophage. The Gifsy prophage is present in three *S.* Typhimurium strains, ATCC14028s (Fields *et al.*, 1986), SL1344 (Hoiseth and Stocker, 1981) and LT2 (Figueroa‐Bossi *et al.*, 2001). The Gifsy-2 prophage plays an essential role in bacterial virulence, as evidenced by the attenuated virulence seen in strains lacking this prophage (Figueroa‐Bossi and Bossi, 1999). Gifsy-2 also encodes a periplasmic Cu/Zn superoxide dismutase named SodCI (De Groote *et al.*, 1997; Farrant *et al.*, 1997), which protects bacteria by clearing peroxides produced by the host cells (De Groote *et al.*, 1997). There are ~10 putative virulence genes encoded within the Gifsy-2 prophage (Fig. 1-6).

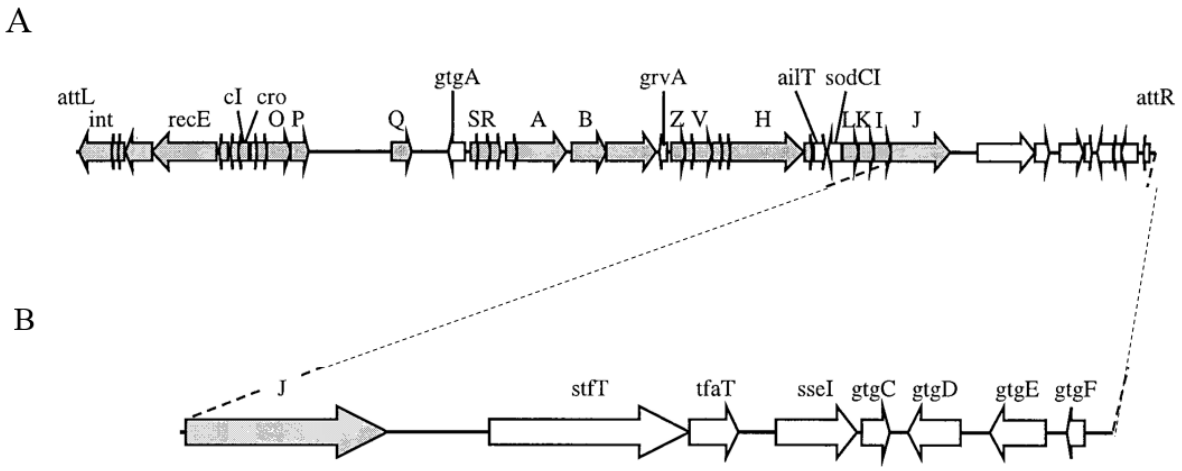

Fig. 1-6. Schematic representation of Gifsy-2 prophage. **A**. Open reading frame of Gifsy-2 prophage. Most of the genes are termed *gft* (Gifsy-2), e.g., *gftO* and are labeled with a single additional letter. White arrows represent putative virulence genes. Gray arrows represent putative phage genes and lines indicate deletion intervals. **B**. Gene organization of the region encoding putative effectors. Genes with no obvious role in phage production are termed *gtg* (Gifsy-2 gene) (Figueroa‐Bossi *et al.*, 2001). The Figure is modified from (Ho *et al.*, 2002) with permission.

To understand the functions of the putative virulence genes, individual putative effector genes were deleted using the λ red recombinase method and the virulence of a target gene was measured by a competition assay (Ho *et al.*, 2002). To conduct a competition assay, mutant and wild-type strains were mixed in a 1:1 ratio and inoculated into mice. After 4-5 days post infection, bacteria from an infected mouse were plated on an LB plate, which selects for the infecting bacteria. In this way, the recovery ratio of mutant and wild-type strains could be determined.

This value is designated as the competition index (CI), which is used to quantify the level of virulence (Wilson *et al.*, 2011). The lower the CI, the less virulent the strain and thus the more significant the deleted gene to virulence. The Δ*sodCI* mutant and the ΔgtgE mutant had a CI of ~0.15 while the ΔGifsy-2 mutant had a CI of ~0.01 (Ho *et al.*, 2002). When the ΔGifsy-2 mutant strain was complemented with the *gtgE*-containing plasmid, bacteria behaved like the wild-type strain (Ho *et al.*, 2002). These experiments identified the *SodCI* and G*tgE* genes as the major virulence determinants carried by Gifsy-2 in *S.* Typhimurium (Ho *et al.*, 2002).

1.5.3 GtgE affects the host specificity of *S.* Typhi

S. Typhimurium has a broad range of hosts, while *S.* Typhi is human-specific. *S.* Typhi produces a unique virulence protein called typhoid toxin, which is an AB toxin with a DNase and an ADP-ribosyltransferase activities (Haghjoo and Galán, 2004). Typhoid toxin is expressed exclusively inside the host cells and is transported to the extracellular environment by vesicular transport (Spanò *et al.*, 2008). Considering that Rab GTPases are usually involved in vesicular trafficking, a siRNA screen targeting human Rab and Rab-like GTPase was performed to identify GTPases that were required for typhoid toxin transport (Spano *et al.*, 2011). It was found that deletion of Rab29 decreased the amount of typhoid toxin transport intermediates (Spano *et al.*, 2011).

Rab29 was further characterized to be present on the SCV membrane of *S.* Typhi, but not on the SCV membrane of *S.* Typhimurium (Spano *et al.*, 2011). The differential recruitment of Rab29 on SCVs was caused by a TTSS-1 substrate GtgE (Spano *et al.*, 2011). GtgE is present in *S.* Typhimurium but not in *S.* Typhi (Spano *et al.*, 2011). When *S.* Typhi was complemented with the *gtgE* gene from *S.* Typhimurium, *S.* Typhi propagated more efficiently within the SCV than its wild-type counterpart (Spano *et al.*, 2011). Moreover, *S.* Typhi complemented with the *gtgE* gene showed significantly increased survival ability in primary bone-marrow-derived macrophages from mice, a non-permissive species (Spanò and Galán, 2012). This indicated that the expression of the *S.* Typhimurium effector GtgE in *S.* Typhi permitted *S.* Typhi to overcome the host restriction barrier.

1.5.4 GtgE directly cleaves Rab29

GtgE is essential for the depletion of Rab29 on the SCV membrane. It was found that Rab29 was present on the SCV membrane in cells infected with *S.* Typhimurium Δ*gtgE* strain,

but not the wild-type strain (Spano *et al.*, 2011). Cleavage of Rab29 by GtgE was confirmed through *in vitro* experiments. The purified GtgE was treated with Rab29-GFP fusion in a buffer containing Ca^{2+} and Mg^{2+} and an anti-GFP antibody was used to detect the GFP-tagged protein on a Western blot. In addition to Rab29-GFP, a specific band with a lower molecular weight was present, confirming that GtgE cleaves Rab29 (Spano *et al.*, 2011).

To identify the cleavage product, Rab29 fused a 3×Flag at the C-terminal was co-expressed with GtgE in *E.* coli (Spano *et al.*, 2011). The cells expressing both proteins were lysed and the supernatant was loaded on an anti-Flag M2 affinity gel to purify the cleaved product. The cleaved product was subjected to N-terminal sequencing, which revealed the cleavage site. It was identified that the Rab29 cleavage occurred after Gly41 (Spano *et al.*, 2011).

Other GTPases were tested as possible GtgE targets. Although most Rabs and Rab-like GTPases exhibit a broad residue conservation of residues in the region around Gly41 of Rab29, only Rab29, Rab32 and Rab38 were identified as GtgE substrates (Fig. 1-7) (Spanò and Galán, 2012). Rab32 and Rab38 function in the biogenesis of lysosome-related organelle complexes that deliver their cargos to lysosome-related organelles. These cargos include enzymes required for melanine synthesis and a variety of antimicrobial proteins, which promote elimination of the SCV (Dell'Angelica, 2004; Bultema *et al.*, 2012). Therefore, GtgE cleavage of Rab29, Rab32 and Rab38 helps to avoid fusion of SCV with lysosomes.

Fig. 1-7. Multiple alignment of the closely related Rab GTPases Rab32, Rab38 Rab29 and Rab23. The arrow represents the cleavage site of Rab GTPases by GtgE. The figure is adapted from (Spanò and Galán, 2012) with permission.

1.5.5 GtgE is a cysteine protease

To identify the mechanism of the GtgE proteolytic activity, its primary sequence was used to search for homologs (Spano *et al.*, 2011). It was found that GtgE showed ~14% sequence identity and ~24% similarity to a cysteine protease caricain (Fig. 1-8). Cysteine proteases are present in all living organisms (Grzonka *et al.*, 2000). The catalytic residues Cys and His are evolutionarily conserved in all cysteine protease and frequently form a Cys-His-Asp catalytic

triad (Grzonka *et al.*, 2001). Cysteine and histidine form an ion pair Cys-S^- … H^+-His at pH 3.5-8.0 (Grzonka *et al.*, 2001). The deprotonated Cys-S^- acts as a nucleophile and attacks the electrophilic carbonyl carbon of the peptide bond of the substrate. The intermediate attracts the proton from H^+-His to form a thioester and releases the amine terminus of the substrate. The thioester is subsequently hydrolyzed to regenerate the nucleophile Cys-S^- with the releasing of the remaining substrate fragment (Polgár and Asbóth, 1986).

```
GtgE              1 -MLRH---IQNSLGSVYRSNTATPQGQIIHHRNFQ--------SQFDTTG     38
                     ||.|   .:|....:||..........|...|.:        ::|....
Caricain         51 WMLNHNKFYENVDEKLYRFEIFKDNLNYIDETNKKNNSYWLGLNEFADLS    100

GtgE             39 NTLYNNCWVCSL-------------------NVIKSRDGNNYSALEDITS     69
                    |..:|..:|.||                   |:.::.|.....|:..:..
Caricain        101 NDEFNEKYVGSLIDATIEQSYDEEFINEDTVNLPENVDWRKKGAVTPVRH    150

GtgE             70 DNQ-----AFNNI--LEGI--------------DIIECEN----------     88
                    ...     ||:.:  :|||               ::::||.
Caricain        151 QGSCGSCWAFSAVATVEGINKIRTGKLVELSEQELVDCERRSHGCKGGYP    200

GtgE             89 ----------------------------------LLKEMNVQKI-PESS    102
                                                     ::|...|.:: |.:.
Caricain        201 PYALEYVAKNGIHLRSKYPYKAKQGTCRAKQVGGPIVKTSGVGRVQPNNE    250

GtgE            103 LFTNIKEALQAEVFNSTVEDDFESFISYELQNHGPLMLIRPSLGSECLHA    152
                      .|:..|:..:..:..||.....|   :|...|   :.....|::..||
Caricain        251 --GNLLNAIAKQPVSVVVESKGRPF---QLYKGG---IFEGPCGTKVDHA    292

GtgE            153 ECIVGYDSEVKK--VLIYDSMNTSPEWQSNIDVYDKLTLAFNDKYKNEDC    200
                    ...|||.....|  :||.:|..|:  |...  .|.::..|     .....
Caricain        293 VTAVGYGKSGGKGYILIKNSWGTA--WGEK--GYIRIKRA-----PGNSP    333

GtgE            201 SICGLYYDGVYEPKPLHSSSWKDWCTIL    228
                    .:||||....|..|.
Caricain        334 GVCGLYKSSYYPTKN-------------    348
```

Fig. 1-8. Sequence alignment of GtgE and caricain. In the middle line a single dot indicates similar residues, double dots mark residues with higher similarity and vertical lines represent identical residues. This sequence allignment was generated through EMBL-EBI Pairwise Sequence Alignment server http://www.ebi.ac.uk/Tools/psa/.

To verify that GtgE is a cysteine protease, each cysteine in GtgE was mutated to an alanine (Kohler *et al.*, 2014). Only the C45A mutant lost the *in vitro* protease activity, indicating that Cys45 is the critical residue in the active site (Kohler *et al.*, 2014). His151 was predicted to be a component of the catalytic triad based on sequence alignment with other cysteine proteases and indeed H151A mutation resulted in a loss of protease activity (Spano *et al.*, 2011; Spanò and

Galán, 2012). The third catalytic residue of the triad was identified as Asp169 by point mutation studies.

A structure of a GtgE fragment spanning residues 80 to 213 was recently reported (Fig.1-9.A) (Kohler *et al.*, 2014). The structure contains five α helices and five anti-parallel β strands, forming a globular structure. The catalytic residue Cys45 is not present in the fragment and the catalytic residues His151 and Asp169 are present on the protein surface and in a conformation that is not consistent with an active state. The substrate binding site is not obvious due to the lack of the first 79 N-terminal residues.

The peptidase database MEROPS classifies peptidases into clans, which contain evolutionary related proteins (Rawlings *et al.*, 2013). Members of cysteine protease families perform various biological functions. The structure of $GtgE^{(80-213)}$ is folded similarly to other cysteine proteases, specifically to the cysteine protease from clan CA family C39 (Kohler *et al.*, 2014). $GtgE^{(80-213)}$ aligns well with the C39 member ComA at the peptidase domain (Fig.1-9.B) (Kohler *et al.*, 2014). The first letter C in the clan CA indicates a cysteine protease family. The C39 family contains bacteriocin-processing endopeptidases from bacteria (Wu and Tai, 2004). ComA from *Streptococcus* is a bacteriocin transporter with a peptidase domain on the N-terminal region (Ishii *et al.*, 2010).

Although the structure of $GtgE^{(80-213)}$ aligns well with the peptidase domain of ComA, the orientations of His151 and Asp169 are different with respect to the catalytic residues His96 and Asp112 from ComA (Fig. 1-9). This difference in orientation may arise from the absence of the N-terminal region of GtgE, which includes Cys45. As a result, the crystallized GtgE fragment represents an inactive conformation.

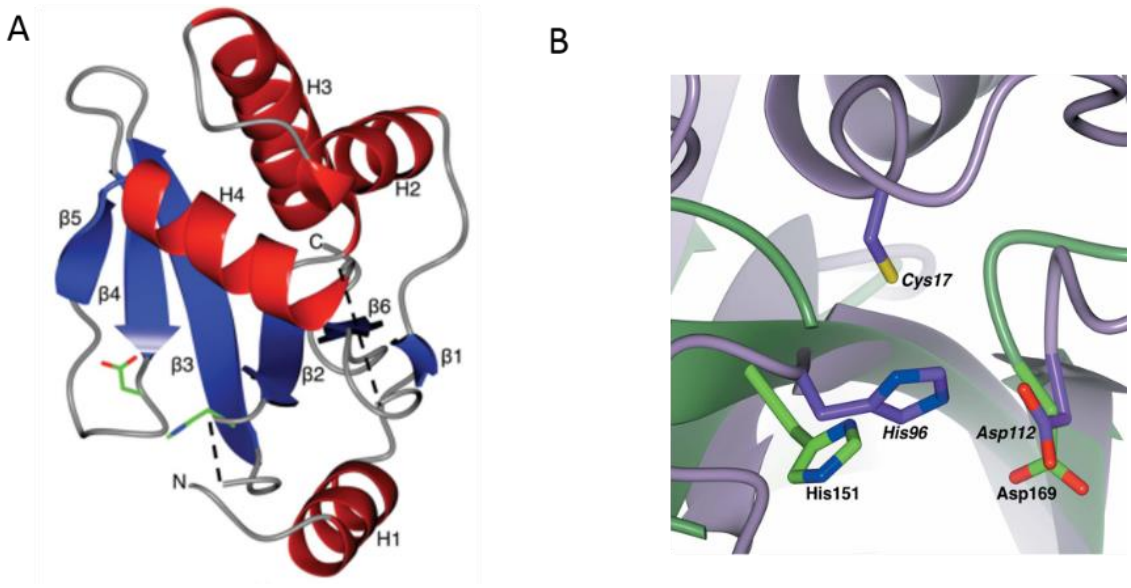

Fig. 1-9. Structure of GtgE$^{(80\text{-}213)}$ and its superposition with ComA. **A**. Cartoon representation of GtgE$^{(80\text{-}213)}$ structure. **B**. Structural alignment of GtgE$^{(80\text{-}213)}$ (green) with the peptidase domain of ComA (PDB entry 3K8U, purple). The active site residues of GtgE$^{(80\text{-}213)}$, His151 and Asp169 (labelled in bold), are in similar location as the active His96 and Asp169 (labelled in bold italics) of the ComA peptidase domain. The figures are adapted from (Kohler *et al.*, 2014) with permission.

1.6 SpvB is a virulence protein disrupting the host actin cytoskeleton

1.6.1 Bacterial proteins (effectors or toxins) affecting actin rearrangement

Actin is a component of microfilaments (Lodish, 2008), one of the three eukaryotic cytoskeletons. Both the monomeric globular actin (G-actin) and polymerized filament (F-actin) play important roles in eukaryotic cell motility, organelle movement, cell division and the maintenance of cell shape (Lodish, 2008). *Salmonella* secretes a series of effectors through TTSS-1 to manipulate the actin cytoskeleton in order to invade the host cell. SPI-1 effectors, SopE and SopE2 are involved in the activation of cytoskeletal regulation proteins Cdc42 and Rac1, resulting in the recruitment of WASP and Scar/WAVE family proteins to the Arp2/3 complex (Buchwald *et al.*, 2002; Williams *et al.*, 2004; Burkinshaw *et al.*, 2012). The Arp2/3 complex is involved in the initialization of actin polymerization (Criss and Casanova, 2003) and is predominantly regulated by proteins belonging to the WASP and Scar/WAVE families (Millard *et al.*, 2004; Pollitt and Insall, 2009). Besides, SPI-1 effectors SipA and SipC interact directly with actin (Hayward and Koronakiss, 2002). SipA functions as a molecular staple, which has a globular domain and two extended non-globular "arms". The globular domain interacts

with the acidic patch on the C-terminus of actin and the extended arms tether to actin protomers on the opposite strands of actin filament (Lilic *et al.*, 2003). The interaction between SipA and actin stabilizes polymerized actin and promotes the formation of F-actin (Lilic *et al.*, 2003). SipC is a component of the SPI-1 translocon and is also secreted into the host. The N-terminal region of SipC bundles actin filament and the C-terminal domain nucleates actin polymerization (Hayward and Koronakis, 1999). The exact role of SipC in actin rearrangement remains unclear, since its genetic deletion, the Δ*sip*C mutant, failed to assemble SPI-1 and was unable to deliver SPI-1 effectors (Guiney and Lesnick, 2005).

Actin rearrangement occurs not only during bacterial invasion but also continues during the intracellular infection process. After *Salmonella* gains entry into the host cell, SPI-1 effectors are downregulated. In spite of this global downregulation, the SPI-1 effector SptP persists in the cytoplasm. SptP acts as a GTPase-activator and a tyrosine phosphatase (Stebbins and Galán, 2000). The GTPase activation domain of SptP reverses the activation of Cdc42 and Rac1, which is caused during *Salmonella* invasion (Stebbins and Galán, 2000; Galán, 2001). SptP is believed to function in the restoration of normal actin cytoskeleton functions, which are disrupted during invasion (Galán, 2001). SPI-2 effectors SspH2 and SseI, which show sequence similarity in their N-terminal regions, co-localize with the polymerized actin, which is believed to result from the interactions of their homologous N-terminal regions with filamin, a protein that holds actin filaments in eukaryotic cells (Miao *et al.*, 2003). It was found that SspH2 also interacts with profilin, a protein involved in actin cytoskeletal dynamics (Miao *et al.*, 2003). A number of *S. enterica* strains employ SpvB to modify actin by ADP-ribosylation, which prevents actin polymerization (Guiney and Lesnick, 2005). Ubiquitously, *Salmonella* secretes a series of effectors to regulate the cytoskeletal dynamics of actin.

1.6.2 *Spv* locus

SpvB is encoded within the *spv* locus, which is located on a separate virulence plasmid in *S. enterica* subspecies I lineage and on the chromosome in some other *S. enterica* linages (Libby *et al.*, 2002). The *spv* locus plays an important role in bacterial virulence. A *S.* Typhimurium strain with a *spv* deletion showed reduced virulence in terms of LD_{50} values in mice (Fierer *et al.*, 1992; Libby *et al.*, 1997). The *spv* operon encodes a transcriptional regulator, SpvR, and four structural proteins SpvABCD (Fig.1-10) (Guiney and Fierer, 2011). The initial transcription of SpvR is regulated by RpoS, a stationary phase sigma factor (Fang *et al.*, 1992; Chen *et al.*, 1996).

Subsequently, SpvR and RpoS upregulate the expression of SpvABCD by interacting with upstream recognition sites of the *spv*R and *spv*A promoters (Sheehan and Dorman, 1998). SpvB and SpvC increase the virulence of *S*. Typhimurium, while the functions of SpvA and SpvD remain unknown. SpvC functions as a phosphothreonine lyase and targets the host mitogen-activated protein kinases (MAPKs), which are essential for the host immune response (Mazurkiewicz *et al.*, 2008). SpvC inactivates MAPKs by removing the phosphate moiety from phosphothreonine in MAPKs and generates a double-bond-containing product by breaking the C-O rather than the O-P bond (Chen *et al.*, 2008). The inactivation of MAPKs suppresses the host's pro-inflammatory responses and thereby facilitates the growth of bacteria (Haneda *et al.*, 2012).

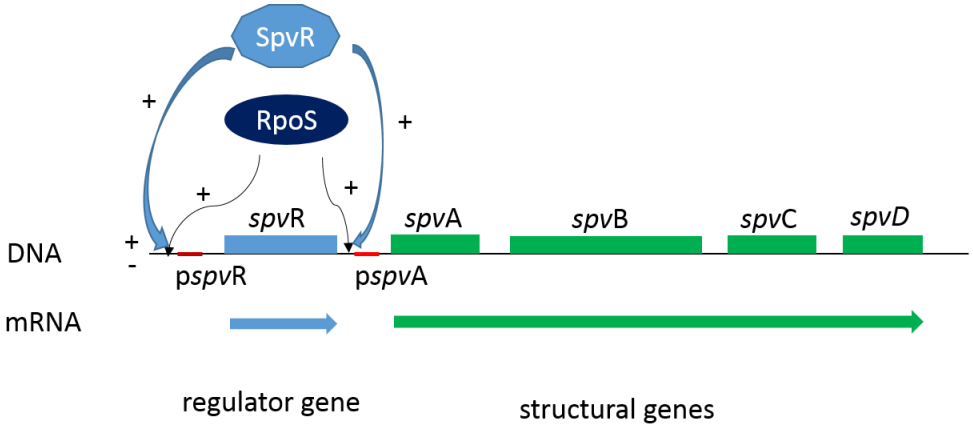

Fig. 1-10. Map of the *spv* operon residing within the virulence plasmid of *S*. Typhimurium. The operon encodes a regulator protein SpvR and four structural proteins, SpvABCD. The transcription of SpvR is initiated by RpoS, a stationary phase sigma factor. SpvR and RpoS upregulate the transcription of *spv*ABCD by binding to the upstream promoters of *spv*R and *spv*A. The red line in the DNA sequence indicates the promoter sequences corresponding the genes.

1.6.3 SpvB ADP-ribosylates G-actin, resulting in de-polymerization of F-actin

SpvB from *S.* Typhimurium is a 591 amino acid long protein, folded into two domains linked by a short proline-rich segment. The C-terminal domain of SpvB shows ~19% sequence identity to *Bacillus cerues* VIP2, which is an actin ADP-ribosylating toxin. SpvB was demonstrated to function as an ADP-ribosyltransferase (ART) and its substrate was identified as actin (Tezcan-Merdol *et al.*, 2001). It was shown that SpvB ADP-ribosylates actin at Arg177 (Hochmann *et al.*, 2006). This modification of actin results in the loss of polymerization activity, leading to the disruption of an equilibrium between G- and F-actin (Fig. 1-11) (Aktories *et al.*,

2011; Barth and Aktories, 2011). Disruption of the cytoskeleton by SpvB, initiates apoptosis (Paesold *et al.*, 2002; Tezcan-Merdol *et al.*, 2005), resulting in the uptake of infected cells by macrophages (Guiney, 2005).

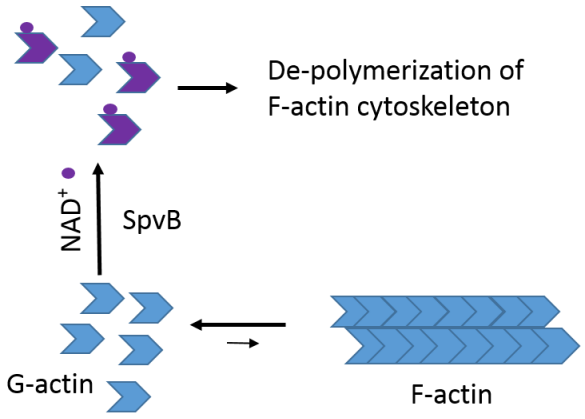

Fig. 1-11. SpvB mediated actin cytoskeleton dynamics. Inside the host cell, G- and F-actin are in an equilibrium. In the presence of NAD^+, SpvB transfers the ADP-ribosyl moiety to G-actin. The modified actin loses the ability to polymerize into F-actin, which shifts the equiliblium towards G-actin and leads to partial F-actin depolymerization. Continous removal of G-actin by SpvB leads to complete depolymerization of F-actin cytoskeleton.

The crystal structure of the SpvB ART domain in complex with NADH has been determined (Margarit *et al.*, 2006). Alignment of the SpvB ART domain structure with other ADP-ribosylating toxins showed similar core structures and active site clefts (Fig. 1-12). Relative to other ART domains, SpvB contains an insertion between the third and forth α-helices (Fig.1-12).

Once ADP-ribosylated, actin loses its polymerization activity. Two possible explanations for this loss of polymerization activity have been proposed, (1) the ADP-ribosylation of actin causes a significant conformational change, which results in a disruption of the actin filaments interfaces; (2) the modification results in a steric disruption of intra-filament contacts (Margarit *et al.*, 2006). To understand why the modification results in a loss of polymerization activity, structures of ADP-ribosylated actin were determined (Margarit *et al.*, 2006). Superposing the structures of the modified and wild-type actin showed only minor conformational differences, result which excludes the possibility that large conformational changes are responsible for the loss in actin polymerization activity. However, the ADP-ribosyl moiety bound to Arg177 is present at the intra-filament interfaces of F-actin (Fig. 1-13), causing steric hindrance to prevent

the binding of another actin monomer. This finding agrees with the latter possibility of abrogating actin polymerization (Margarit *et al.*, 2006).

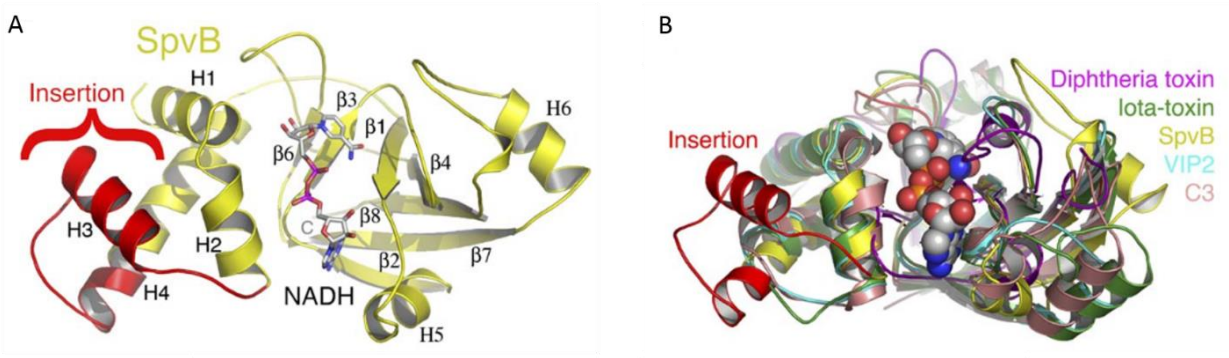

Fig. 1-12. Structures of SpvB$^{(390\text{-}591)}$ and its superimposition with other ART toxins. **A**. Ribbon representation of the structure of SpvB ART domain in complex with NADH, shown as a ball-and-stick model. The conserved ADP-ribosylating toxin core structure is shown in yellow, and the insertion specific for SpvB is highlighted in red. **B**. Structural alignment of SpvB with other ADP-ribosylating toxins (Diphtheria toxin, Iota-toxin, VIP2 and C3). NADH is shown in a space-filling representation. The figures are adapted from (Margarit *et al.*, 2006) with permission.

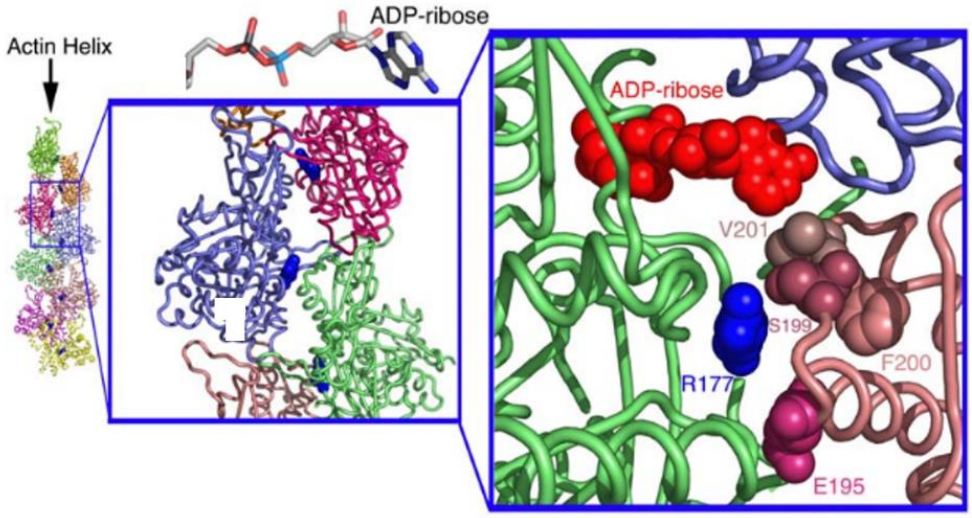

Fig. 1-13. Steric clash due to the ADP-ribosylation in the actin helix. The left panel shows the Holmes model of actin helix. The middle panel is the magnification of the several actin protomers with Arg177 (blue) shown in space-filling representation. The last panel is the superimposition of ADP-ribose (red) in space-filling representation with actin interfaces. Putative residues (E195, S199, F200 and V201) interacting with Arg177 were shown in space-filling representation. The relative size of ADP-ribose is much larger than other residues of the interface. Thus the ADP-ribose actin would increase steric clash when it conjugated to Arg177. The figure is adapted from (Margarit *et al.*, 2006) with permission.

1.6.4 Comparison of the N-terminal domain of SpvB with the ABC toxins

The structure and funtion of the SpvB ART domain are well characterized. However, the structure and funtion of the larger N-terminal domain remain unknown. The N-terminal domain of SpvB shows 47% sequence identity with the N-terminal region of YenB from *Yersinia entomophaga* and 49% with TcdB2 from *Photorhabdus luninescens*(Fig. 1-14).

Fig. 1-14. Sequence allignment of the N-terminal domain of SpvB with the N-terminal segments of TcdB2 and YenB. Residues in red are hyphophobic, green are neutral, blue are negatively charged and purple are positively charged. Symbols below the sequences indicate: a single dot marks similar residues, a double dot marks closer similarity and a star marks identical residues. This sequence allignment was generated through EMBL-EBI multiple sequence allignment ClustalW2 server, http://www.ebi.ac.uk/Tools/msa/clustalw2/.

YenB and TcdB2 (~1,500 amino acid long) are the B components of ABC toxins (also called Tc toxins), a group of toxins that are comprised of three components A, B and C. The ABC toxin complex is assembled to translocate the cytotoxic domain of the C component (TcC) into the cytosol of the host cell (Busby *et al.*, 2013). Crystal structures of ABC toxins from *Yersinia entomophaga* and *Photorhabdus luninescens* were recently determined (Busby *et al.*, 2013; Meusch *et al.*, 2014). When inserted into the host membrane, the A component (TcA) forms pentamers with a translocation channel in the center (Meusch *et al.*, 2014). The B component (TcB) and the N-terminal region (NTR) of the TcC form a bell-shaped canister (Fig. 1-15). The C terminal region (CTR) of TcC is buried inside the canister (Busby *et al.*, 2013). The canister (TcB-TcC^{NTR}) and the cargo (TcC^{CTR}) complex is then docked onto the pentamer formed by TcA. When induced by low pH, the TcA pentamer opens the central channel and the TcC is autocatalytically cleaved to free the cytotoxic domain which is then transported through the TcA channel. The cytotoxic domain of TcC is released into the cytosol of the host cells.

Genes encoding the ABC toxin components are usually located in the same locus. Interesteringly, there is some similarity between Tc components and Spv proteins. The 255 residues long SpvA encoded upstream of SpvB shows 19% sequence identity to the N-terminal region of TcA, a large protein of ~2,500 residues (Fig. 1-16). SpvA is predicted to be an outer membrane-associated protein and the TcA is a transmembrane protein. As discussed above, the N-termianl domain of SpvB shows sequence identity to the N-terminal segment of TcB. Moreover, the C-terminal domain of SpvB has the same activity as the C-terminal domain of some TcCs, like TccC3 and TccC5. Although some similarity could be found between SpvA/SpvB and the Tc toxin, SpvA and SpvB might function differently because they are much smaller than TcA and TcB, respectively. The N-terminal domain of the TcA homologous to SpvA accounts for only 10% of the TcA sequence and the N-terminal domain of TcB homologous to the N-termianl domain of SpvB spans only ~20% of the TcB sequence. As no transmembrane helices are predicted within the SpvA and SpvB sequences, these proteins are unlikely to form a transmembrane channel to translocate the C-terminal domain of SpvB. Furthermore, from the structure of the Tc complex, the TcB-TcA interface inolves domains with no homologs in SpvA and SpvB (Fig. 1-16).

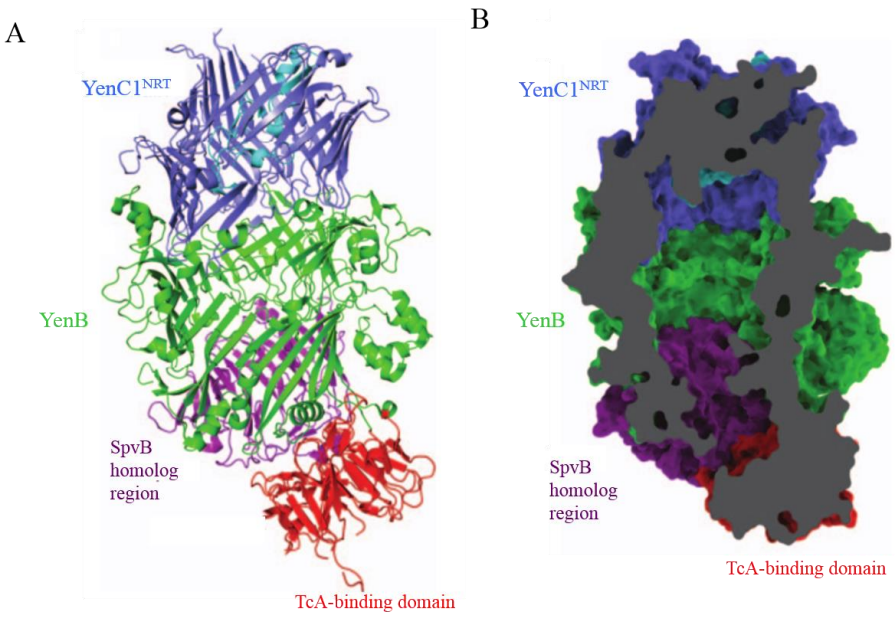

Fig. 1-15. The structure of YenB-YenC1^{NTR} complex. **A**. Cartoon representation of the complex. The YenC1^{NTR} is colored blue, except for the C-terminus, which is cyan, the N-terminal domain of YenB is colored magenta (homolog of SpvB), the middle domain is red and the C-terminal domain is green. **B**. The complex contains a central cavity shown here in a slice through the surface representation of the complex. The color coding is the same as in A.

Sequence map of Tc toxin components	*Yersinia Entomophaga*	*Photorhabdus Luninescens*
TcB-binding domain Homolog of SpvA TcA →2516*	YenA1, YenA2	TcdA1
Homolog of SpvB TcA-binding domain TcB → 1474*	YenB	TcdB2
N-terminal domain Cytotoxic domain TcC →960*	YenC1, YenC2	TccC3, TccC5
Homolog of TcdB2 ART domain SpvB → 591		

Fig. 1-16. Components of the ABC toxin from *Photorhabdus luninescens* and *Yersinia entomophaga*. Domain structure of each component is marked in different colors and the known functions are annotated. Protein residues number are labelled according to TcdA1, TcdB2 and TccC3.

1.6.5 Comparison of SpvB with actin ADP-ribosylating toxins

A number of pathogens like *Clostridium, Bacillus* and *Photorhabdus luminescens,* secrete toxins and effectors that mediate actin cytoskeleton rearrangement (Barbieri *et al.*, 2002; Aktories and Barbieri, 2005). One of the common approaches to interfere with actin dynamics is actin ADP-ribosylation. Actin ADP-ribosylating toxins can be classified into two groups, (1) those that modify actin at Arg177, which results in the depolymerization of F-actin, and (2) those that modify actin at Thr148, which promotes actin polymerization and actin aggregation (Aktories *et al.*, 2011). Toxins modifying Arg177 of actin normally contain two components, an enzyme component and a binding component (Aktories *et al.*, 2011). Thus this group of toxins are also called binary actin ADP-ribosylating toxins and includes the C2 toxin from *Clostridium botulinum,* Iota from *Clostridium perfringens,* VIP from *Bacillus cerues,* CDT from *Clostridium difficile* and CST from *Clostridium spiroforme* (Barth and Stiles, 2008; Simon *et al.*, 2014).

The mechanism of the delivery of the C2 toxin is well understood (Fig. 1-17). The binding component (C2II) is activated by the pre-cleavage of the N-terminal region and then the remaining C-terminal part polymerized into a heptameric prepore structure (Schleberger *et al.*, 2006). The heptamer interacts with the N-terminal binding domain of the enzyme component (C2I). The C2II heptamer is then recognized by the receptor on the host membrane, resulting in the ruffling of the host membrane and leads to internalization of the toxin within an endosome. Triggered by low pH, the C2 toxin inserts into the endosomal membrane and the C2I component is then delivered to the cytoplam of the host cytosol where it modifies actin (Aktories and Barth, 2004a, b). The function of the C-terminal domain of SpvB is similar to that of C2I toxins. However, since SpvB is not associated with a C2II-like component, the delivery of SpvB is rather different from the binary actin-ADP-ribosylating toxins and likely occurs through the type three secretion system.

1.6.6 The secretion of SpvB

The delivery of SpvB appears to be different from the ABC toxins and binary actin-ADP-ribosylating toxins. TTSS are the major translocation pathways for a large number of virulence proteins. However, the previously reported *in vitro* secretion assay of SpvB in *Δspi-1* mutant strain (Δ*inv*A) and *Δspi-2* mutant strain (Δ*ssr*A) indicated that SpvB was secreted into medium in both mutant strains, leading the authors to conclude that the secretion of SpvB is TTSS-independent (Gotoh *et al.*, 2003). However, no secretion pathway for SpvB was as yet identified.

To firmly confirm that TTSS are indeed not utilized for SpvB secretion one would need to show that SpvB is secreted when both SPI-1 and SPI-2 secretion systems are non-functional. However, indirect evidence suggests that SpvB is likely secreted primarily through the SPI-2 secretion system. The expression of *spv* genes and SPI-2 TTSS is upregulated when *Salmonella* gains entry into the host cells (Fierer *et al.*, 1993; Chen *et al.*, 1996). Moreover, several SPI-2 TTSS effectors such as SsaV, SsaB and SseB-D are required for the secretion of SpvB (Browne *et al.*, 2008).

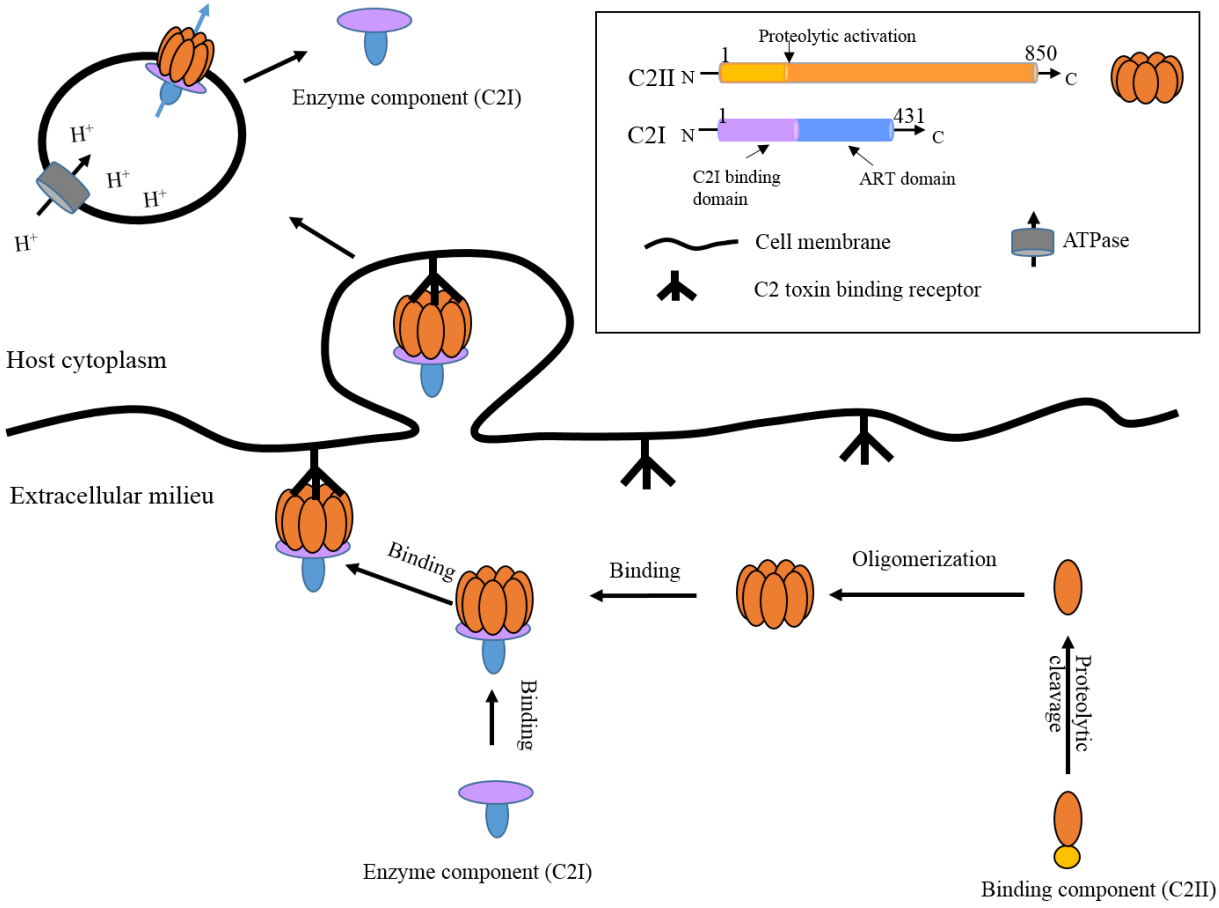

Fig. 1-17. Model of action of the C2 binary actin ADP-ribosylating toxin. The C2 toxin consists of an enzyme component (C2I) and a binding component (C2II). The N-terminal region of C2II is cleaved and the remaining C-terminal part oligomerizes into a hepatmer, which subsequently binds to the N-terminal domain of C2I. The C2 toxin complex binds to the receptor on the cell surface and triggers endocytosis. Upon endosome acidification the C2 complex is inserted into the endosomal membrane, releasing the C2I component into the host cytosol to modify actin.

1.7 Project objectives

S. Typhimurium can invade a broad range of hosts, while *S.* Typhi is human-specific. Expression of a single protein GtgE from *S.* Typhimurium in *S.* Typhi helped to overcome host restriction. This indicated that GtgE plays a role in host permissiveness. The GtgE was shown to cleave several Rabs but not all, despite their high sequence similarity in the cleaved region. To understand how GtgE differentiates between closely related Rabs,the three-dimensional structure of the active form of GtgE alone and with a bound substrate is needed. Currently, only the crystal structure of the GtgE fragment of lacking ~80 N-terminal residues is known and represents an inactive form of GtgE. The missing segment includes the cysteine nucleophile, and represents. The objectives of this project were to acquire structural information about the active form of GtgE and to understand the substrate specificity of GtgE. Therefore the main efforts on this project were directed toward crystallization of GtgE, its structure determination and its complex with Rab32 or a peptide containing the cleavage site.

SpvB is another important effector in *S.* Typhimurium. It is known that SpvB ADP-ribosylates actin and disrupts actin cytoskeleton. The structure and function of the ART domain is well characterized. However, the function and structure of the N-terminal domain remains unknown. The objectives of this project were to obtain structural information about the N-terminal domain of SpvB and to identify the function of this domain.

2. Methods and materials

2.1 Materials and reagents

The reagents used in this project are listed in Table 2-1. Antibodies used for Western blot and immunocytochemistry are listed in Table 2-2. Cell lines used are listed in Table 2-3. Vectors and plasmids used in this project are listed in Table 2-4.

Table 2-1. Important reagents used in this project

	Reagents	Supplier
For cloning	KOD hot start DNA polymerase kit, 71086	EMD Millipore
	T4 DNA polymerase, M0203L	NEB
	T4 DNA ligase and corresponding buffer, M0202S	NEB
	*Dpn*I, R0176L	NEB
	*Xho*I, R0146L	NEB
	*EcoR*I, M0211L	NEB
	*Bgl*II, R0144L	NEB
	*Pst*I, R0140S	NEB
	100×BSA	NEB
	100 mM dCTP,and 100 mM dGTP, N0446S	NEB
	NEBuffer 2, B7002S	NEB
	NEBuffer 3.1, B7203S	NEB
	DNA loading buffer, 28129	Norgen
	Gelgreen nucleic acid gel stain, 41005	Biotium
	QIAquick Gel Extraction Kit (250), 28706	Qiagen
	QIAprep Spin Miniprep Kit (250), 27106	Qiagen
For protein expression, purification and crystallization	Isopropyl β-D-1-thiogalactopyranoside (IPTG), BP1755-100	Thermo Fisher Scientific
	Yeast Extract, YEX401.205	BioShop
	Tryptone, BP1421-2	Thermo Fisher Scientific
	Sodium chloride (NaCl), SOD002.10	BioShop
	Magnesium chloride hexahydrate, MAG520.500	BioShop
	Potassium chloride, POC999.500	EMD Millipore
	Glycerol, G31-4	Thermo Fisher Scientific
	Potassium phosphate monobasic (KH_2PO_4), P285-500	Thermo Fisher Scientific
	Potassium phosphate dibasic (K_2HPO_4), PPD303.1	BioShop
	Dithiothreitol (DTT), BP17225	Thermo Fisher Scientific
	4-(2-hydroxyethyl)-1-piperazineethanesulfonic acid (HEPES), HEP001.1	BioShop

	Bis-Tris, BST602.250	BioShop
	Imidazole, IMD508.1	BioShop
	Nickel (II) sulfate hexahydrate, 227676-500G	Sigma-Aldrich
	L-Glutathione (GSH), GTH003.25	BioShop
	Formaldehyde, 04018	Polysciences, Inc.
	Protein marker, 161-0377	Bio-Rad
	Borane dimethylamine complex, 180238-5G	Sigma-Aldrich
	Glycine, BP381-5	Thermo Fisher Scientific
	Sodium dodecyl sulfate (SDS), SDS001.1	BioShop
	30% Acrylamide/Bis-acrylamide(29:1), ACR009.500	Bioshop
	Ammonium persulfate (APS), AMP001.25	BioShop
	N,*N*,*N*,*N*-Tetramethylethane-1,2-diamine (TEMED), TEM001.25	BioShop
	Bromophenol Blue, 114413-5G	Sigma-Aldrich
	Coomassie Brilliant Blue R-250, (0427-25G)	AMRESCO
	Tween-20,170-6531	BioShop
	Polyethylene glycol 3350 (PEG3350), P4338-1KG	Sigma-Aldrich
	Polyacrylic acid 5100 sodium salt, 1132	Sigma-Aldrich
	Halt Protease Inhibitor Cocktail EDTA free, PI78439	Thermo Scientific
	Ni-NTA agarose, 142338540	Qiagen
	Hitrap chelating column, 17-0409-03	GE Healthcare Life Science
	Glutathione superflow resin, 635608	Clontech
	MonoQ 4.6/100PE, 17-5179-01	GE Healthcare Life Science
	Superdex 75 10/300, 17-5174-01	GE Healthcare Life Science
For Cell culture	Dulbecco's Modified Eagle's medium,D5796	Sigma
	XtremeGENE HP DNA Transfection reagent, 06366236001	Roche
	Trysin-EDTA solution, T4049-500ML	Sigma
	Triton X-100, BP151-500	Thermo Fisher Scientific
	Ethylenediaminetetraacetic acid (EDTA), EDS-500G	Sigma-Aldrich
	Paraformaldehyde, P6148-500G	Sigma-Aldrich
	Fetal Bovine Serum (FBS), 10437-028	Life technologies
	4',6-diamidino-2-phenylindole (DAPI), D9542	Thermo Fisher Scientific
	Acti-stain 555 phalloidin, PHDH1-A	Cytoskeleton Inc.
	Nitroblue tetrazolium/ 5-bromo-4-chloro-indolyl phosphate (BNT/BCIP), 34042	Life Technologies
	ECL reagent 1 and 2, RPN2109	GE Healthcare Life Science

Table 2-2. List of primary and secondary antibodies used in this project

Antibody	Supplier
Mouse anti-HA (1:1000)	Santa-Cruz-Biotechnology
Mouse anti-FLAG (1:1000)	Sigma-Aldrich
Mouse anti-DnaK (1:10000)	Sigma-Aldrich
Rabbit anti-SseL serum (1:2000)	W. Koester, Vaccine and Infectious Disease Organization (VIDO), Saskatoon
Rabbit anti-SopE serum (1:2000)	
Goat anti-mouse-alkaline phosphatase (1:2000)	
Goat anti-Rabbit-alkaline phosphatase (1:10000)	
Goat anti-mouse- horseradish peroxidase (HRP) (1:5000)	Santa-Cruz-Biotechnology

Table 2-3. List of cell lines used in this project

	Cell lines	Source
Mammalian cell lines	HeLa	Dr. W. Xiao, Department of Microbiology and Immunology, University of Saskatchewan (Usask)
	Human embryonic kidney 293 (HEK293)	
E. coli strains	DH5α	Dr. M. Cygler, Department of Biochemistry, Usask
	BL21	
	BL21(DE3)	
	Bl21(DE3)STAR	
Salmonella strains	*Salmonella* Enteritis strain 18	Dr. W. Koester, VIDO, Saskatoon
	Salmonella Enteritis Strain 18 with Δ*spi-1*::*Amp* & Chloramphenicol (Δ*spi-1* strain)	
	Salmonella Enteritis Δ*spi-2*::*Amp* & Chloramphenicol (Δ*spi-2* strain)	
	Salmonella Enteritis Δ*spi-1&2*::*Amp* & Chloramphenicol (Δ*spi*-1&2 strain)	

Table 2-4. List of plasmids used in this project

Plasmid	Description	Source
pMSCG7	Ampcillin^{resistant} (Amp^r), cloning vector for N-His constructs with a TEV cleavage site	Dr. M. Cygler, Department of Biochemistry, Usask
pRL652	Amp^r, cloning vector for N-GST constructs with a TEV cleavage site	
pHis-GtgE$^{(2-228)}$	Amp^r, GtgE$^{(2-228)}$ cloned into pMSCG7	This work
pHis-GtgE$^{(14-214)}$	Amp^r, GtgE$^{(14-214)}$ cloned into pMSCG7	This work
pHis-GtgE$^{(31-214)}$	Amp^r, GtgE$^{(31-214)}$ cloned into pMSCG7	This work
pGST-GtgE$^{(2-228)}$	Amp^r, GtgE$^{(2-228)}$ cloned into pRL652	This work
pGST-GtgE$^{(14-214)}$	Amp^r, GtgE$^{(14-214)}$ cloned into pRL652	This work
pGST-GtgE$^{(21-214)}$	Amp^r, GtgE$^{(21-214)}$ cloned into pRL652	This work
pGST-GtgE$^{(31-214)}$	Amp^r, GtgE$^{(31-214)}$ cloned into pRL652	This work

pHis-GtgE$^{(2-228)}$(C45S)	Amp^{r}, pHis-GtgE$^{(2-228)}$ derivative containing C45S mutation	This work
pHis-GtgE$^{(2-228)}$(H151S)	Amp^{r}, pHis-GtgE$^{(2-228)}$ derivative containing H151S mutation	This work
pGST-GtgE$^{(14-214)}$(C45S)	Amp^{r}, pGST-GtgE$^{(14-214)}$ derivative containing C45S mutation	This work
pHis-GtgE$^{(2-228)}$ (KNE196ANA)	Amp^{r}, pHis-GtgE$^{(2-228)}$ derivative containing KNE196ANA mutation	This work
pHis-GtgE$^{(2-228)}$ (KK163AA)	Amp^{r}, pHis-GtgE$^{(2-228)}$ derivative containing KK163AA mutation	This work
pECFP-Rab32	Amp^{r}, Rab32 cloned into pECFP-C3	J. Brunell, Department of Molecular Genetics, University of Toronto
pGST-Rab32	Amp^{r}, Rab32 cloned into pRL652	This work
pHis-SpvB$^{(26-355)}$	Amp^{r}, SpvB$^{(26-355)}$ cloned into pMSCG7	Dr. M. Cygler, Department of Biochemistry, Usask
pCDNA4TO	Amp^{r}, cloning vector for C-HA constructs	Wei's lab
pSpvB$^{(26-355)}$-HA	Amp^{r}, SpvB$^{(26-355)}$ cloned into pCDNA4TO	This work
pSpvB$^{(1-591)}$-HA	Amp^{r}, SpvB$^{(1-591)}$ cloned into pCDNA4TO	This work
pSpvB$^{(26-591)}$-HA	Amp^{r}, SpvB$^{(26-591)}$ cloned into pCDNA4TO	This work
pSpvB$^{(390-591)}$-HA	Amp^{r}, SpvB$^{(390-591)}$ cloned into pCDNA4TO	This work
pEGFP-N1	Kanamycin^{resistant} (Kana^{r}), cloning vector for C-GFP constructs	Dr. B. Roesler, Department of Biochemistry, Usask
pSpvB$^{(1-355)}$-GFP	Kana^{r}, SpvB$^{(1-355)}$ cloned into pEGFP-N1	This work
pSpvB$^{(1-591)}$-GFP	Kana^{r}, SpvB$^{(1-591)}$ cloned into pEGFP-N1	This work
pSpvB$^{(26-591)}$-GFP	Kana^{r}, SpvB$^{(26-591)}$ cloned into pEGFP-N1	This work
pSpvB$^{(390-591)}$-GFP	Kana^{r}, SpvB$^{(390-591)}$ cloned into pEGFP-N1	This work
pFLAG-CTC	Amp^{r}, cloning vector for C-FLAG constructs	Dr. A. White, VIDO, Saskatoon
pSpvB$^{(1-591)}$-Flag	Amp^{r}, SpvB$^{(1-591)}$ cloned into pFLAG-CTC	This work

2.2 Structural studies of GtgE

2.2.1 Constructions of GtgE and Rab32 expression vectors using ligase independent cloning (LIC) method

Target genes (*S.* Typhimurium GtgE, NCBI reference NP_460029.1 and human Rab32, NCBI reference NP_006825.1) were amplified by the polymerase chain reaction (PCR) using the

commercial KOD hot start DNA polymerase kit (EMD Millipore, Darmstadt, Germany). The PCR reactions were set up in a 50 µL volume according to the manufacturer's instructions. The used primers are listed in Table 2-5. The PCR reaction started with polymerase activation at 95 ℃ for 2 min, followed by 25 cycles of denaturing DNA at 95 ℃ for 20 s, annealing DNA and primers at primer denaturing midpoint temperature (normally 57 ℃) for 10 s and DNA extension at 70 ℃ for 20 s/kb. The amplified DNA product was mixed with DNA loading buffer (Norgen Thorold, ON, Canada) and loaded onto 1% (w/v) agarose gel. The agarose gel was made by heat dissolving 1% agarose in 1×TAE buffer, which consists of 40 mM Tris-acetate, pH 8.2-8.4 and 1 mM ethylenediaminetetraacetic acid (EDTA). DNA dye, Gelgreen nucleic acid gel stain, was added to the mixture at 10,000 times dilution when the agarose mixture cooled down to ~37 ℃. The gel was cast in a mold with combs to form loading wells. After loading the samples, 120 V was applied to the gel for 30 min and the DNA was visualized under UV light. The target DNA band was excised and purified using the QIAquick Gel Extraction Kit (Qiagen, Valencia, CA, USA).

The vectors of interest (pMSCG7 vector for His-tagged constructs and pRL652 vector for GST-tagged constructs) were amplified using vector-specific primers (Table 2-5) in a 50 µL reaction system. The PCR was set up in a similar way as described above except the extension time at 70 ℃ was set to 5 min. The amplified vector DNA products were purified using QIAquick Gel Extraction Kit (Qiagen, Valencia, CA, USA) and further treated with DpnI restriction enzyme at 37 ℃ for 1 h to digest the circular template.

DNA insert was treated with T4 DNA polymerase, which has 3' to 5' exonuclease activity, in the presence of dCTP to form sticky ends. The sticky end formation reaction was set up in a 40 µL reaction volume, which consisted of 200 ng DNA, 1×NEBuffer2, 5 mM dithiothreitol (DTT), 1×NEB BSA, 0.3 µL T4 DNA polymerase and 2.5 mM dCTP for treating insert. To form sticky ends, the vector was treated with 2.5 mM dGTP instead of dCTP. The reaction was set at 22 ℃ for 1 h, followed by deactivation enzyme at 75 ℃ for 20 min.

T4 DNA polymerase-treated insert DNA and vector were mixed together at a ratio of 5:1~10:1 in a 10 µL reaction volume to form circular plasmid. The mixture was incubated at room temperature for 1 h. Subsequently, the DNA mixture was mixed with 50 µL *E. coli* DH5α competent cells and incubated on ice for 20 min. Afterwards, the competent cells were heat-shocked at 42 ℃ for 45 s and cold-shocked on ice for 5 min. 300 µL of antibiotic-free Luria broth

media (LB, 1% (w/v) tryptone, 0.5% (w/v) yeast extract, 1% (w/v) NaCl) was added to the mixture, which was further incubated at 37 ℃ for 40 min. After the incubation, 100 µL of the cell mixture was plated onto LB agar plate (1.5% (w/v) agar in LB medium), which was complemented with 100 µg/mL ampicillin. After 16 h incubation at 37 ℃, a single colony was picked and grown in LB medium at 37 ℃for 16 h. The cell culture was spun down at 15,000×g for 2 min and used for plasmid extraction using QIAprep Spin Miniprep Kit (Qiagen, Valencia, CA, USA). The sequence of the insert was further confirmed by Sanger sequencing using services of the National Research Council (Saskatoon, Canada) or Eurofins (Huntsville, USA).

Table 2-5. Primers for GtgE and Rab32 constructs using LIC

	Primer sequence	Supplier
GtgE (F014)	TACTTCCAATCCAATGCCAGAAGTAATACAGCAACTCCTCAGGGT	IDT
GtgE (F021)	TACTTCCAATCCAATGCCCAGGGTCAGATTATTCACCATCGTAAC	IDT
GtgE (F031)	TACTTCCAATCCAATGCCCAAAGCCAGTTTGATACCACAGGC	IDT
GtgE (R214)	TTATCCACTTCCAATGTTACTATTTTGGCTCATAAACACCGTCATAGTAAAG	IDT
Rab32 (F001)	TACTTCCAATCCAATGCCATGGCGGGCG	IDT
Rab32 (R225)	TTATCCACTTCCAATGTCAGCAACACT	IDT
pMSCG7 F	ATTGGAAGTGGATAACGGATCCGAATTCGAGC	IDT
pMSCG7 R	ATTGGATTGGAAGTACAGGTTCTCGGTACCCA	IDT
pRL652 F	ATTGGAAGTGGATAACGGATCCGAATTCGAGC	IDT
pRL652 R	ATTGGATTGGAAGTACAGATTCTCGCTATCCG	IDT

2.2.2 Site-directed mutagenesis

Primers for constructing the desired GtgE mutations are listed in Table 2-6. The paired primers encoding the mutation were used to amplify the plasmid with the gene of interest. The PCR reaction was set up as previously described in the LIC method. Afterwards, the 50 µL PCR product was treated with 1 µL DpnI at 37 ℃ for 1 h to digest the added template. Five microliters of mixture was transformed into 50 µL DH5α competent cells. Sequences of the mutants were confirmed by Sanger sequencing using services at the National Research Council (Saskatoon, Canada) or Eurofins (Huntsville, USA).

Table 2-6. Primers for site-directed mutagenesis for GtgE constructs (F - forward, R - reverse).

	Primer sequence	Supplier
GtgE(C45A) F	GGCAACACCCTCTACAATAATGCCTGGGTTTGC TCATTAAATG	IDT
GtgE(C45A) R	CATTTAATGAGCAAACCCAGGCATTATTGTAGA GGGTGTTGCC	IDT
GtgE(C45S) F	GGCAACACCCTCTACAATAATAGCTGGGTTTGC TCATTAAATG	Eurofins
GtgE(C45S) R	CATTTAATGAGCAAACCCAGCTATTATTGTAGA GGGTGTTGCC	Eurofins
GtgE(H151A) F	GCTCGGAATGTCTAAGCTCAGAGTGCATTG	IDT
GtgE(H151A) R	CAATGCACTCTGAGCTTAGACATTCCGAGC	IDT
GtgE(H151S) F	CTTGGCTCGGAATGTCTAAGCGCAGAGTGCATT GTAGG	IDT
GtgE(H151S) R	CCTACAATGCACTCTGCGCTTAGACATTCCGAG CCAAG	IDT
GtgE(H151N) F	GCTCGGAATGTCTAAATGCAGAGTGCATTG	IDT
GtgE(H151N) R	CAATGCACTCTGCATTTAGACATTCCGAGC	IDT
GtgE(D169A) F	GAAGGAAAAAAGTATTAATTTATGCTTCAATGA ATACCTCACCTGAATGG	Eurofins
GtgE(D169A) R	CCATTCAGGTGAGGTATTCATTGAAGCATAAAT TAATACTTTTTTCCTTC	Eurofins
GtgE(KK163AA) F	GGCTATGATAGTGAAGTGGCAGCAGTATTAATT TATGATTCAATG	IDT
GtgE(KK163AA) R	CATTGAATCATAAATTAATACTGCTGCCACTTC ACTATCATAGCC	IDT
GtgE(KNE163ANA) F	GCATTCAATGATAAATATGCAAATGCAGATTGC AGTATTTGTGGTC	IDT
GtgE(KNE163ANA) R	GACCACAAATACTGCAATCTGCATTTGCATATT TATCATTGAAGTC	IDT

2.2.3 Purification and crystallization trials of GtgE constructs

2.2.3.1 Protein expression

Plasmids containing the target genes were transformed into *E. coli* expression cell lines (BL21 for GST-tagged protein and BL21(DE3)STAR for His-tagged protein). A single colony was picked and grown at 37 ℃ for 12-16 h. The cell culture was scaled up into 1 L terrific broth (TB) media (1.2% (w/v) tryptone, 2.4% (w/v) yeast extract, 72 mM K_2HPO_4, 17 mM KH_2PO_4, and 0.4% (v/v) glycerol). When the optical density at 600 nm (OD_{600}) reached 0.6, 1 mM isopropyl β-D-1-thiogalactopyranoside (IPTG) was added to induce expression of the target gene and the culture was incubated in the shaker for 12-16 h at 20 ℃.

2.2.3.2 Purification of the His-tagged GtgE constructs

Cell cultures expressing His-tagged GtgE were spun down at 7000×g for 20 min. The harvested cells were re-suspended in 50 mL lysis buffer (15 mM 4-(2-hydroxyethyl)-1-piperazineethanesulfonic acid (HEPES) pH 7.5, 150 mM NaCl) and the cells were lysed in a cell disrupter (Constant Systems Ltd, TS Series Benchtop). The cell lysate was centrifuged at 30,000×g for 45 min. The supernatant was loaded to nickel-nitrilotriacetic acid (Ni-NTA) agarose resin (Qiagen, Valencia, CA, USA). The Ni^{2+}-charged column was washed with 3 column volumes of lysis buffer, followed by 2 column volumes of high salt buffer (15 mM HEPES pH 7.5, 500 mM NaCl). Subsequently, the His-tagged protein was eluted by applying imidazole gradient. Column fractions were analyzed by sodium dodecyl sulfate--polyacrylamide gel electrophoresis (SDS-PAGE). Fractions containing the target protein were combined and treated with Tobacco Etch Virus (TEV) protease, which is His-tagged, at a 1:50 (w/w) ratio. The cleavage reaction was set up inside a dialysis bag and dialyzed against a buffer containing 15 mM HEPES pH 7.5, 150 mM NaCl and 1 mM DTT at 4 ℃ for 16 h. The treated sample was loaded onto a Ni-NTA column to remove un-cleaved His-tagged protein and TEV. The reaction progress was followed by SDS-PAGE. All the His-tagged GtgE was purified except for His-$GtgE^{(2\text{-}228)}$(KNE196ANA). After cell lysis, supernatant was filtered through 0.22 μm filter and then applied to a GE pre-packed Hitrap chelating column, which had been charged with Ni^{2+} and equilibrated with lysis buffer, controlled by the NGC™ chromatography Quest 10 plus system (Bio-Rad, Mississauga, ON, Canada). Step gradient of imidazole in buffer was used to elute protein. The TEV protease was also applied to remove the His-tag. Whenever TEV protease was applied to remove the tag, the mixture was loaded onto a Ni^{2+} column to remove TEV.

2.2.3.3 Purification of the GST-tagged GtgE constructs

The cell culture was spun down and the cells were re-suspended in 50 mL lysis buffer (15 mM HEPES pH 7.5, 150 mM NaCl, 1 mM DTT). The cells were lysed in a cell disrupter, centrifuged, and the supernatant was mixed with glutathione (GSH) agarose resin pre-equilibrated with lysis buffer. The protein solution and GSH resin was incubated at 4 ℃ for 1 h for binding. After binding, the resin mixture was loaded into a column with a filter. The resin was washed with 3 column volumes of lysis buffer. The GST-tagged protein bound to the GSH resin was treated with TEV protease in a ~1:50 (w/w) ratio in 10 ml of lysis buffer at room temperature for 12 h. The amount of protein bound to the resin was estimated by measuring the

concentration of protein, which was eluted from a fraction of protein-resin mixture using a 20 mM GSH solution. After the cleavage reaction, the protein solution was loaded onto a Ni-NTA column to remove TEV protease. Protein fractions were analyzed on SDS-PAGE throughout the purification process.

2.2.3.4 Size exclusion chromatography

Size exclusion chromatography was the last step in the protein purification protocol. Target protein was concentrated to about 5-10 mg/mL and then loaded onto a size exclusion Superdex 75 or Superdex 200 column, which was pre-equilibrated with buffer containing 15 mM HEPES, 150 mM NaCl and 1 mM DTT. This buffer was further used to elute protein from the column. Proteins were separated according to their molecular weight. Protein fractions eluted from the column were monitored by measuring the absorption at 280 nm and the peak fractions were analyzed by the SDS-PAGE.

2.2.3.5 SDS-PAGE analysis

The SDS-PAGE gel is comprised of a stacking gel (at the top) and a separating gel (at the bottom). The extent of separation used in the gel varies from 10 to 15% acrylamide and bis-acrylamide mixture (29:1), depending on the molecular weight of the protein in question. For a 15% gel, the separating gel was composed of 375 mM Tris, pH 8.8, 15% (v/v) acrylamide/bis-acrylamide (29:1), 0.1% (w/v) SDS, 0.1% (w/v) ammonium persulfate (APS) and 0.1% (v/v) *N*,*N*,*N*',*N*'-tetramethylethane-1,2-diamine (TEMED). The 5% stacking gel consisted of 125 mM Tris, pH 6.8, 5% (v/v) acrylamide/bis-acrylamide (29:1), 0.1% (w/v) SDS, 0.1% (w/v) APS and 0.1% (v/v) TEMED. A multi-well comb was inserted into the stacking gel to form multiple lanes for loading samples. Protein samples were loaded into the stacking gel after being mixed with loading buffer (62.5 mM Tris, pH 6.8, 2% (w/v) SDS, 0.002% (w/v) bromophenol blue, 100 mM DTT, 10% (v/v) glycerol) and denatured at 95 ℃ for 10 min. Finally, protein markers were loaded on the gel to indicate molecular weight. The gel was put in the electrophoresis system with ~500 mL running buffer containing 24.8 mM Tris, 192 mM glycine and 0.1% SDS (w/v). Then the gel was run at 200 V for 55 min. When the electrophoresis was completed, the gel was removed, stained with a solution containing 40% (v/v) ethanol, 10% (v/v) acetic acid and 0.025% (w/v) Coomassie brilliant blue R-250 for 20 min, and de-stained with a solution containing 10% acetic acid (v/v) and 10% ethanol (v/v) for 30 min. After destaining, the gel was scanned on an imager (Syn-Gene, ChemlXX9).

2.2.3.6 Crystallization trials

GtgE constructs were purified and concentrated to approximately 20 mg/mL. Crystallization trials were carried out on GtgE mutants in the absence and presence of peptides corresponding to the known Rab32 cleavage site. The screens were performed in 96-well plates in a sitting drop format using the Gryphon crystallization robot (Art Robbins Instruments, Sunnyvale, CA, USA). Micro-batch crystallization approach was also used to set up screens. Crystallization screening was performed using both commercial (Hampton Research, Aliso Viejo, CA, USA and Qiagen, Valencia, CA, USA) and home-made incomplete factorial screens. Promising conditions were explored further by systematic modifications of the initial conditions within a narrow range.

2.2.4 Protease activity of the GtgE constructs

GST-Rab32 was purified in a similar fashion to GST-tagged GtgE except for omitting the GST tag cleavage step. GST-Rab32 was eluted with 20 mM GSH in buffer containing 15 mM HEPES pH 7.5, 150 mM NaCl and 1 mM DTT. Eluted GST-Rab32 was dialysis against buffer containing 15 mM HEPES pH 7.5, 30 mM NaCl and 1 mM DTT at 4 ℃ for 16-20 h. After dialysis, the protein was loaded onto an anion exchange HitrapQ column, which was pre-equilibrated with buffer A, composed of 15 mM HEPES pH 7.5 and 1 mM DTT. After loading the protein, the column was washed with 2 column volumes of buffer A. Protein was eluted with a salt step gradient in buffer A, which salt steps of 50 mM, 100 mM, 200 mM, 300 mM, 500 mM and 1M NaCl. Fractions were collected and analyzed by SDS-PAGE.

GtgE constructs were incubated with GST-Rab32 at 1:2 and 1:20 molar ratio in the presence of 10 mM Mg^{2+} and 10 mM Ca^{2+}. The reactants were incubated at room temperature for 2 h. An aliquot of the reaction mixture was removed at 1 h. The reactions were terminated by adding SDS-PAGE loading buffer and by denaturing the proteins at 95 ℃ for 10 min. The sample was analyzed by SDS-PAGE.

2.2.5 Expression and purification of ^{15}N-GtgE$^{(14-214)}$(C45S)

GST-GtgE$^{(14-214)}$(C45S) was transformed into BL21 for expression, 5 mL LB media supplemented with ampicillin was inoculated with a single colony and grown at 37 ℃ for 16-20 h. The overnight cell culture was inoculated into 4 L LB media and incubated at 37 ℃ in a shaker. When an OD_{600} of the cell culture reached 0.6, cells were harvested using sterilized centrifuged tubes at 7000×g for 20 min. The cell pellet was re-suspended into 1 L M63 washing solution

containing 100 mM KH_2PO_4, 70 mM KOH, 15 mM NH_4Cl, 15 mM Na_2SO_4, 3 μM $FeSO_4$, 18 μM thiamine, 0.02% (w/v) $MgSO_4 \cdot 7H_2O$ and 0.3% glucose. The mixture was centrifuged at 7000 ×g for 20 min and the pellet was resuspended into M63 medium, which contained 15 mM $^{15}NH_4Cl$, and supplemented with 50 μg/mL ampicillin. The cell culture was then induced with 1 mM IPTG and incubated at 20 ℃ for 20 h. The cells were harvested and ^{15}N-GtgE$^{(14-214)}$(C45S) purified in the same way as described for GST-tagged GtgE.

2.2.6 ^{1}H-^{15}N HSQC spectra of ^{15}N-GtgE$^{(14-214)}$(C45S) and protein titration with peptide

The 4,4-dimethyl-4-silapentane-1sulfonic acid (DSS) was added to purified ^{15}N-GtgE$^{(14-214)}$(C45S) solution to a final concentration of 1 mM. D_2O was added into protein mixture to a final concentration of 10%. The ^{1}H-^{15}N heteronuclear single quantum correlation (HSQC) spectrum was recorded at 298 K on a Bruker NMR spectrometer operating at 600 MHz frequency. After recording the protein spectrum, a 5-fold excess of peptide (RATIGVDFALK) was added to the protein solution and a second spectrum was recorded. The NMR data acquisition was performed by Mr. Corey Yu, Department of Biochemistry, University of Saskatchewan (Dr. Oleg Dmitriev's laboratory).

2.2.7 Nanopore analysis of GtgE constructs

The lipid, 2-dipheytanoyl-sn-glycero-3-phosphocholine, was dissolved in chloroform, dried under vacuum condition for 4 h and redissolved in decane to a final concentration of 30 mg/mL (Stefureac *et al.*, 2006). The lipid solution was painted onto the aperture in a Teflon perfusion cup to form lipid bilayer. 1 mL of buffer solution containing 10 mM HEPES, pH 7.8 and 1 M KCl was added onto both the *cis* and *trans* compartments of the cup. Alpha-hemolysin, which is a protein used for pore formation, was added into the *cis* compartment in the cup at a concentration of 1.25 μg/mL. A direct current potential of 100 mV was applied to insert α-hemolysin into the lipid to form a stable pore. The protein of interest (GtgE constructs) at a final concentration of 1 μM was added into the *cis* compartment of the cup. A 100 mV potential was applied to the cup and the signals were recorded with a computer running PClamp 10.1 program (Axon Instruments, Molecular Devices, Sunnyvale, CA, USA). The data was processed with the programs Clampfit 10.1 (Axon Instruments) and Origin 7.0 (Meller and Branton, 2002). The blockade current histograms peaks were obtained by fitting the blockade current distribution with a Gaussian function. The lifetime curve was obtained by fitting each blockade time distribution

with a single-exponential function. The nanopore experiments were performed by Ms. Elisabet Jakova, Department of Biochemistry, University of Saskatchewan (Dr. Jeremy Lee's laboratory).

2.3 Structure determination of SpvB$^{(26-355)}$

2.3.1 Purification and methylation of SpvB$^{(26-355)}$

His-SpvB$^{(26-355)}$ expression plasmid was constructed by Ms. Linhua Zhang (Dr. Cygler's laboratory). The plasmid was transformed into the BL21(DE3)STAR cell line. The protein was expressed and harvested as described above. The cells were resuspended in 50 mL lysis buffer (15 mM HEPES pH 7.5, 200 mM NaCl) supplemented with protease inhibitors cocktail. The protein was purified in a similar manner as described for His-GtgE. The protein was treated with TEV protease at 1:50 (w/w) ratio and dialyzed against 15 mM HEPES pH 7.5, 200 mM NaCl and 1 mM DTT buffer at 4 ℃ for 16 h to remove the His-tag. The protein mixture was subsequently loaded on a Ni-NTA column to remove the uncleaved His-SpvB$^{(26-355)}$ and TEV, which also contained a His tag at the N-terminus. SDS-PAGE analysis was used to follow the reaction progress.

SpvB$^{(26-355)}$ was methylated using formaldehyde and dimethylamine borane complex. 20 µL of 1.0 M dimethylamine borane solution was added to 1.0 mL containing 10 mg/mL protein in HEPES pH 7.5. Subsequently 40 µL of 1.0 M formaldehyde was added to the solution. After 2h incubation at 4 ℃ an additional 20 µL of 1.0 M dimethylamine borane solution and 40 µL of 1.0 M formaldehyde were added. After another 2h incubation at 4 ℃ 10 µL of 1.0 M dimethylamine borane was added to the mixture and incubated at 4 ℃ overnight. Afterward, 125 µL of 1.0 M glycine and 125 µL of 50 mM DTT were added to stop the reaction. The mixture was incubated at 4 ℃ for 2 h. When the reaction was completed, the mixture was dialyzed at 4 ℃ for 12 h against buffer containing 15 mM HEPES pH 7.5, 200 mM NaCl and 1mM DTT. Dialysis buffer was changed once after 2 h. The methylated protein was concentrated using a Milipore concentration tube (30K cut-off). Protein concentration was measured using absorption at 280 nm and the protein extinction coefficient (65320 M^{-1} cm^{-1}) was calculated using the ProtParam server (http://web.expasy.org/protparam/).

2.3.2 Crystallization, X-ray diffraction and data collection of SpvB$^{(26-355)}$

Methylated SpvB$^{(26-355)}$ was concentrated to 10 mg/mL. Initial screening was performed using commercial incomplete screens by the application of a sitting drop vapor diffusion method.

Crystallization plates were set up using Gryphon robot. Initial crystallization conditions were optimized by fine-tuning protein concentration, pH, precipitant concentration, additive concentrations, size of the drop and the crystallization temperature. The best crystal were obtained from well solution containing 0.1 M Bis-Tris pH 6.5, 14% poly(acrylic acid) 5100 sodium, 4% PEG3350, 1 mM DTT and 20 mM $MgCl_2$. These crystals belong to the space group of $P4_32_12$ with cell dimensions of 101.4, 101.4, 211.3 Å and contain 2 molecules in the asymmetric unit, corresponding to Vm =3.61 $Å^3$/Da and solvent content of 66%. Crystals were mounted within a fiber loop, transferred into the cryo-protectant solution containing mother liquor supplemented with 20% glycerol, and flash-cooled in liquid nitrogen. Diffraction data were collected from a single crystal at the 08ID beamline, Canadian Light Source (CLS) equipped with a CCD X-ray detector and controlled by the CLS MXDC software. The crystal-to-detector distance was set at 300 mm. The oscillation range was 1 ° per frame and 180 frames were collected. The frames were indexed, integrated and scaled using the HKL3000 software package (Minor *et al.*, 2006).

2.3.3 Structure determination of SpvB$^{(26-355)}$

The structure was solved by molecular replacement method using the Phaser-MR program (McCoy *et al.*, 2007) within the PHENIX package (Adams *et al.*, 2010). The search model consists of residues 28 to 366 of YenB from *Yersinia Entomophaga* ABC toxin (PDB entry 4IGL). The sequence identity between the search model and SpvB$^{(26-355)}$ is 47%. Two molecules were identified in the asymmetric unit. The initial R-factor for the molecular replacement solution was 0.263. Refinement of the model was carried out in Phenix.refine (Adams *et al.*, 2010) and manual rebuilding was performed with the program Coot (Emsley *et al.*, 2010b). Five percent of randomly selected reflections were set aside for monitoring R_{free}. The final model comprise residue 34-353 in chain A and chain B. There was not interpretable electron density for residue 26-33 and 353-354 in both chains. The final R-factors: R_{work}=0.200 and R_{free}=0.239.

2.4 Functional studies of SpvB$^{(26-355)}$

2.4.1 Construction of SpvB-HA

The inserted gene was amplified and purified the same way as previously described and inserted into the pCDNA4TO vector. The primers for the restriction enzyme digestion cloning

method are listed in Table 2-7. The DNA insert and the pCDNA4TO vector were digested with restriction enzymes in 50 μL reaction volume, which consisted of 1×NEB buffer 3.1, 200 ng DNA, 1 μL each of two restriction enzymes *Pst*I and *Xho*I. The digestion reactions were set at 37 ℃ for 2 h. After digestion DNA was loaded on 1% agarose gel. The target DNA-containing band was cut out and the DNA was purified using QIAquick gel extraction kit. Subsequently, insert DNA and vector were mixed at a 5:1~10:1 ratio in 20 μL reaction volume containing 1 μL T4 DNA ligase and supplemented buffer. The mixture was incubated at room temperature for 1 h. After ligation, 5 μL of the mixture was used for transformation of 50 μL DH5α competent cells. Correct sequences of targets were confirmed by Sanger sequencing.

Table 2-7. Primers for SpvB constructs used for restriction enzyme digestion cloning method

	Primer sequence	Restriction enzyme	Supplier
SpvB*Pst*I (F001)	TCCAATCTGCAGCCATGTTGATACTAAATGGTTT	*Pst*I	IDT
SpvB*Pst*I (F026)	ATCTGCAGCCGCGCTGAGTCAGTCAGGCCCT	*Pst*I	IDT
SpvB*Pst*I (F390)	AATGGGCTGCAGTAGAGGAATCAAAGCAGATTCA	*Pst*I	IDT
SpvB*Xho*I (R355)	CTTCCACTCGAGGTCGCCTTCATAGGCCAGCGT	*Xho*I	IDT
SpvB*Xho*I (R591)	CTTCCACTCGAGCTATGAGTTGAGTACCCTCAT	*Xho*I	IDT

The recognition sites for the restriction enzymes were underlined.

2.4.2 Co-immunoprecipitation (Co-IP) of SpvB constructs with actin

2.4.2.1 Transfection of mammalian cells

Mammalian cells (HeLa or HEK293) were recovered from the -80 ℃ freezer on OPTI-MEM medium and incubated in a humidified CO_2 incubator (Thermo Fisher Scientific, HERAcell 150i) with 5% CO_2 at 37 ℃ for 24 h. 4 μg of plasmids were added to 1 mL of OPTI-MEM medium and the mixture was incubated at 37 ℃ for 20 min. Eight microliters of XtremeGENE HP DNA Transfetion reagent was added into the mixture, which then was added to cell culture. Cell culture containing plasmid was further incubated at 37 ℃ for 24 h for overexpression.

2.4.2.2 Co-IP using anti-HA antibody

After transfection with plasmids for 24 to 48 h, the medium was aspirated and the cells were washed with the phosphate buffered saline (PBS), which consisted of 10 mM phosphate pH 7.4, 137 mM NaCl and 2.7 mM KCl. Cells were detached by treating them with 0.25% (w/v) trypsin at 37 ℃ for 3 min and the reaction was terminated with 2 mL 10% fetal bovine serum (FBS). Subsequently, cells were dispersed and transferred to a clean 15 mL falcon tube. Cells still remaining in the plate were washed by adding 2 mL 10% FBS and the solution was added to the falcon tube. The mixture was spun down at 1500 ×g at 4 ℃ for 5 min. The cells were resuspended in 750 µL of ice-cold PBS and transferred to a 1.5 mL Eppendorf tube. Another 500 µL ice-cold PBS was added to the falcon tube and transferred to the same Eppendorf tube. The cells were spun down at 5000 ×g at 4 ℃ for 1 min. The cells were re-suspended in 3 times their volume in ice-cold lysis buffer (50 mM Tris, pH 8.0, 150 mM NaCl, 1 mM EDTA, 1% (v/v) Nonidet P-40, 10% (v/v) glycerol, 1 ×protease inhibitor cocktail and 200 mM PMSF). After incubation on ice for 30 min, the cell mixture was centrifuged at 15,000 ×g at 4 ℃ for 15 min. The supernatant was carefully transferred to another 1.5 mL Eppendorf tube. Protein concentration was measured using the Bradford method. Part of the lysate was saved for running the Western blot. The rest of the cell lysate was mixed with mouse anti-HA antibody (0.2 µg/µL) and 25 µL Protein G agarose resin, which was pre-equilibrated with lysis buffer. After incubation at 4 ℃ for 16 h the mixture was centrifuged at 3000 ×g for 1 min and the supernatant was transferred to another clean 1.5 mL tube. The resin was washed with 1 mL lysis buffer 3 times for 5 min each and re-suspended in 60 µL lysis buffer. Finally, 20 µL of 4 ×SDS-PAGE loading buffer was added to the resin. The sample was denatured at 95 ℃ for 10 min.

2.4.2.3 Western blot for detecting SpvB and actin

An SDS-PAGE gel containing target samples (equal amount) and a positive control was washed with double distilled H_2O (ddH_2O) and then with the transfer buffer (1.0 L transfer buffer consisted of 2.9 g glycine, 5.8 g Tris, 0.37 g SDS and 200 mL methanol). A sandwich was assembled with the filter paper (pre-soaked with transfer buffer) at the bottom, polyvinylidene fluoride (PVDF) membrane (pre-soaked in methanol for 5 min and washed with transfer buffer), SDS-PAGE gel, and another filter paper (pre-soaked with transfer buffer) on the top. Air bubbles inside the sandwich were carefully removed. The sandwich was then placed in a semi-dry transferring apparatus (Bio-Rad, 170-3940). The transferring process was set at constant

amperage of 0.1 A for 1 h. After transferring protein from the gel to the membrane, the membrane was removed from the apparatus and washed with PBST (0.1% (v/v) Tween-20 in PBS). Blocking solution (5% (w/v) of skim milk in PBST) was applied to the membrane at room temperature for 1 h. The blocking solution was aspirated, the primary mouse anti-HA antibody in blocking solution was applied and the membrane was incubated at room temperature for 1 h or at 4 ℃ overnight. The membrane was then washed with PBST three times for 10 min each time. The secondary goat anti-mouse-IgG antibody conjugated with horseradish peroxidase (HRP) in blocking solution was applied to the membrane at room temperature for 1 h. Subsequently, the membrane was washed three times for 10 min with PBST. The membrane was covered with ECL reagent mixture (GE healthcare, RPN2109) (HPR substrate) and after 1 min incubation the membrane was overlaid on an X-ray film, which was later developed using X-ray Film Processor (PROTECT Processor Technology, OPTIMAX).

2.4.3 Localization of SpvB constructs

In order to test the secretion of SpvB in *Salmonella*, different SpvB truncations, *spv*B$^{(1-591)}$, *spv*B$^{(1-355)}$, *spv*B$^{(390-591)}$ were inserted into the pEGFP-N1 vector (provided by Dr. Bill Roesler, Department of Biochemistry, University of Saskatchewan), which was used to express protein with a GFP-tag fused at the C-terminus. Primers needed for construction are listed in Table 2-8. The constructs were completed by the same approach as described above to make HA tagged constructs. The EAE536AAA mutants were made to inactivate the ADP-ribosyltransferase activity of SpvB. Site directed mutagenesis was performed by the same method as described above for mutating GtgE.

Cells were plated on glass coverslips, which were placed at the bottom of the six-well plates. After transfection with SpvB plasmids, the cultures were aspirated and the cells were washed with PBS. Hereafter, the cells were covered with aluminum foil to avoid lights. Each well was supplemented with 4% (w/v) of paraformaldehyde and incubated for 30 min at room temperature to fix the cells. Cells were washed three times for 10 min with PBST. After fixation, the cells were washed with 0.5% (v/v) Triton-X100 in PBST for 5 min, followed by another wash with PBST for 10 min. Subsequently, the cells were blocked with 5% FBS for 30 min at room temperature. When blocking was completed, the cells were incubated with 0.5 µM 4',6-diamidino-2-phenylindole (DAPI) and 0.1 µM Acti-stain 555 phalloidin (Cytoskeleton, PHDH1-A) at room temperature for 30 min. The cells were washed three times for 10 min with PBST.

The coverslips carrying the cells were fixed and sealed on glass plates. The slides were imaged under confocal laser fluorescent microscope (Zeiss LSM 510 Meta, Zeiss).

Table 2-8. Primers for the GFP-tagged SpvB constructs

	Primer sequence	Enzyme	Supplier
SpvB*Xho*I (F001)	AATTCTCTCGAGATGTTGATACTAAA TGGTTT	*Xho*I	Eurofin
SpvB*Xho*I (F026)	TGGAATCTCGAGATGGCGCTGAGTCA GTCAGGCCCT	*Xho*I	Eurofin
SpvB*Xho*I (F390)	TGGAATCTCGAGATGGAGGAATCAA AGCAGATTCA	*Xho*I	Eurofin
SpvB*EcoR*I (R355)	TCTAGAGAATCCGGTCGCCTTCATAG GCCAGCGT	*EcoR*I	Eurofin
SpvB*EcoR*I (R591)	AGACTCGAATCCGTGAGTTGAGTACC CTCATGTT	*EcoR*I	Eurofin
Primer for mutation			
SpvB(EAE536AAA) F	GTTGCACATTTTAAGGGAGCGGCAGC GATGCTTTTCCC	N.A	Eurofin
SpvB(EAE536AAA) R	GGGAAAAGCATCGCTGCCGCTCCCTT AAAATGTGCAAC	N.A	Eurofin

2.4.4 Cytotoxicity of SpvB constructs in the host cells

HeLa cells were transfected with pEGFP-N1, pSpvB$^{(1-591)}$-GFP, pSpvB$^{(1-355)}$-GFP and pSpvB$^{(390-591)}$-GFP. After transfection for 24 h, cells were harvested as described above. The lactate dehydrogenase (LDH) activity in the cells transfected with different constructs was measured following the protocol of a lactate dehydrogenase activity assay kit (Sigma, MAK066). At least three dilutions of all the samples were measured with the kit and each measurement was in duplicate. The experiments were repeated three times.

2.4.5 Secretion of SpvB$^{(1-591)}$-Flag in wild-type and mutant *Salmonella*

In order to test the secretion of SpvB in *Salmonella*, *spv*B$^{(1-591)}$ was inserted into pFLAG-CTC vector (provided by Dr. Aron White, Vaccine and Infectious Disease Organization, Saskatoon), which was used to express proteins with a Flag-tag fused at the C-terminus. The primers used are listed in Table 2-9. The construction of the plasmid was similar to the construction of the HA-tagged SpvB except for the application of different restriction enzymes.

Table 2-9. Primers for construction of SpvB$^{(1-591)}$-Flag

	Primer sequence	Restriction enzyme	Supplier
SpvB*Xho*I(F001)	AATTCTCTCGAGATGTTGATACTAAATG GTTT	*Xho*I	Eurofin
SpvB*Bgl*II(R591)	GCGAGAAGATCTTGAGTTGAGTACCCTC ATGTT	*Bgl*II	Eurofin

The recognition site of the restriction enzymes are underlined.

The plasmids were transformed into wild-type *S*. Enteritis strain 18 to express SpvB$^{(1-591)}$-Flag. The bacteria were first grown overnight in the LB medium and 2 mL of this cell culture was used to inoculate 300 mL fresh LB medium, which was then incubated in a shaker at 37 ℃ until OD_{600} reached 0.7. To stimulate SPI-1 secretion system, 1.7 mL of overnight cell culture was inoculated into 250 mL LB-0.3 M NaCl medium at 1:150 ratio and grew at 37 ℃ incubator under static anaerobic conditions for 16 h. To stimulate SPI-2 system, 10 mL of the overnight cell culture was spun down and the pellet was resuspended in 500 mL low pH medium (LPM), which consisted of 337 mM phosphate buffer, 5 mM KCl, 7.5 mM $(NH_4)_2SO_4$, 0.5 mM K_2SO_4, 0.1% (w/v) casamino acids, 38 mM glycerol, 8 μM $MgCl_2$, and pH adjusted to 5.8 by using 80 mM MES. This culture grew in a shaker at 37 ℃ for 16-18 h and then induced with 1 mM IPTG for 2 h.

All cell cultures were centrifuged at 8000 ×g for 30 min. The supernatants were filtered with 0.22 μm polyethersulfone (PES) membrane to remove the remaining bacteria from the supernatants. Trichloroacetic acid (TCA) was added to the filtered supernatant to a final concentration of 15% (w/v) in order to precipitate proteins. The mixture was incubated at -20 ℃ for 30 min and further incubated at 4 ℃ for 16-20 h. Subsequently, the mixture was centrifuged at 10,000 ×g for 30-60 min. The TCA supernatant was discarded and the protein pellet was washed with ice-cold acetone. After drying the acetone, PBS buffer was added to dissolve the remaining proteins. The protein samples were prepared for Western blotting. Anti-Flag antibody was used to detect the expression of SpvB-Flag. To demonstrate that the presence of SpvB in the medium was not due to cell leakage, a cytosolic heat shock protein DnaK was used as a control. To confirm that the TTSS was fully functional, anti-SopE2 serum was used to detect SopE2, a SPI-1 effector, and anti-SseL serum for SseL, a SPI-2 substrate.

Western blots were performed in a similar way as described above except for: (1) using nitrocellulose membrane instead of PVDF membrane for protein support, (2) using alkaline phosphatase conjugated secondary antibody instead of using HRP conjugated secondary antibody and (3) using Nitroblue tetrazolium/ 5-bromo-4-chloro-indolyl phosphate (BNT/BCIP) substrate solution instead of ECL substrates to detect secondary antibody.

The plasmid carrying *spv*B$^{(1\text{-}591)}$ was also transformed into a *Salmonella* Δ*spi-1* mutant strain, Δ*spi-2* mutant strain and Δ*spi-1&2* mutant strain. The Δ*spi-1* mutant harboring SpvB was grown in the SPI-2 stimulating medium; Δ*spi-2* mutant was grown in the SPI-1 stimulating medium and Δ*spi-1&2* mutant was grown in LB medium in the same way as described above. Proteins were precipitated as described above. The presence of proteins was detected by Western blot as described above.

3. Results

3.1 Structural studies of GtgE

3.1.1 Purification and crystallization trials of GtgE$^{(2-228)}$

His- and GST-tagged constructs of GtgE$^{(2-228)}$ were made as a part of high-throughput cloning of bacterial effectors (Linhua Zhang, Dr. Cygler laboratory). His-GtgE$^{(2-228)}$ was highly expressed and was purified using Ni-NTA affinity chromatography. The His-tag was removed by digestion with TEV protease. The digest was loaded again on the Ni-NTA column to remove any remaining His-GtgE as well as the His-tagged TEV protease. Subsequently, GtgE-containing fractions were loaded on a Superdex75 size exclusion chromatography column. Eluted fractions were analyzed by SDS-PAGE (Fig. 3-1) and the GtgE-containing fractions were pooled together. Similarly, GST-GtgE$^{(2-228)}$ was loaded on the glutathione agarose resin and the tag was cleaved on the column by adding TEV protease and incubating for 16 h. The GtgE protein was eluted from the column in the wash step and was further purified on a Superdex 200 gel filtration column. The quality of the protein sample was assessed by dynamic light scattering for the homogeneity of the protein in solution. Light scattering shows monodisperse molecular behavior when the particles/protein in solution are uniform. When the particles form various multimers or aggregates, the dynamic light scattering shows a polydisperse behavior. Monodispersity correlates with the propensity of protein to crystallize (Ferré-D'Amaré and Burley, 1994). The protein sample was concentrated to ~20 mg/mL and subjected to crystallization screening in a sitting drop format using multiple commercial screens. The screens were set up using the Gryphon Crystallization Robot. Crystallization trials were carried out at room temperature and at 4 ℃. Despite screening nearly one thousand conditions, no crystals were formed. In an effort to facilitate crystallization, GtgE was methylated; the chemical methylation of accessible lysines alters the surface properties of a protein. These changes can make a protein more likely to crystallize. Unfortunately, methylated GtgE did not yield any crystals either.

3.1.2 Mutation of the active site His151

GtgE was shown to be a cysteine protease containing a Cys-His-Asp triad (Spano *et al.*, 2011; Spanò and Galán, 2012; Kohler *et al.*, 2014). The critical base was identified as H151 (Spano *et al.*, 2011). I mutated this His151 to Ala (H151A), Ser (H151S) or Asn (H151N) to render the protein inactive. I reasoned that a loss of catalytic activity would allow for co-

crystallization of GtgE with peptide substrates. Interestingly, of the three mutants only H151S was soluble. GST-GtgE$^{(2-228)}$(H151S) was purified and the tag removed as described above for the wild type protein (Fig. 3-2). This protein was used for more crystallization trials, albeit without success.

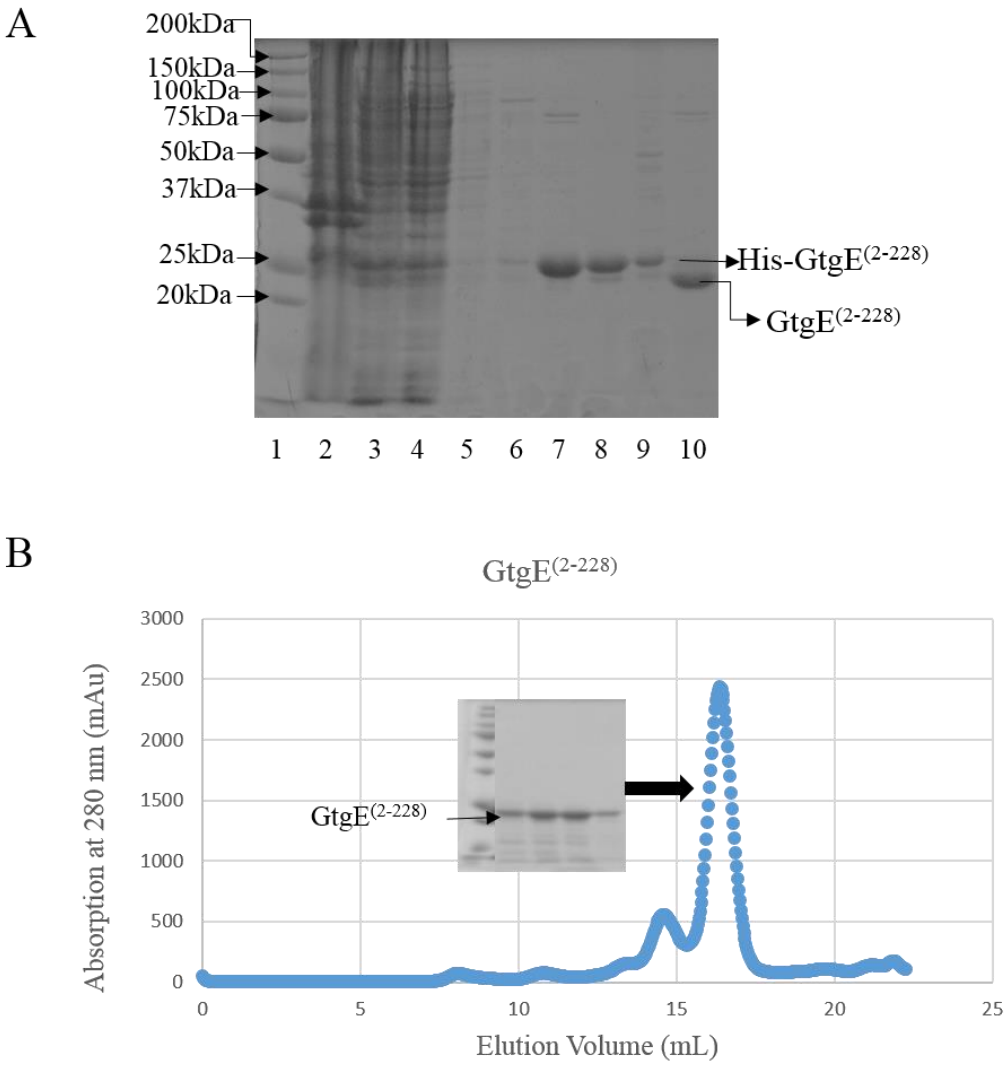

Fig. 3-1. Expression and purification results for the His-GtgE$^{(2-228)}$ construct. **A**. The SDS-PAGE gel showing fractions collected during affinity purification of His-GtgE$^{(2-228)}$ using Ni-NTA resin. Lane 1: protein markers, 2: content of the protein pellet, 3: supernatant, 4: proteins not retained on the resin, 5: proteins washed away with the lysis buffer, 6: protein eluted with 10 mM imidazole, 7: protein eluted with 200 mM imidazole, 8: protein eluted with 400 mM imidazole, 9: proteins retained on the column, 10: cleavage the His tag with TEV protease. **B**. Elution profile of affinity purified GtgE$^{(2-228)}$ on the Superdex 200 size exclusion column. The insert shows the SDS-PAGE gel of fractions across the main peak.

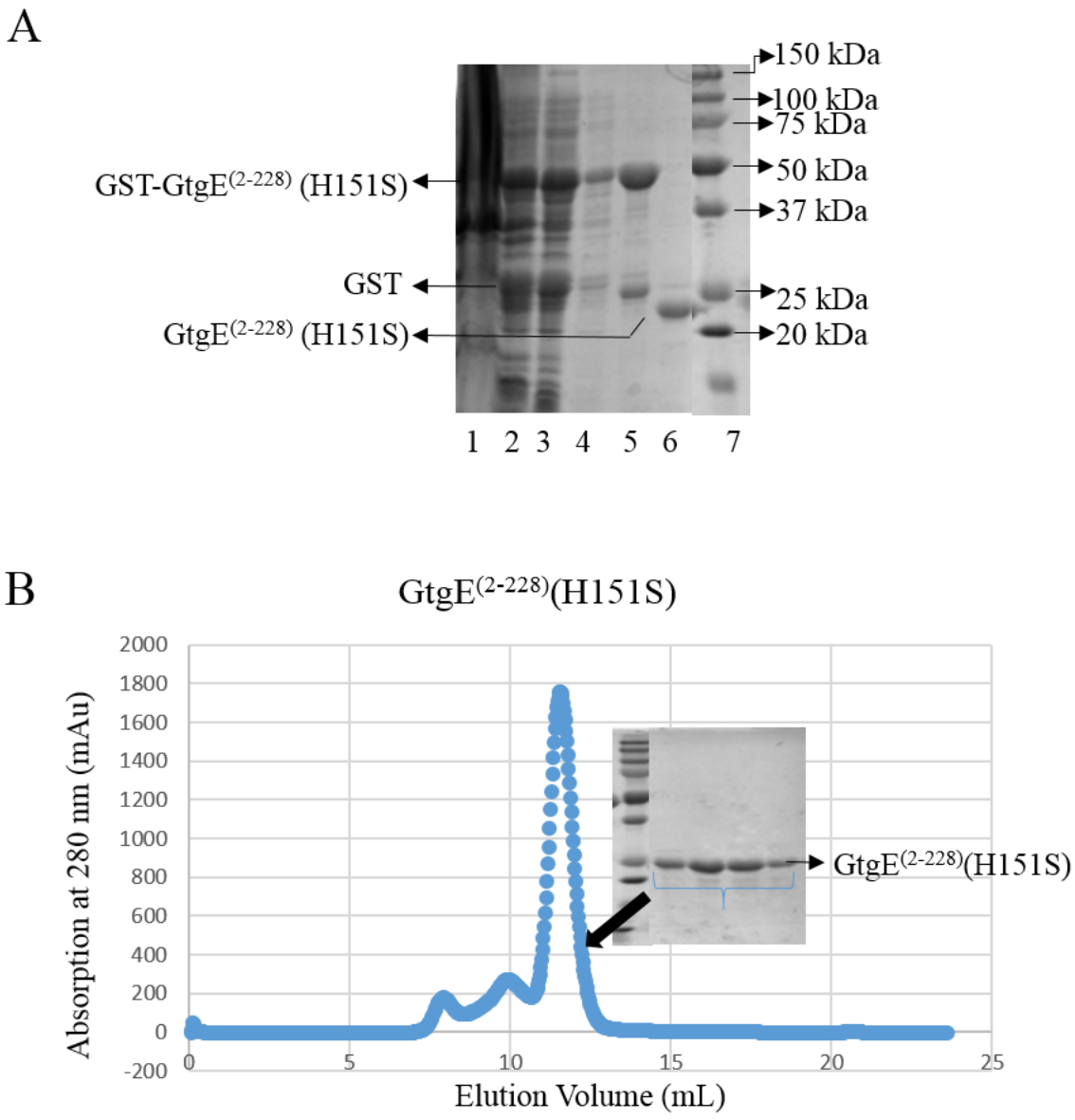

Fig. 3-2. Expression and purification results for the GST-GtgE$^{(2-228)}$(H151S) construct. **A**. The SDS-PAGE gel showing fractions progress of affinity purification of GST-GtgE$^{(2-228)}$(H151S) on Glutathione (GSH) agarose resin. Lane 1: content of the protein pellet, 2: supernatant, 3: proteins not retained on the resin, 4: proteins washed away with lysis buffer, 5: protein bound to resin, 6: untagged proteins after TEV cleavage, 7: protein markers. **B**. Elution profile of the affinity purified GtgE$^{(2-228)}$(H151S) from the Superdex 75 size exclusion column. The insert shows the SDS-PAGE gel of fractions from the largest peak.

3.1.3 Protease activity assay for GtgE$^{(2-228)}$ and GtgE$^{(2-228)}$(H151S)

To test the activity of the recombinant His-GtgE$^{(2-228)}$ and GtgE$^{(2-228)}$(H151S), GST-Rab32 was used as the GtgE substrate. GST-Rab32 was purified using glutathione resin and further purified through an anion exchange chromatography (Fig. 3-3). The cleavage of Rab32 was analyzed by SDS-PAGE. According to literature, the cleavage occurs after Gly59 (Spanò and Galán, 2012). The GST tag was fused to the N-terminus of Rab32. Thus, after the cleavage by GtgE, a ~35 kDa fragment should be detected.

GST-Rab32 was treated with His-GtgE$^{(2-228)}$ and GtgE$^{(2-228)}$(H151S) at 2:1 (GST-Rab32:GtgE) and 20:1 molar ratio in the presence of Mg^{2+} and Ca^{2+} at room temperature. To exclude the spontaneous degradation of proteins, GST-Rab32 without GtgE proteins were treated the same way as a negative control. Samples were aliquoted and the reactions were determined by adding SDS-PAGE loading buffer and denaturing the samples at 95 ℃ for 10 min. These samples were analyzed on an SDS-AGE gel. A 35 kDa band increased in intensity with the treatment of His-GtgE$^{(2-228)}$, which indicated activity of His-GtgE$^{(2-228)}$, albeit the activity was relatively low. This was evidenced by the detection of uncleaved substrate 2 h after the onset of the reaction at room temperature.

The protease activity of GtgE$^{(2-228)}$(H151S) was tested. A new batch of the GST-Rab32 substrate was used. This preparation of Rab32 was less pure and contained a band with molecular weight similar to the expected cleavage fragment. No change in intensity of the 35 kDa band was observed, nor the decrease in the amount of the intact substrate. This result confirmed that the GtgE$^{(2-228)}$(H151S) was indeed inactive

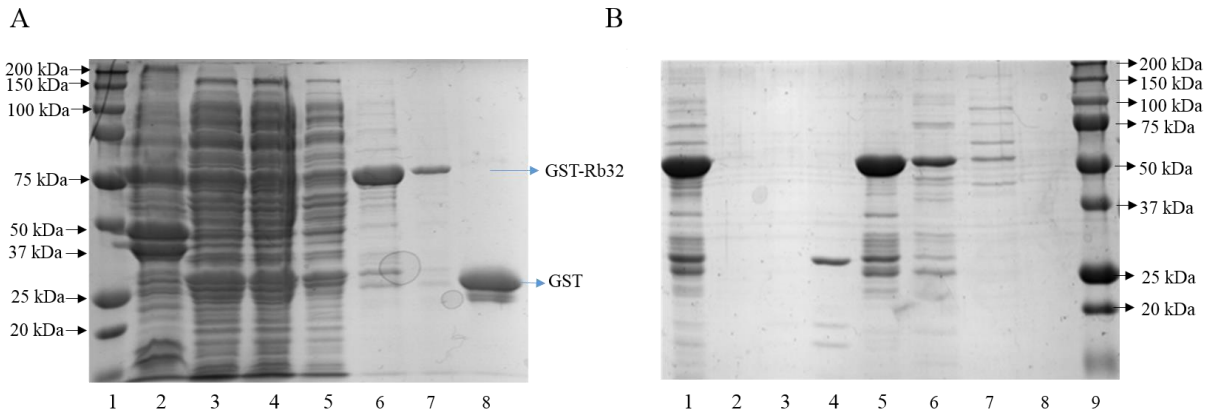

Fig. 3-3. Expression and purification of the GST-Rab32 construct. **A**. SDS-PAGE gel showing fractions collected during affinity purification of GST-Rab32 using GSH resin. Lane 1: protein markers, 2: content of the protein pellet, 3: supernatant, 4: proteins not retained on the affinity column, 5: proteins washed away with lysis buffer, 6: protein eluted with 20 mM GSH, 7: protein eluted with 30 mM GSH, 8: protein retained on the resin. **B**. SDS-PAGE showing fractions collected from an anion exchange HitrapQ column. Lane 1: Affinity purified sample loaded to HitrapQ column, 2: proteins eluted with buffer containing of 15 mM HEPES and 1 mM DTT , 3: proteins eluted with the buffer in addition of 50 mM NaCl, 4: proteins eluted with the buffer in addition of 100 mM NaCl, 5: proteins eluted with the buffer in addition of 200 mM NaCl, 6: proteins eluted with the buffer in addition of 300 mM NaCl, lane 7: proteins eluted with the buffer in addition of 500 mM NaCl, 8: proteins eluted with the buffer in addition of 1 M NaCl, 9: protein marker. GST-Rab32 from B. lane 5 was used as substrate for testing GtgE activity.

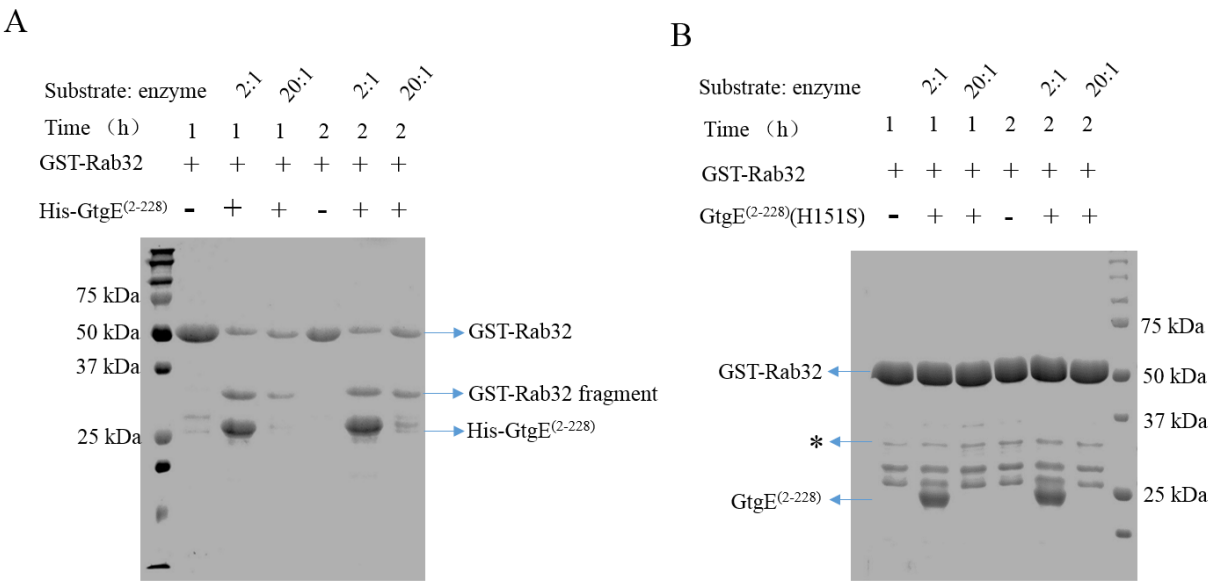

Fig. 3-4. Determination of protease activity of His-GtgE$^{(2-228)}$ and GtgE$^{(2-228)}$(H151S) using GST-Rab32 as a substrate. The reaction was performed at room temperature. **A**. The activity of His-GtgE$^{(2-228)}$ based on SDS-PAGE gel result. Lane 1: protein markers, 2: GST-Rab32 substrate to control after 1 h, 3: Cleavage of GST-Rab32 by His-GtgE$^{(2-228)}$ in 2:1 (substrate : enzyme) in molar ratio after 1 h incubation, 4: Cleavage of GST-Rab32 by His-GtgE$^{(2-228)}$ in 20:1 ratio for 1 h, 5: GST-Rab32 substrate to control after 2 h, 6, Cleavage of GST-Rab32 by His-GtgE$^{(2-228)}$ in 2:1 ratio for 2 h, 7: Cleavage of GST-Rab32 by His-GtgE$^{(2-228)}$ in 20:1 ratio for 2 h incubation. **B**. The activity of His-GtgE$^{(2-228)}$(H151S) based on SDS-PAGE gel result. The substrate was purified from a new batch substrate (which contains some impurities). The pre-existed band with the * mark had the similar molecular weight to the expected product fragment of Rab32 during cleavage by GtgE. Lane 1: GST-Rab32 substrate to control after 1 h, 2: Cleavage of GST-Rab32 by GtgE$^{(2-228)}$(H151S) in 2:1 ratio after 1 h incubation, 3: Cleavage of GST-Rab32 by GtgE$^{(2-228)}$(H151S) in 20:1 ratio for 1 h, 4: GST-Rab32 substrate to control after 2 h, 5: Cleavage of GST-Rab32 by GtgE$^{(2-228)}$(H151S) in 2:1 ratio for 2 h, 6: Cleavage of GST-Rab32 by GtgE$^{(2-228)}$(H151S) in 20:1 ratio for 2 h incubation, 7: protein markers.

3.1.4 Purification and crystallization trials of entropy-reduced surface mutants of GtgE

Another rescue strategy employed in crystallization of 'difficult' proteins is to mutate a cluster of large, flexible sidechain residues on the protein surface into smaller residues to reduce protein entropy (Derewenda, 2004). Two promising mutations, KK161AA and KNE196ANA, predicted by the SERp sever (http://services.mbi.ucla.edu/SER/) were introduced into the His-GtgE$^{(2-228)}$ construct. The expression level of His-GtgE$^{(2-228)}$(KK163AA) was very low but His-GtgE$^{(2-228)}$(KNE196ANA) expressed well. His-GtgE$^{(2-228)}$(KNE196ANA) was purified using Ni-NTA affinity column (Fig. 3-5.A). Fractions containing target protein was subjected to TEV

cleavage to remove the His-tag (Fig. 3-5.B). This purified protein was also used for crystallization screening, albeit without success.

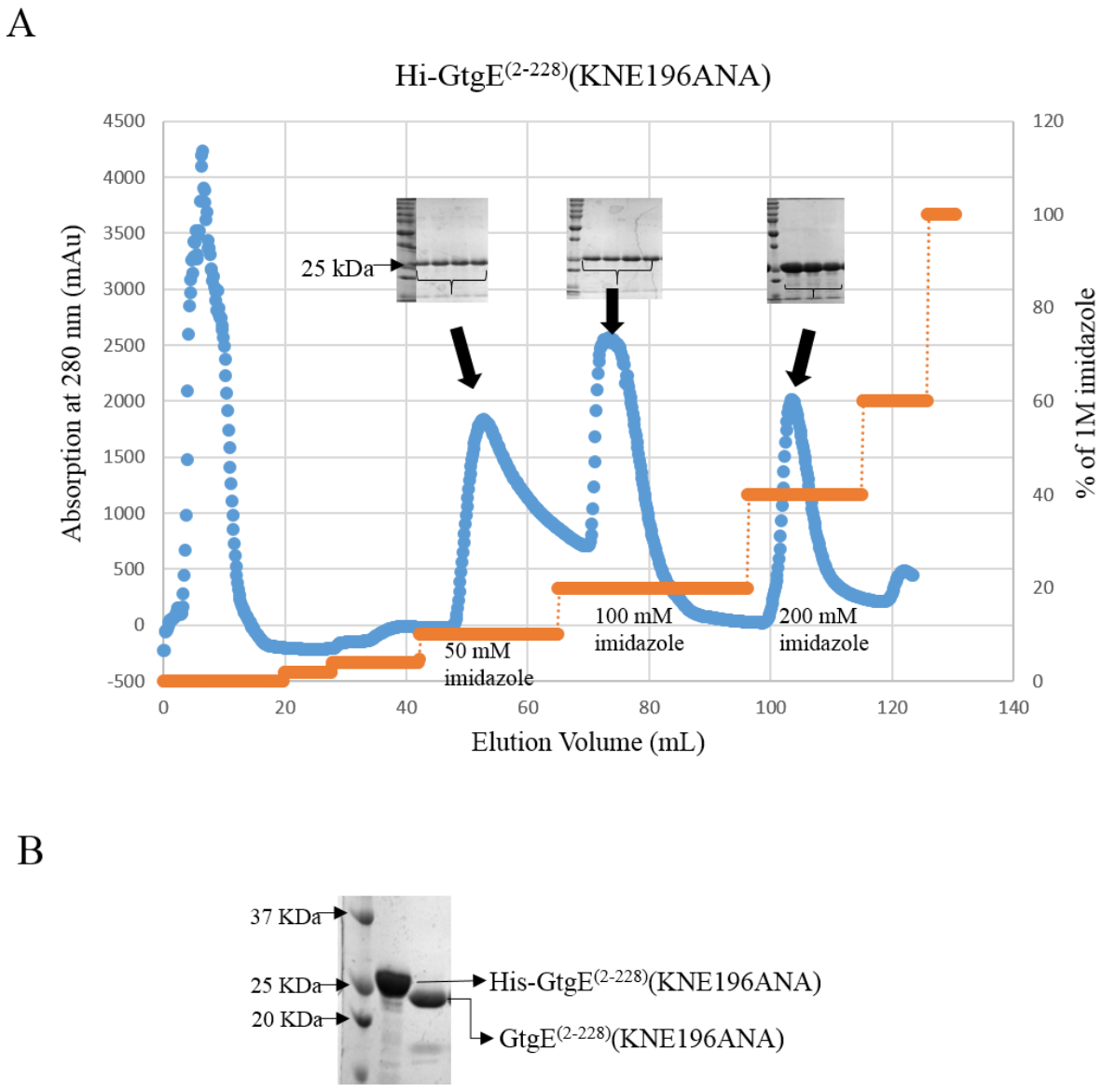

Fig. 3-5. Purification results for the His-GtgE$^{(2-228)}$(KNE196ANA) construct. **A**. Elution profile of His-GtgE$^{(2-228)}$(KNE196ANA) from Ni-NTA column using imidazole step gradient. The blue curve shows absorption at 280 nm and the orange shows the imidazole concentration. The inserts show SDS-PAGE gels of the fractions across the peaks. **B**. Cleavage of the His-tag from the construct by TEV protease. Lane 1: protein markers, 2: His-tagged protein. 3: untagged protein.

3.1.5 New GST-tagged constructs, GtgE$^{(14-214)}$, GtgE$^{(21-214)}$ and GtgE$^{(31-214)}$

While this research was in progress, the structure of the inactive GtgE$^{(80-213)}$ fragment has been published (Kohler *et al.*, 2014). This structure, which contains only residues 80 to 213, suggests that the N- and C-terminal regions are hampering crystallization of the full length protein. The active site Cys45 is not part of the crystallized fragment. In order to probe if a longer construct containing this cysteine could still be crystallized, I designed several new constructs guided by the disorder prediction (Fig. 3-6) and the secondary structure prediction (Fig. 3-7).

The GST-GtgE$^{(14-214)}$, GST-GtgE$^{(21-214)}$ and GST-GtgE$^{(31-214)}$ constructs were made. Hereafter, all the described GtgE constructs were expressed as a GST fusion with a cleavable GST tag. GST-GtgE$^{(14-214)}$ and GST-GtgE$^{(31-214)}$ expressed as soluble proteins with a good yield, while GST-GtgE$^{(21-214)}$ was insoluble. Untagged GtgE$^{(14-214)}$ (Fig. 3-8) and GtgE$^{(31-214)}$ (Fig. 3-9) were purified to near homogeneity by the methods described above and were concentrated to ~25 mg/mL. These two proteins were used in crystallization trials at 4 ℃ and at room temperature. In addition, methylation was carried out for both proteins, but no crystals were observed.

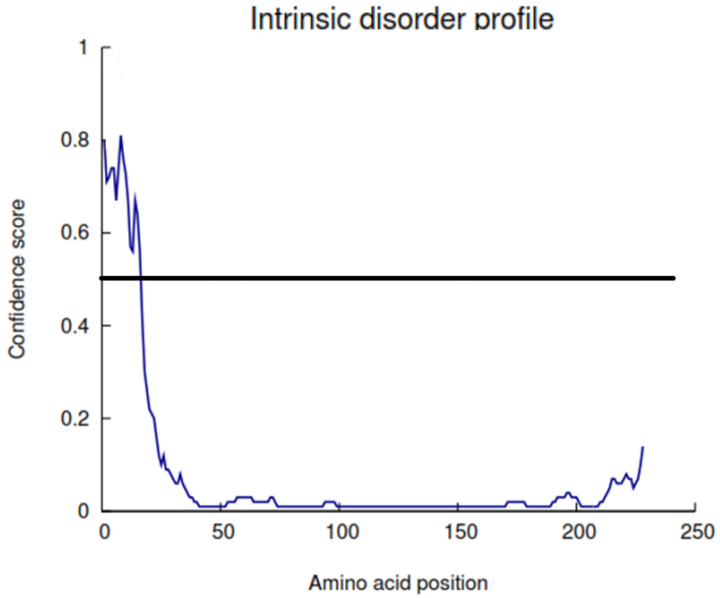

Fig. 3-6. The intrinsic disorder profile of GtgE. The prediction was performed by the DISOPRED3 predictor (http://bioinf.cs.ucl.ac.uk/psipred/). The blue line indicates the disordered state. Amino acid residues with the confidence score higher than 0.5 are considered as disordered.

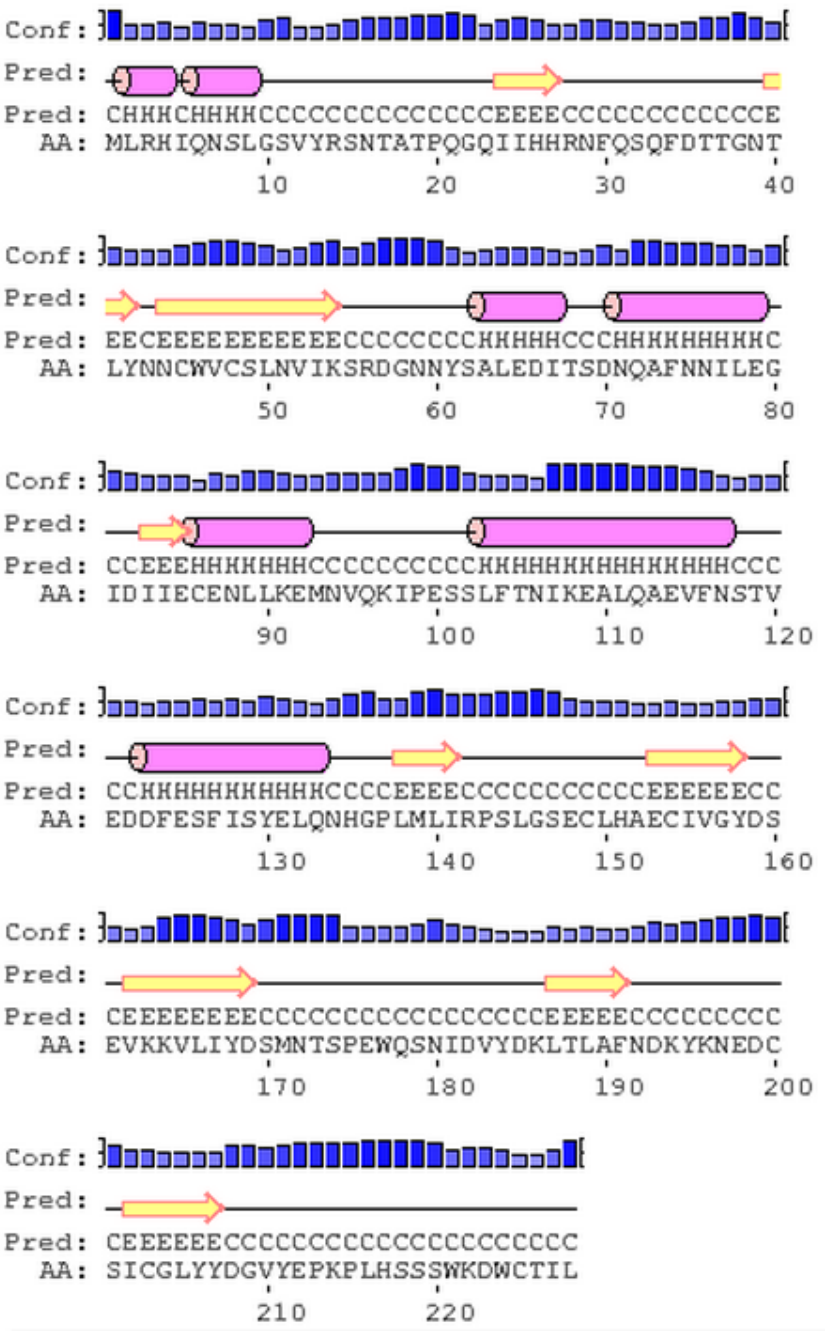

Fig. 3-7. Secondary structure prediction of GtgE. The prediction was performed by the Psipred protein sequence analysis workbench (http://bioinf.cs.ucl.ac.uk/psipred/). The label on the left side are Conf, which indicates the confidence of prediction, Pred, which shows the predicted secondary structure, and AA, which is the target sequence. The secondary structure prediction presents in two ways: one using a pink cylinders for a representing α-helix, a yellow arrow for β-strand and a black line for a coil and the other one using letters, C for coil, H for helix and E for strand.

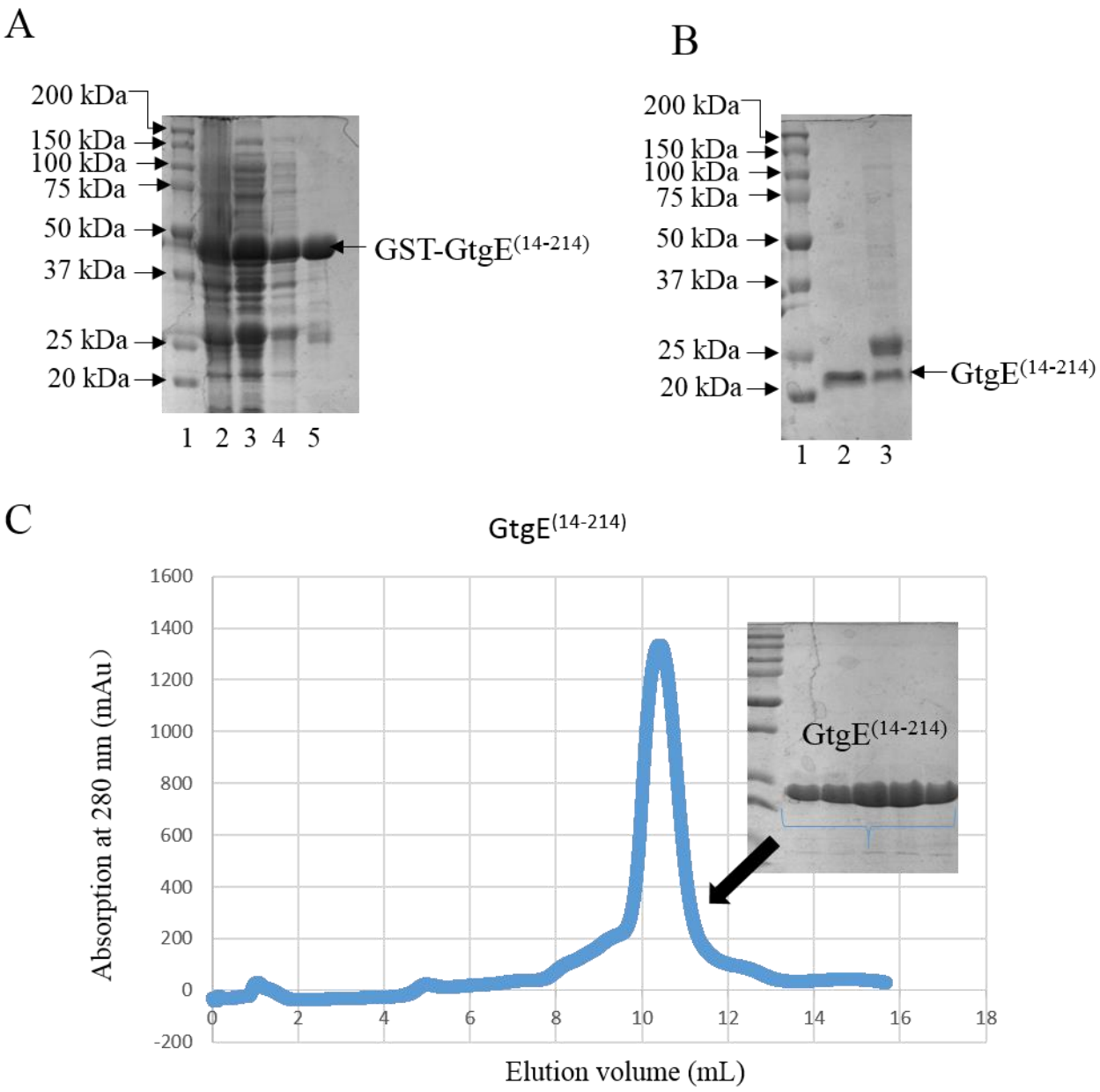

Fig. 3-8. Expression and purification results for the GST-GtgE$^{(14-214)}$. **A**. The SDS-PGAE gel showing fractions collected while purifying GST-GtgE$^{(14-214)}$ on a GSH resin. Lane 1: protein markers, 2: content of the protein pellets, 3: supernatant, 4: proteins not retained on the resin, lane 5: protein retained to the resin. **B**. SDS-PGAE gel showing the GST-tag cleavage result by TEV protease. TEV protease was added to the protein bound resin at an approximate ratio 1:50 (TEV:substrate). Lane 1: protein markers, 2: protein not retained on the resin after cleavage, 3: proteins retained on the GSH resin after cleavage. **C**. The elution profile of affinity purified GtgE$^{(14-214)}$ from the Superdex 75 size exclusion column. The insert shows the SDS-PAGE gel of fractions from the largest peak.

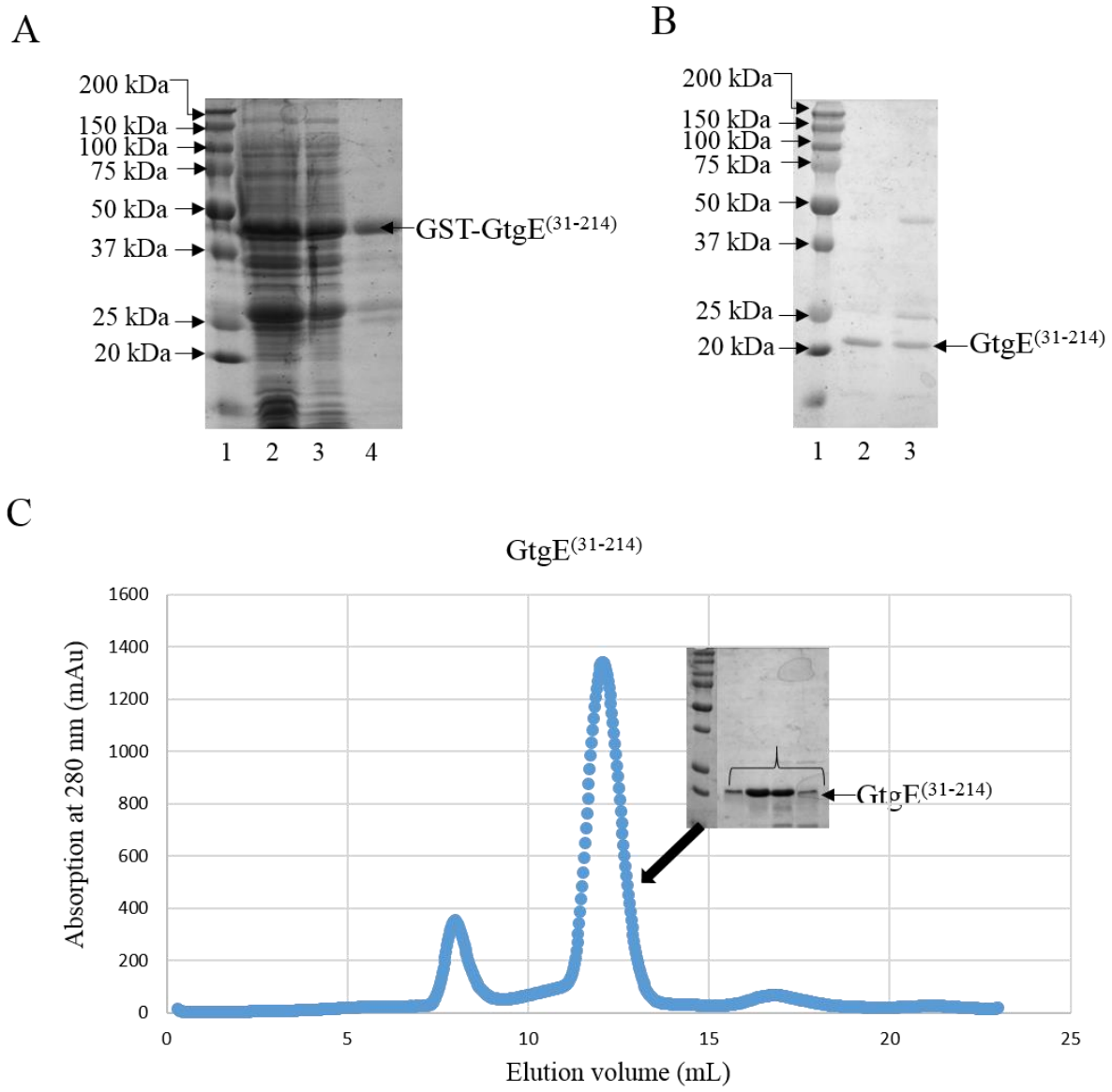

Fig. 3-9. Purification results for the GST-GtgE$^{(31-214)}$ construct. **A**. The SDS-PGAE gel showing fractions collected while purifying GST-GtgE$^{(31-214)}$ on a GSH resin. Lane 1: protein markers, 2: supernatant, 3: proteins not retained on the resin, 4: protein retained to the resin. **B**. The SDS-PGAE gel showing the GST-tag cleavage by TEV protease. Lane 1: protein markers, 2: protein not retained on the resin after cleavage, 3: proteins retained on the GSH resin after cleavage. **C**. Elution profile of the affinity purified GtgE$^{(31-214)}$ from the Superdex 75 size exclusion column. The insert shows the SDS-PAGE gel of fractions from the largest peak.

3.1.6 Protease activity assay for GtgE$^{(14-214)}$ and GtgE$^{(31-214)}$

The proteolytic activity of GtgE$^{(14-214)}$ and GtgE$^{(31-214)}$ was tested with GST-Rab32 as a substrate. His-GtgE$^{(2-228)}$ was used as a positive control and GtgE$^{(2-228)}$(H151S) as a negative control in the protease activity assay. GST-Rab32 was treated with GtgE$^{(14-214)}$ and GtgE$^{(31-214)}$ in the molar ratio of 2:1 (GST-Rab32:GtgE) and 20:1 in the presence of Mg^{2+} and Ca^{2+}. The reactions were performed at room temperature. After the reaction, protein samples were loaded on an SDS-PAGE gel to visualize the cleavage of GST-Rab32. The 35 kDa band increases in intensity upon treatment with GtgE$^{(14-214)}$ (Fig. 3-10). Conversely, no such increase was observed in the sample treated with inactive GtgE$^{(2-228)}$(H151S). In fact, the amount of cleaved product produced by GtgE$^{(14-214)}$ was similar to that of His-GtgE$^{(2-228)}$. This result indicated that GtgE$^{(14-214)}$ is active. For GtgE$^{(31-214)}$, however, the 35 kDa band shows only a slight increase in intensity. In accordance with this observation, GtgE$^{(31-214)}$ exhibited much lower activity than that of His-GtgE$^{(2-228)}$ and GtgE$^{(14-214)}$ (Fig. 3-10). These results indicate that residues 14-30 are important for maintaining protease activity of GtgE.

3.1.7 Mutation of the active site Cys45

Despite extensive efforts and using several rescue strategies, I was not able to crystallize GtgE. The rationale for these difficulties is likely the intrinsic flexibility of the N-terminal and C-terminal segments of GtgE. Only removal of the first ~80 and the last 14 residues led to the crystallization of the remaining GtgE fragment. In an attempt to reduce the flexibility of the protein, I proceeded with the co-crystallization of GtgE with the peptide corresponding to the Rab32 cleavage site. Considering that GtgE is a protease, the cleavage reaction might occur quickly and the substrate might leave the active site after the reaction. To avoid this, an inactive mutant of GtgE was used. The nucleophile Cys45 was mutated to Ala or Ser, GST-GtgE$^{(14-214)}$(C45A) and GST-GtgE$^{(14-214)}$(C45S), and these two mutants were transformed into the *E. coli* BL21 for expression. GST-GtgE$^{(14-214)}$(C45S) was soluble but GST-GtgE$^{(14-214)}$(C45A) was insoluble. GtgE$^{(14-214)}$(C45S) was further purified using the method described for GtgE$^{(14-214)}$ (Fig. 3-11). Purified GtgE$^{(14-214)}$(C45S) was mixed with the RATIGVDFALK peptide (Rab32 cleavage site) and subjected to crystallization screening. Unfortunately, no crystals were obtained by this method.

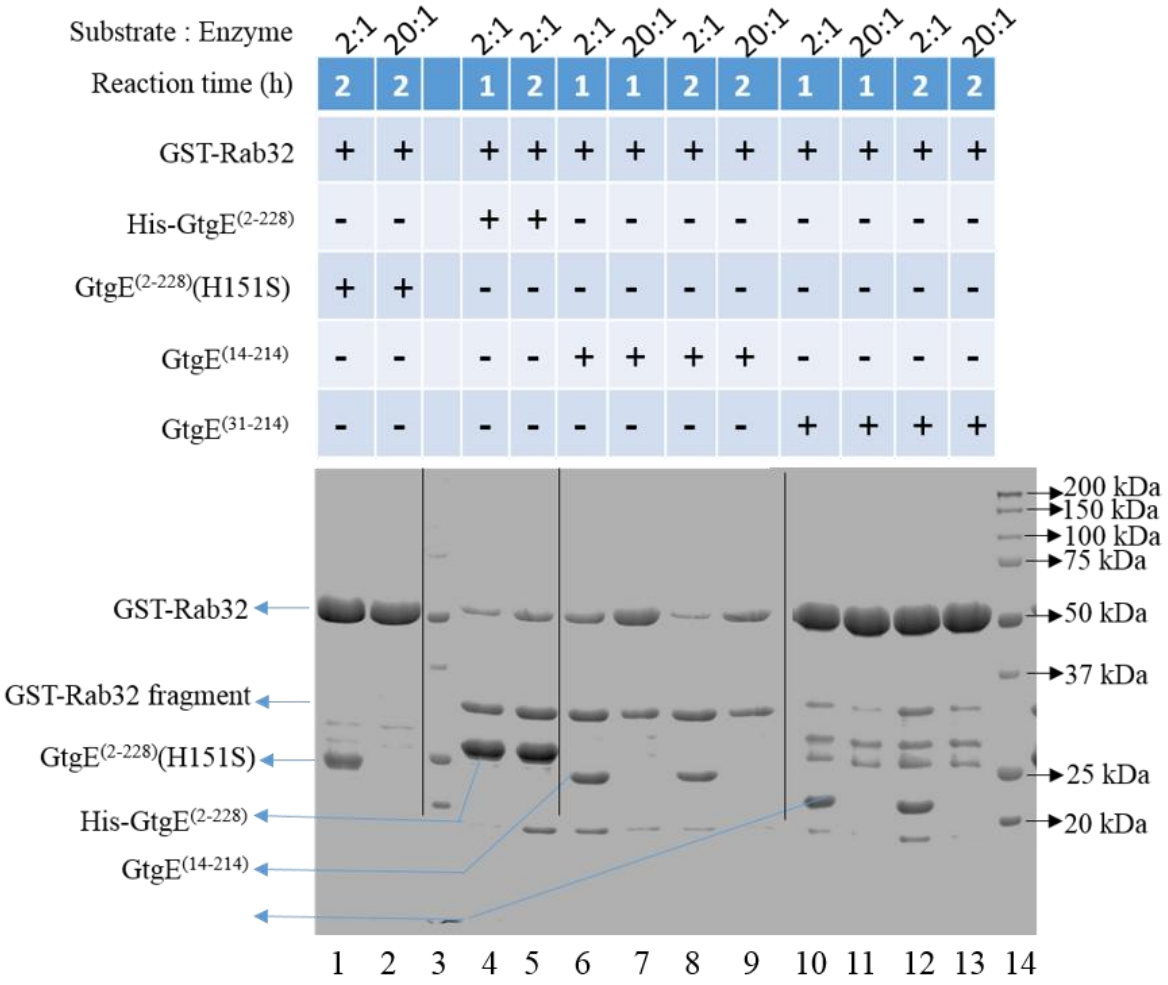

Fig. 3-10. Determination of the protease activity of GtgE$^{(14-214)}$ and other construct using GST-Rab32 as a substrate. The reactions were conducted at room temperature. Equal volume of the reaction mixture was loaded to each lane. Lane 1: Cleavage of GST-Rab32 by GtgE$^{(2-228)}$(H151S) in 2:1 (substrate : enzyme) in molar ratio after 2 h incubation, 2: Cleavage of GST-Rab32 by GtgE$^{(2-228)}$(H151S) in 20:1 ratio after 2 h incubation , 3: protein markers, 4: Cleavage of GST-Rab32 by His-GtgE$^{(2-228)}$ in 2:1 ratio after 1 h incubation, 5: Cleavage of GST-Rab32 by His-GtgE$^{(2-228)}$ in 2:1 ratio after 2 h incubation, 6: Cleavage of GST-Rab32 by GtgE$^{(14-214)}$ in 2:1 ratio after 1 h incubation, 7: Cleavage of GST-Rab32 by GtgE$^{(14-214)}$ in 20:1 ratio after 1 h incubation, 8: Cleavage of GST-Rab32 by GtgE$^{(14-214)}$ in 2:1 ratio after 2 h incubation, 9: Cleavage of GST-Rab32 by GtgE$^{(14-214)}$ in 20:1 ratio after 2 h incubation, 10: Cleavage of GST-Rab32 by GtgE$^{(31-214)}$ in 2:1 ratio after 1 h incubation, 11: Cleavage of GST-Rab32 by GtgE$^{(31-214)}$ in 20:1 ratio after 1 h incubation, 12: Cleavage of GST-Rab32 by GtgE$^{(31-214)}$ in 2:1 ratio after 2 h incubation, 13: Cleavage of GST-Rab32 by GtgE$^{(31-214)}$ in 20:1 ratio after 2 h incubation, 14: protein markers.

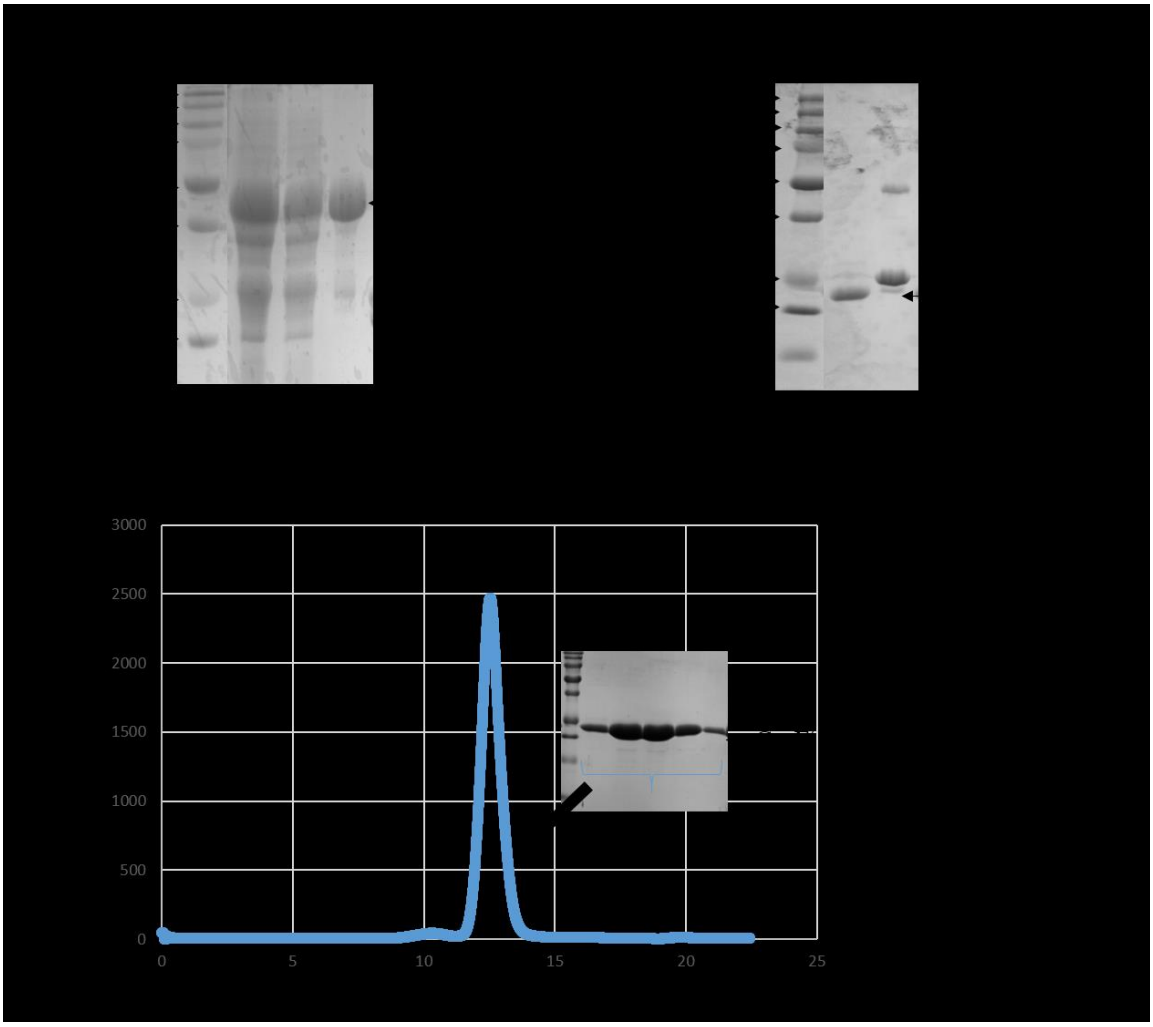

Fig. 3-11. Purification results for the GST-GtgE$^{(14-214)}$(C45S). **A**. SDS-PGAE gel showing fractions collected while purifying GST-GtgE$^{(14-214)}$(C45S) on GSH resin. Lane 1: protein markers, 2: supernatant, 3: proteins not retained on the resin, 4: protein retained to the resin. **B**. SDS-PGAE gel showing the GST-tag cleavage result by TEV protease. Lane 1: protein markers, 2: protein not retained on the resin after cleavage, 3: proteins retained on the GSH resin after cleavage. **C**. The elution profile of affinity purified GtgE$^{(14-214)}$(C45S) from the Superdex 75 size exclusion column. The insert shows the SDS-PAGE gel of fractions from the largest peak.

3.1.8 Protease activity of GtgE$^{(14-214)}$(C45S)

The activity of GtgE$^{(14-214)}$(C45S) mutants was tested by the same method as other constructs. The reactions were set up at a substrate to enzyme ratio of 2:1 and 20:1 at room temperature for 1 h and 2 h. From the SDS-PAGE, the cleavage product was not observed and the amount of the substrate was not decreasing. The Cys45 mutation was therefore sufficient to inactivate GtgE (Fig. 3-12).

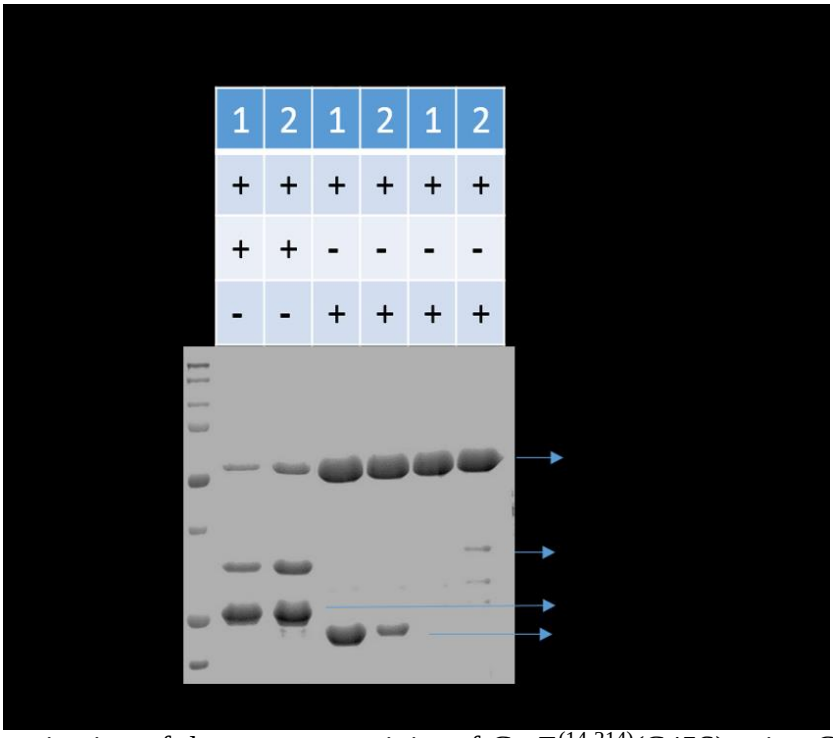

Fig. 3-12. Determination of the protease activity of GtgE$^{(14-214)}$(C45S) using GST-Rab32 as a substrate. The reactions were conducted at room temperature. Equal volume of the reaction mixture was loaded to each lane. Lane 1: protein markers, 2: Cleavage of GST-Rab32 by His-GtgE$^{(2-228)}$ in 2:1 ratio after 1 h incubation, 3: Cleavage of GST-Rab32 by His-GtgE$^{(2-228)}$ in 2:1 ratio after 2 h incubation, 4: Cleavage of GST-Rab32 by GtgE$^{(14-214)}$(C45S) in 2:1 ratio after 1 h incubation, 5: Cleavage of GST-Rab32 by GtgE$^{(14-214)}$(C45S) in 2:1 ratio after 2 h incubation, 6: Cleavage of GST-Rab32 by GtgE$^{(14-214)}$(C45S) in 20:1 ratio after 1 h incubation, 7: Cleavage of GST-Rab32 by GtgE$^{(14-214)}$(C45S) in 20:1 ratio after 2 h incubation.

3.1.9 ^{1}H-^{15}N HSQC spectra of GtgE$^{(14-214)}$(C45S) and the protein titration with peptide

Nuclear magnetic resonance (NMR) is another common approach for determining protein structure (Wuthrich, 2001). It is based on the principle that only isotopes containing an odd number of protons and/or neutrons have intrinsic magnetic moments in the magnetic field. NMR active stable isotopes ^{13}C and ^{15}N are often introduced into the protein for NMR experiment. The expression of ^{15}N-labeled protein was obtained by growing the *E. coli* cell culture in minimal growth medium where the nitrogen source is fully ^{15}N-labeled (Zhao *et al.*, 2007). The NH group is present in every amino acid residue with the exception of proline. The ^{1}H-^{15}N HSQC (heteronuclear single quantum correlation) spectrum is used to record the interaction within NH group (Kwan *et al.*, 2011). In this spectrum we follow the ^{15}N chemical shift along one axis and the ^{1}H chemical shift along the second axis. Since the chemical shifts are affected by the environment of the nuclei, the ^{1}H-^{15}N HSQC spectrum provides information about the folded

state of the protein. Following a standard protocol for ^{15}N labeling, GST-GtgE$^{(14-214)}$(C45S) was expressed enriched in ^{15}N. ^{15}N-GtgE$^{(14-214)}$(C45S) was purified by the same method as GtgE$^{(14-214)}$ (Fig. 3-13). The ^{1}H-^{15}N HSQC spectrum of ^{15}N-GtgE$^{(14-214)}$(C45S) was recorded on a 600 MHz Bruker spectrometer by Mr. Corey Yu (Department of Biochemistry, University of Saskatchewan). The protein solution was then titrated with the RATIGVDFALK peptide and the spectrum was recorded. The two spectra were superimposed to visualize any differences. The red spectrum represents GtgE and the blue shows GtgE titrated with a 5-fold molar excess of the peptide. The HSQC spectrum of ^{15}N-GtgE$^{(14-214)}$(C45S) titrated with peptide was very similar to that of ^{15}N-GtgE$^{(14-214)}$(C45S) (Fig. 3-14). This result indicates that there is, at most, only a weak interaction between ^{15}N-GtgE$^{(14-214)}$(C45S) and the peptide.

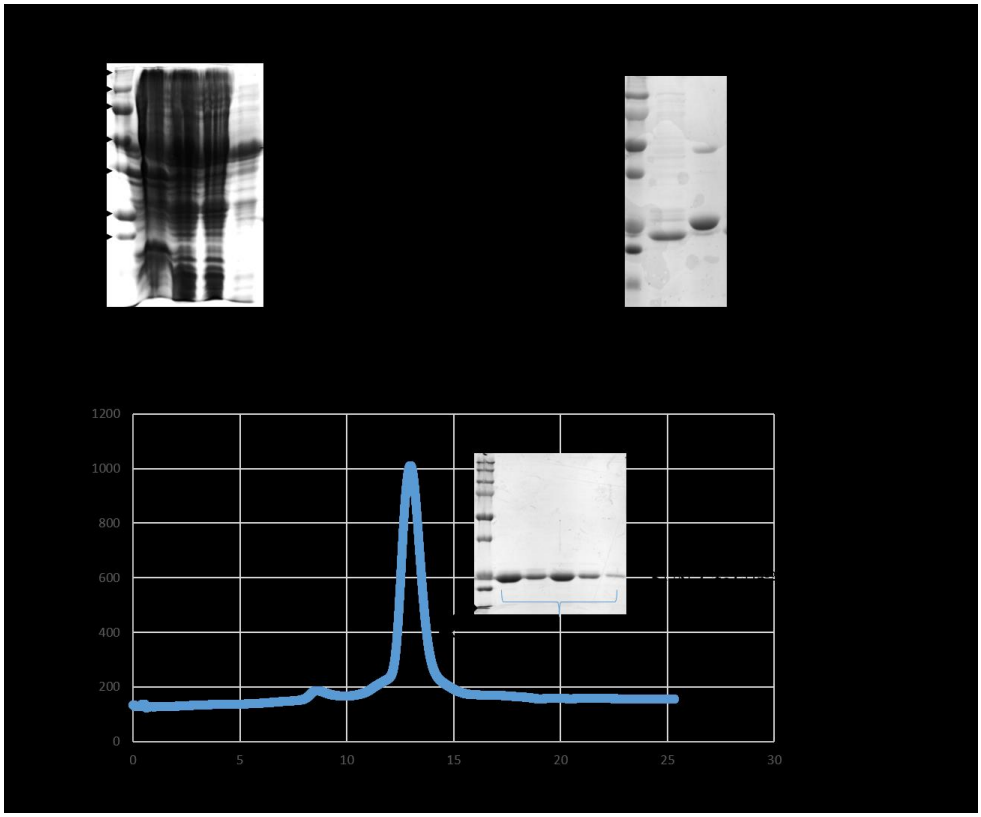

Fig. 3-13. Purification results for the GST-^{15}N-GtgE$^{(14-214)}$(C45S) construct. **A**. SDS-PGAE gel showing fractions collected while purifying GST-GtgE$^{(14-214)}$(C45S) on a GSH resin. Lane 1: protein markers, 2: content of the protein pellets, 3: supernatant, 4: proteins not retained on the resin, 5: protein retained to the resin. **B**. SDS-PGAE gel showing the GST-tag cleavage result by TEV protease. Lane 1: protein markers, 2: protein not retained on the resin after cleavage, 3: proteins retained on the GSH resin after cleavage. **C**. The elution profile of affinity purified ^{15}N-GtgE$^{(14-214)}$(C45S) from the Superdex 75 size exclusion column. The insert shows the SDS-PAGE gel of fractions from the largest peak.

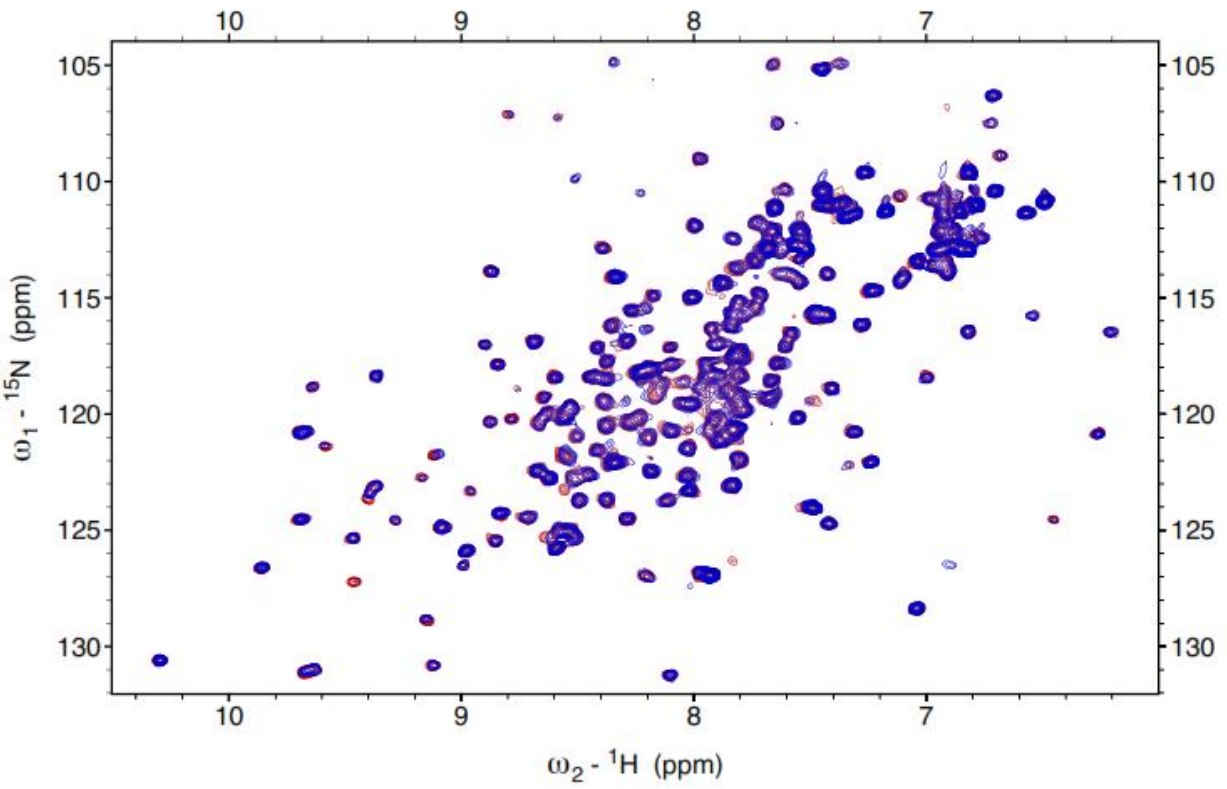

Fig. 3-14. The HSQC spectra of ^{15}N-GtgE$^{(14-214)}$(C45S) and that titrated with the RATIGVDFALK peptide. The spectrum of protein without peptide is in red and that of protein titrated with 5-fold excess of peptide is in blue. The two spectra overlaid almost completely. Experiments performed by Mr. Corey Yu, Department of Biochemistry, University of Saskatchewan.

3.1.10 Nanopore analysis as a potential method to identify unfolded termini in proteins

A nanopore is a pore with an internal diameter of approximately 10 nanometers. Many bacterial transmembrane proteins can be utilized as nanopores if they have an internal cavity crossing the entire membrane. In particular, α-hemolysin is frequently used as a nanopore (Jetha *et al.*, 2009). Applying a voltage across the membrane results in an electrochemical gradient, which drives ions (including proteins and DNA) through the pore. Depending on the properties of the molecule inserted into the pore, three kinds of events can be observed, 1) a translocation event, where the molecule passes through the pore; 2) an intercalation event, where the molecule became trapped in the entrance of the pore and 3) a bumping event, where the molecule approaches close to the pore blocking it temporarily but defuses away without entering (Meng *et al.*, 2010).

To test if nanopore analysis could provide information about the order or disorder of the termini in proteins, I have subjected His-GtgE$^{(2-228)}$, GtgE$^{(14-214)}$ and GtgE$^{(31-214)}$ constructs to this analysis. Indeed, each of the constructs exhibited unique behavior in these experiments. His-GtgE$^{(2-228)}$ showed 63% bumping events at -29 pA and 30% intercalation events at -63 pA (Fig. 3-15.A). GtgE$^{(14-214)}$ showed decreased bumping to 54% at -24 pA, and 35% intercalation events at -51 pA with an additional 5% translocation event peak at -80 pA (Fig. 3-15.B). GtgE$^{(31-214)}$ showed a decreased bumping events to 27% relative to the GtgE$^{(14-214)}$ profile at -26 pA, and an increase intercalation events to 60% at -66 pA (Fig. 3-15.C). Given that GtgE is a 25 kDa protein, the main factor affecting its translocation efficiency is its packing. That is, a loosely packed structure will translocate more easily through the pore than one with tight packing. The additional translocation peak from GtgE$^{(14-214)}$ indicates that the structure of GtgE$^{(14-214)}$ is less compact than His-GtgE$^{(2-228)}$ and GtgE$^{(31-214)}$. Compared with His-GtgE$^{(2-228)}$, GtgE$^{(31-214)}$ showed a big decrease in bumping events, which indicates that GtgE$^{(31-214)}$ is less compact than the full length protein.

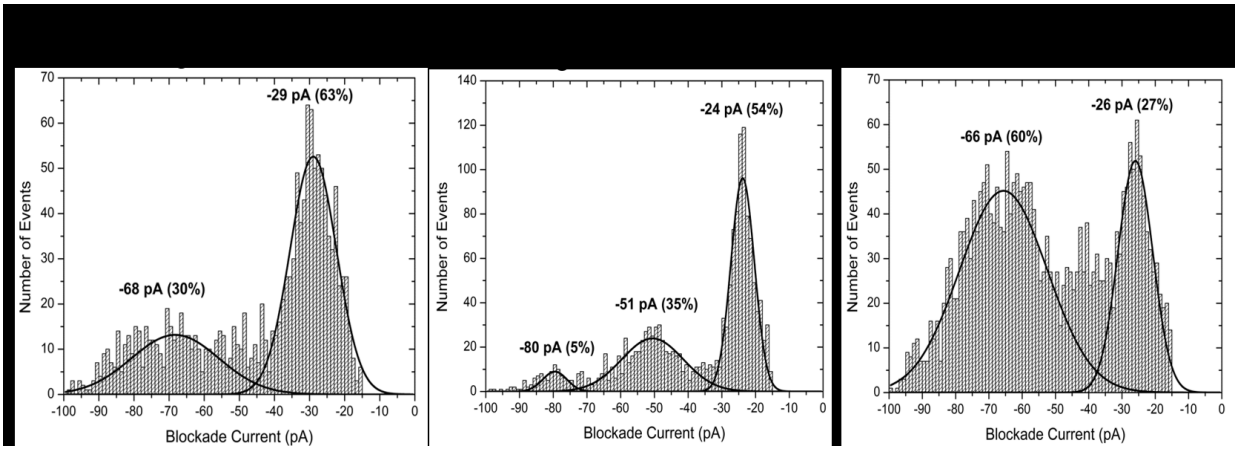

Fig. 3-15. Nanopore analysis of His-GtgE$^{(2-228)}$, GtgE$^{(14-214)}$ and GtgE$^{(31-214)}$ constructs. All experiment was conducted with 100 mV voltage across the membrane. Blockade current histograms for **A**. His-GtgE$^{(2-228)}$, **B**. GtgE$^{(14-214)}$, **C**. GtgE$^{(31-214)}$. Experiment performed by Ms. Elisabet Jakova, Dr. Lee laboratory, Department of Biochemistry, University of Saskatchewan.

3.1.11 Summary

Despite extensive efforts I was unable to crystallize full length GtgE or its shorter constructs containing the entire catalytic triad (Cys45-His151-Asp169). In addition to investigating multiple constructs, I have followed several rescue strategies that are commonly

applied to proteins that are difficult to crystallize. One strategy relied on methylation of surface-accessible lysines to change the surface properties of GtgE constructs. Another approach, termed surface entropy reduction, relied on replacing a cluster of charged residues on the surface by alanines, thereby reducing the conformational freedom on the surface. Finally, co-crystallization of GtgE(H151S) or GtgE(C45S) constructs with a peptide corresponding to the cleavage site of Rab32 were attempted. Crystallization screening was performed at 20 ℃ and 4 ℃ because temperature is an important parameter in determining protein solubility. Although I did not obtain crystals, I have learned much about cloning, protein expression, purification and characterization, as well as crystallization methods. The quality of GtgE HSQC spectra suggests that more information about its three-dimensional structure could be obtained with NMR spectroscopy methodology.

3.2 Structural studies of SpvB$^{(26\text{-}355)}$

3.2.1 Purification results for SpvB$^{(26\text{-}355)}$

Although the structure of the SpvB C-terminal, catalytic domain has been determined, neither the structure nor the function of its larger N-terminal domain is known. The construct encompassing this domain includes residues 26 to 355. This protein was expressed with an N-terminal His-tag. His-SpvB$^{(26\text{-}355)}$ was expressed in the *E. coli* BL21(DE3)STAR cell line and purified in a manner similar to the His-tagged GtgE constructs (Fig. 3-16).

3.2.2 SpvB crystallization, diffraction data collection and processing

Crystallization screening of the SpvB-N with commercial and in-house screens did not produce crystals. As a rescue strategy, the protein was methylated on surface-accessible lysine residues. Continued screening of the methylated protein did eventually lead to the production of crystals. The initial conditions were further optimized and the best conditions were established in the hanging drop format by mixing 1 μL of 27 mg/mL protein with 1 μL of reservoir solution containing 0.1 M Bis-Tris pH 6.5, 14% poly (acrylic acid) 5100 sodium, 4% PEG3350, 1 mM DTT and 20 mM $MgCl_2$ (Fig. 3-17). These crystals were grown at 15 ℃. Diffraction data to 2.4 Å resolution were collected at the Canadian Light Sources CMCF-ID beamline and processed with the program HKL3000 (Minor *et al.*, 2006). The diffraction data and refinement statistics are listed in Table 3-1.

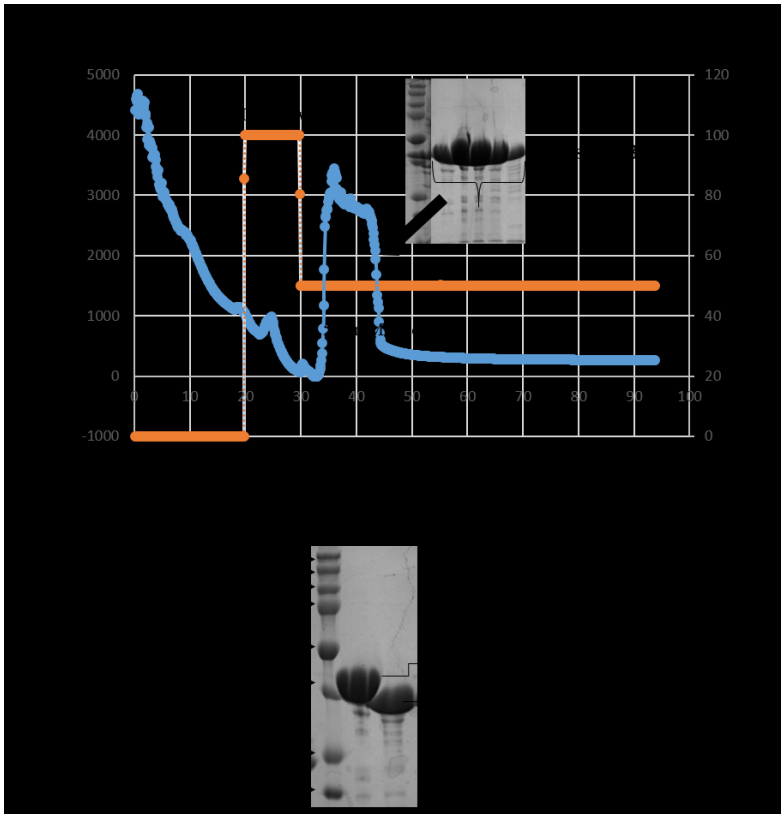

Fig. 3-16. Purification results for the His-SpvB$^{(26-355)}$ construct. **A**. The elution profile of His-SpvB$^{(26-355)}$ on the Ni-NTA. The blue curve indicates the absorption at 280 nm and the orange curve indicates the elution imidazole gradient. The column was washed with 1 M NaCl in 15 mM HEPES pH 7.5 before subjected to imidazole elution. The insert shows the SDS-PAGE gel of fraction from the peak. **B**. Cleavage of the His tag from the construct by TEV protease. Lane 1: protein markers, 2: His-tagged protein. 3: untagged protein.

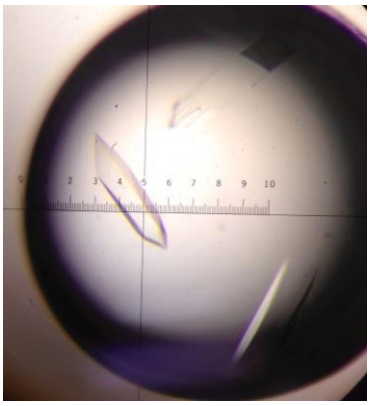

Fig. 3-17. Crystals of SpvB$^{(26-355)}$. Crystals were obtained by the hanging drop method. One microliter of the protein protein at 27 mg/mL was mixed with one microliter of reservoir solution containing 0.1 M Bis-Tris pH 6.5, 14% poly (acrylic acid) 5100 sodium, 4% PEG3350, 1 mM DTT and 20 mM $MgCl_2$. The crystallization plate was incubated at 15^{o}C.

Table 3-1. SpvB$^{(26-355)}$ crystallographic data collection and processing statistics

Diffraction data	
Diffraction source	Canadian Light Sources CMCF-ID
Wavelength (Å)	0.97949
Temperature (K)	100
Space group	$P4_32_12$
Unit-cell parameters (Å)	101.4, 101.4, 211.3, 90, 90, 90
No. of copies in the asymmetric unit	2
Resolution range (Å)	50 - 2.4 (2.44 - 2.4)
Total No. of reflections	646923
No. of unique reflections	43823 (4131)
Completeness (%)	99.52 (95.36)
Redundancy	14.7 (14.1)
I/σ(I)	26.62 (4.79)
R_{syms}	0.074 (0.92)
$CC_{1/2}$	0.980 (0.920)
Refinement	
R_{work}/R_{free}	0.200 / 0.239
Mean B factor	
Bond lengths	0.009
Bond angles	1.13

R_{syms} is defined as $R_{syms}= \sum | I - <I>| / \sum I$, where I = individual intensity measured and <I> = average intensity of the symmetry-related reflections. $CC_{1/2}$, the correlation coefficient, is another indicator of the quality of diffraction data (Karplus and Diederichs, 2012). Values in parentheses are for the outer shell, 2.44-2.40 Å resolution.

3.2.3 Structure determination and refinement

The structure was solved by the molecular replacement method using residues 26-388 of YenB (PDB entry 4GIL) as a search model with the Phenix program suite (Adams *et al.*, 2002). The refinement was performed using Phenix software and the manual rebuilding was done using the program Coot (Emsley *et al.*, 2010a). The crystal structure of SpvB$^{(26-355)}$ was determined at a resolution of 2.4 Å. After refinement, the final values of R_{work} and R_{free} were 0.200 and 0.239 respectively. Each molecule contains only 2 lysine and the electron density shown that the lysines were monomethylated or dimethylated.

The protein is elongated, with dimensions of 70 x 50 x 20 Å^3 (Fig. 3-17). The molecules interact within the crystal through the side surfaces, leaving both large faces accessible to the solvent (Fig. 3-18). Each molecule contacts three other molecules. The larger intermolecular contact area is ~700 Å^2 while the other two contacts are smaller and comprise only ~300 Å^2 (Fig. 3-18). These contact surfaces are rather small in comparison to the total surface area of SpvB$^{(26-}$

$^{355)}$ of ~14,500 Å^2 and are in agreement with a monomeric form of SpvB$^{(26-355)}$ observed in solution. The protein surface and contact surfaces were calculated using the PISA server (http://www.ebi.ac.uk/pdbe/pisa/).

The structure of SpvB$^{(26-355)}$ consists of 21 β-strands and 3 short α-helices (Fig. 3-19). The β-strands are anti-parallel as indicated on the topology diagram (Fig. 3-20). The secondary structure elements are displayed along the primary sequence, produced by the program PDBsum (https://www.ebi.ac.uk/thornton-srv/databases/cgi-bin/pdbsum/) (Laskowski, 2009) (Fig. 3-21). The crystal structure of SpvB$^{(26-355)}$ is relatively flat on one side, while there is a long and deep groove on the other side (Fig. 3-19). The long groove on the structure of SpvB is also present in YenB. This canyon in YenB participates in the formation of a central cavity that forms the path through which the cytotoxic domain of YenC passes to reach the host cell cytosol. It is very likely that the groove in SpvB acts as a binding site for a target protein.

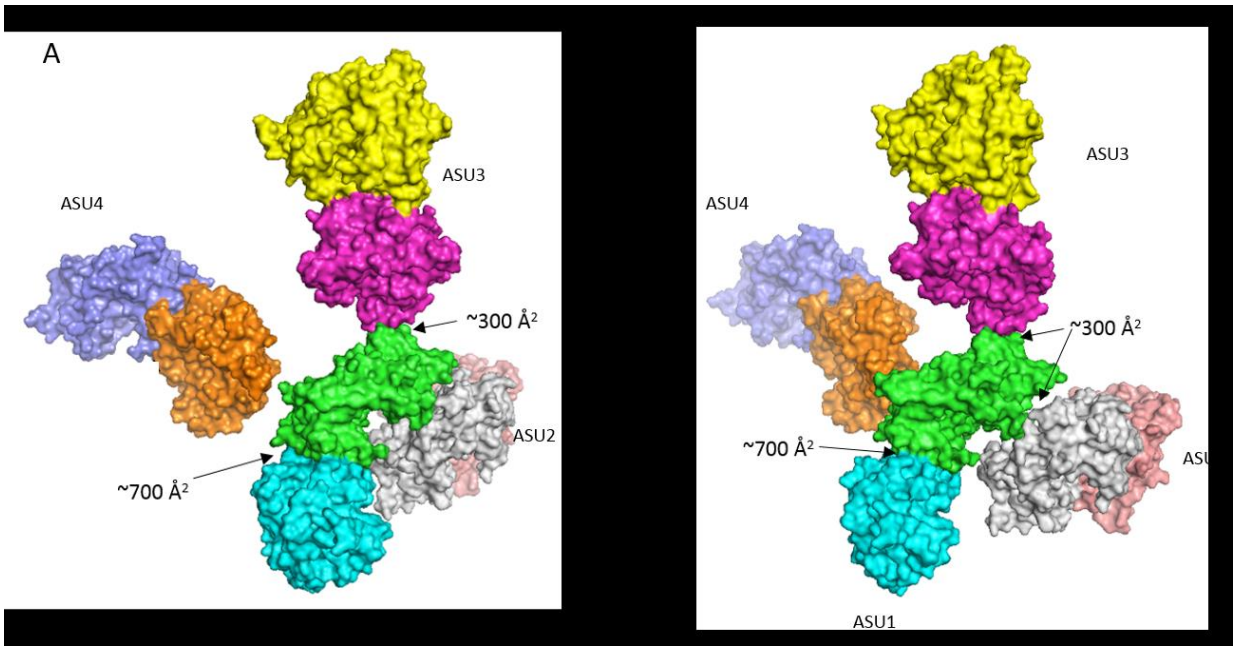

Fig. 3-18. Crystal contacts of SpvB$^{(26-355)}$. There are two SpvB$^{(26-355)}$ molecules in the asymmetric unit (ASU). Each molecule contacts three other molecules. The larger contact area is ~700 Å^2, calculated by Pisa sever (http://www.ebi.ac.uk/pdbe/pisa/). The other contacts cover ~300 Å^2. Each molecule is shown in a different color. Molecules colored green and cyan are in an asymmetric unit, molecules colored grey and pink, yellow and purple, blue and orange are symmetry related to the former.

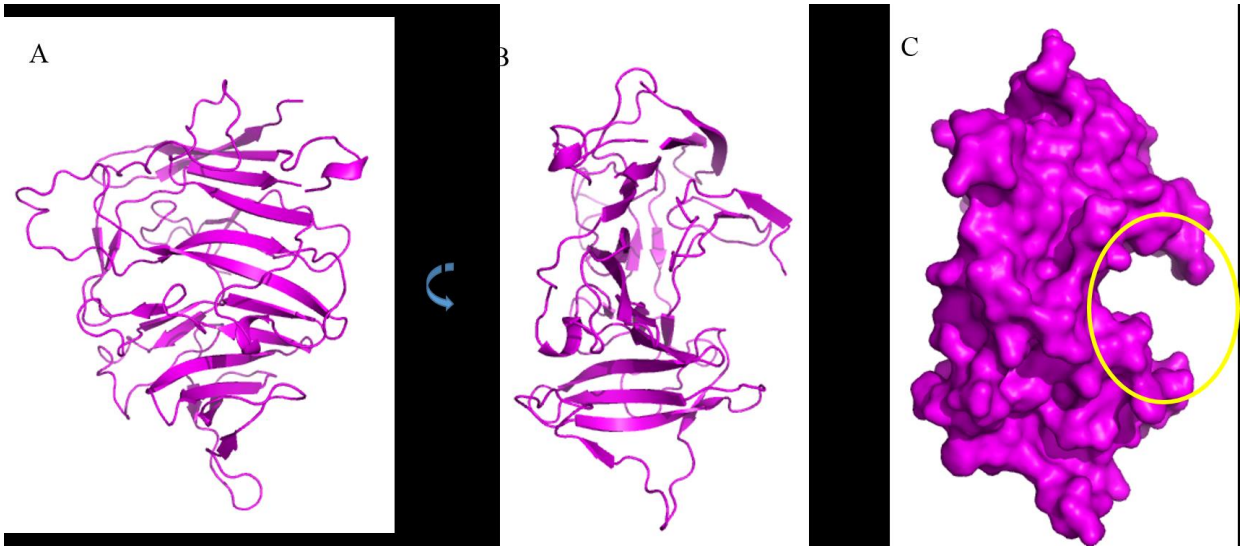

Fig. 3-19. Structural of SpvB$^{(26-355)}$. **A**. Cartoon representation of the protein. **B**. A view after rotating A 90 °counter-clockwise. **C**. The surface representation of the protein in the same view of B. The yellow circle region indicates the groove in the protein surface. Images were generated by Pymol Software (DeLano, 2002).

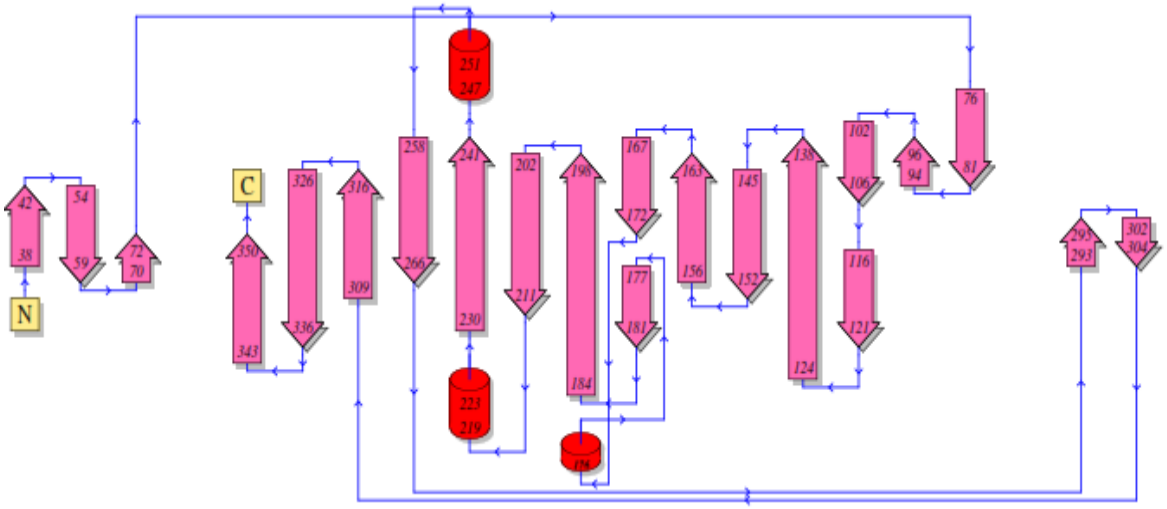

Fig. 3-20. Topology diagram of SpvB$^{(26-355)}$ generated in PDBsum server. The β strands are anti-paralleled.

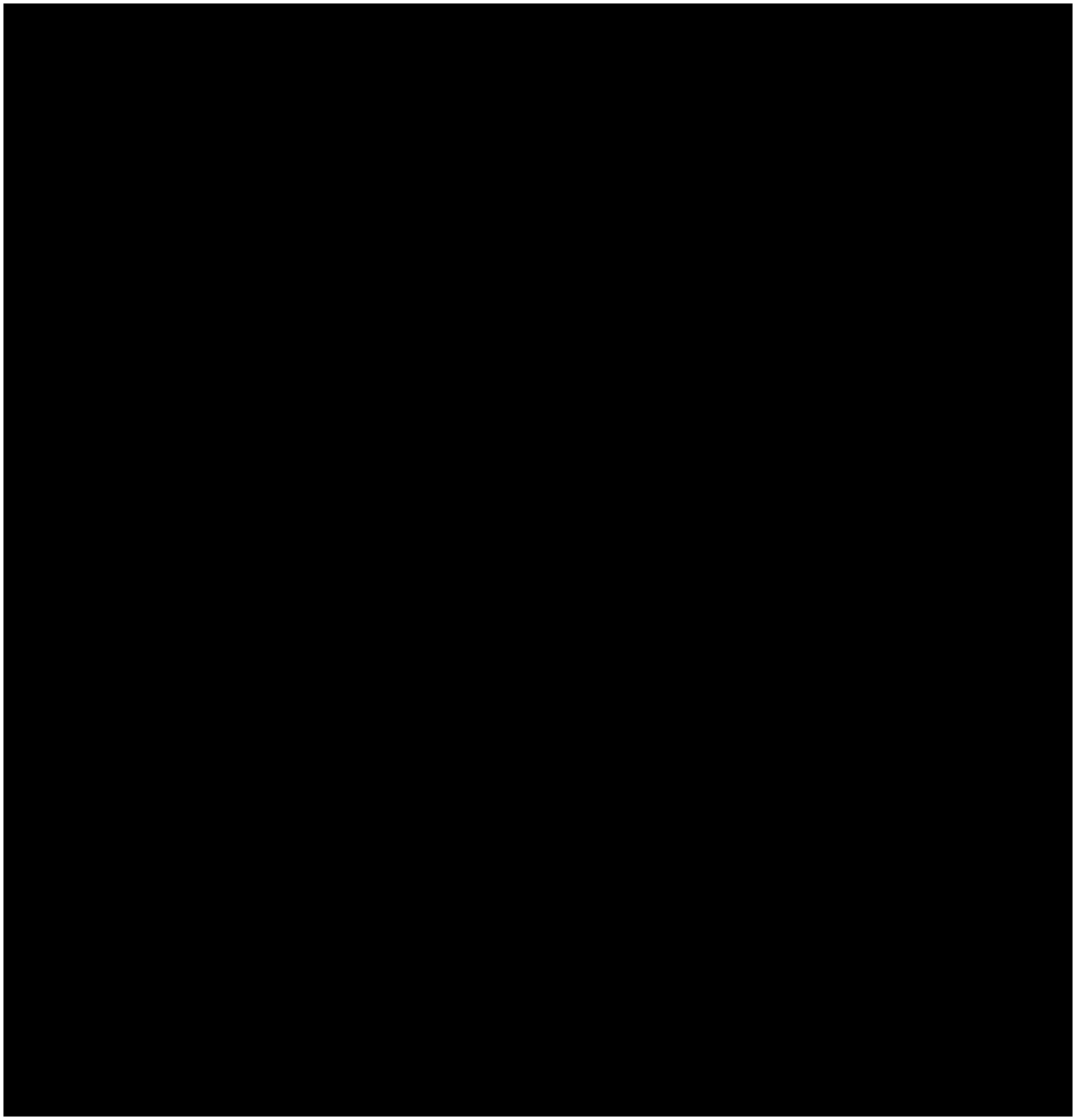

Fig. 3-21. The sequence of SpvB$^{(26\text{-}355)}$ with secondary-structure elements displayed above. The diagram was generated by PDBsum. There are 21 β-strands (labelled with B), colored in purple, and 3 short α-helices (labelled with A), colored in magenta in the structure. The β-turns are represented by β, γ-turns by γ and β-hairpins by @. The positions of the secondary structure elements are labelled according to the topology diagram.

3.3 Functional studies of SpvB$^{(26-355)}$

3.3.1 Interaction between SpvB and actin

Considering that the C-terminal domain of SpvB ADP-ribosylates actin, the first hypothesis about the function of SpvB N-terminal region was that this domain binds actin to promote the ADP-ribosyltransferase activity. To examine if the N-terminal domain binds actin *in vivo*, mammalian cells (HeLa or HEK293) were transfected with SpvB$^{(1-591)}$, SpvB$^{(26-355)}$, SpvB$^{(26-591)}$ or SpvB$^{(390-591)}$ constructs that were HA-tagged on the C-termini. Once SpvB had been overexpressed, the host cells were harvested and lysed. A co-immunoprecipitation (Co-IP) assay was performed using an anti-HA antibody and Protein G agarose resin. On the Western blot, the anti-HA antibody was used to detect HA-tagged SpvB and anti-actin antibody was used to detect actin. Actin was detected in all cell lysates, but not in the sample precipitated with anti-HA antibody (Fig. 3-22). The strong signal of SpvB-HA on the Western blot indicates that SpvB expressed and precipitated well in the host cells, but showed no significant binding to actin. Lack of clear evidence for the interaction between SpvB and actin suggests that the interaction is either weak or transient.

3.3.2 Localization of SpvB in the host cells

Another formulated hypothesis was that the function of SpvB$^{(26-355)}$ was to guide the subcellular localization of the protein. SpvB constructs, SpvB$^{(1-591)}$, SpvB$^{(1-355)}$ and SpvB$^{(390-591)}$ were fused at the C-terminus to GFP. SpvB was expressed and the cells were subjected to immuno-fluorescent approaches. Cells expressing SpvB$^{(1-355)}$-GFP and the control cells expressing only GFP grew well, while cells expressing SpvB$^{(1-591)}$ and SpvB$^{(390-591)}$ detached from the glass slide and became round. In the confocal fluorescent microscope, SpvB$^{(1-355)}$-GFP showed a similar localization pattern to the GFP alone, which predominantly localized to the nucleus (Fig. 3-23). Cells expressing SpvB$^{(1-591)}$-GFP and SpvB$^{(390-591)}$-GFP showed abnormal cell shape, nuclear fragmentation, and de-polymerization of F-actin (Fig. 3-23). Due to changes in the cell caused by active SpvB$^{(1-591)}$-GFP and SpvB$^{(390-591)}$-GFP, it was not possible to reliably determine their localization. Therefore, an inactivating mutation (EAE536AAA) was introduced at the active site of the C-terminal ART domain. The localization of both mutants was clearly in the cytosol (Fig. 3-23). These results indicate that the C-terminal domain directs the localization of SpvB to the cytosol to modify G-actin and to induce apoptosis.

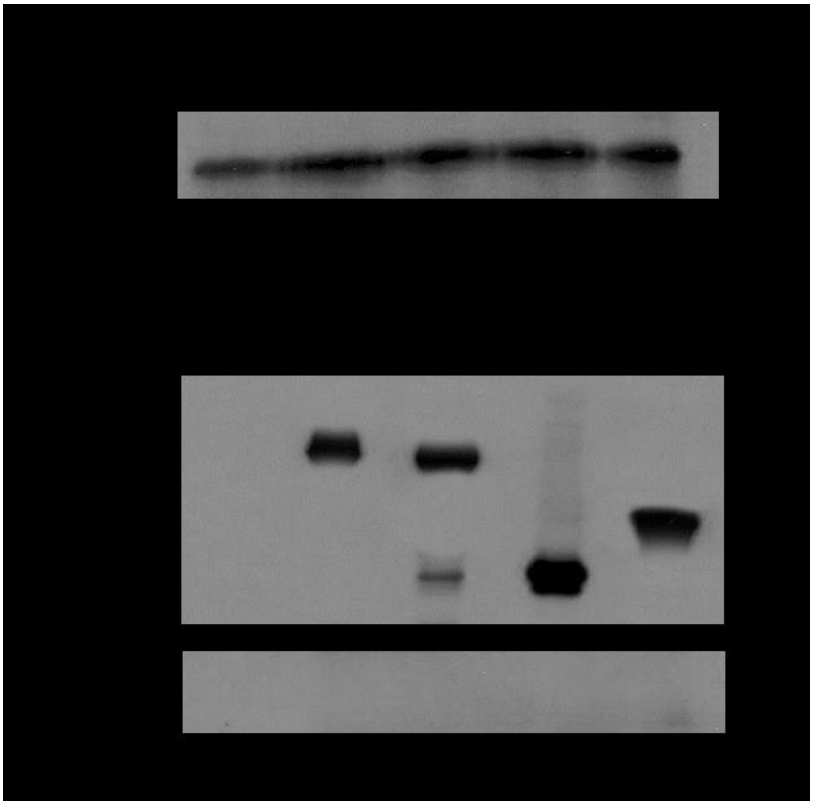

Fig. 3-22. Co-immunonoprecipitation (Co-IP) of SpvB-HA constructs. The upper panel shown the results for input using anti-actin antibody to detect actin. The bottom panel shown the Co-IP result using anti-HA antibody and protein G agarose resin to precipitate SpvB. The expression and precipitation of SpvB was detected by anti-HA antibody and actin was detected by anti-actin antibody. No actin was detected in the precipitant. Lane 1: HEK293 cell transfected with empty vector pCDNA4TO, 2: cells transfected with SpvB$^{(1-591)}$-HA, 3: cells transfected with SpvB$^{(26-591)}$-HA, 4: cells transfected with SpvB$^{(390-591)}$-HA, 5: cells transfected with SpvB$^{(26-355)}$-HA.

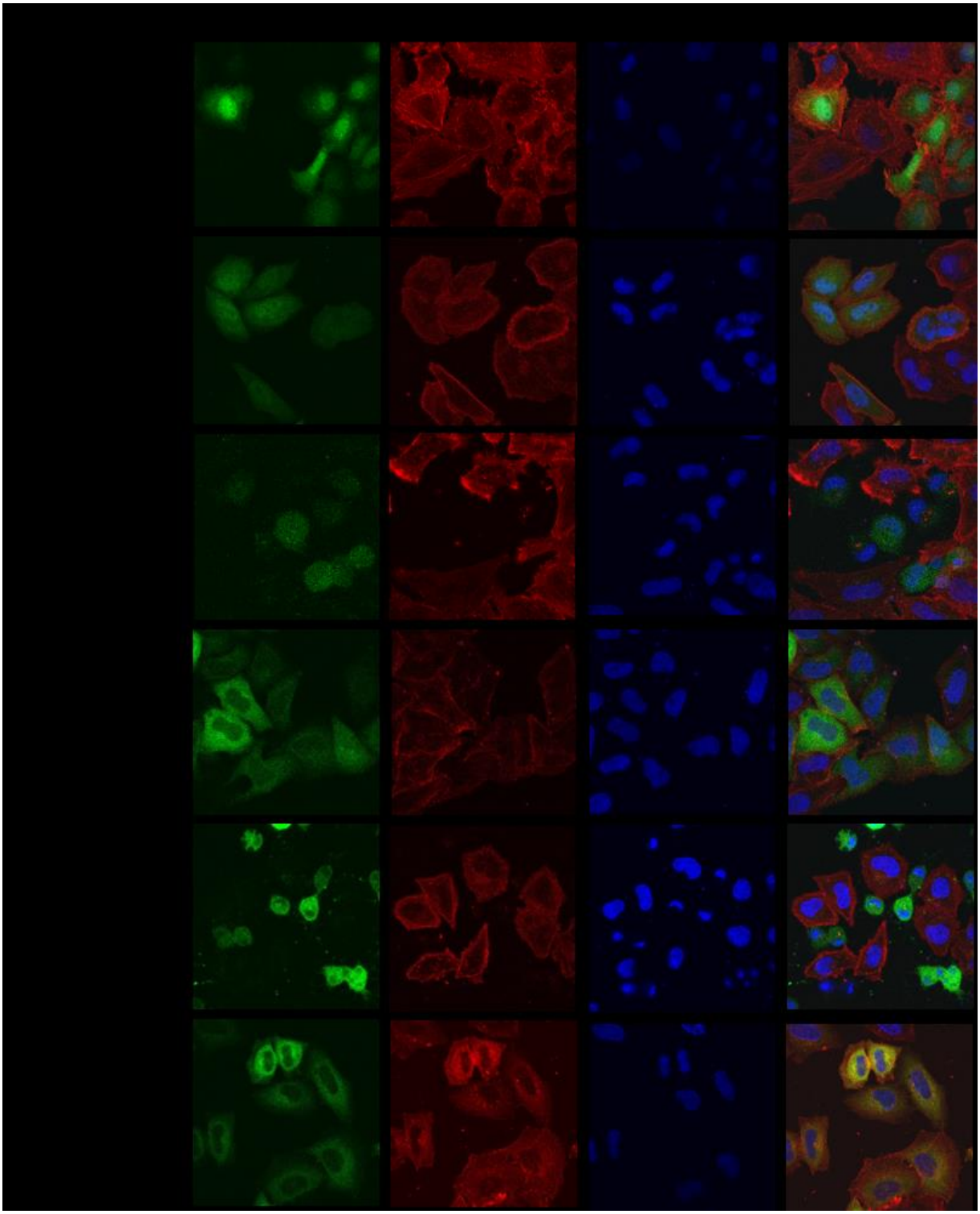

Fig. 3-23. Co-localization of SpvB and actin. Cells were transfected with plasmids carrying SpvB-GFP constructs (indicated on the left of the images). The green fluorescent light indicates the localization of GFP-tagged SpvB, the red fluorescent light stains F-actin filament and the blue fluorescent light shows the nuclei. The yellow color results from the merger of red and green.

3.3.3 Detection of cytotoxicity of SpvB constructs with LDH assay

Considering that the N-terminal domain of SpvB shows 47% sequence identity to YenB, another considered hypothesis was that SpvB$^{(26-355)}$ is cytotoxic and helps in host cell breakdown without directly interfering in actin dynamics. A cytotoxicity assay was performed to test the cytotoxicity of SpvB constructs. A common method to measure protein cytotoxicity is to measure the levels of lactate dehydrogenase (LDH), which is upregulated and released when the cells are damaged. HeLa cells expressing SpvB-GFP constructs were harvested and lysed. The lysate was used to measure the amount of LDH present. The LDH cytotoxicity results showed that the cells expressing SpvB$^{(1-355)}$-GFP had 15% increase in cytotoxicity relative to the cells expressing only GFP. SpvB$^{(390-591)}$-GFP showed 43% increase in cytotoxicity compared to the GFP background and SpvB$^{(1-591)}$-GFP presented a 2.3-fold increase in cytotoxicity (Fig. 3-24). These results showed that by itself the N-terminal domain of SpvB had only marginal effect on cytotoxicity.

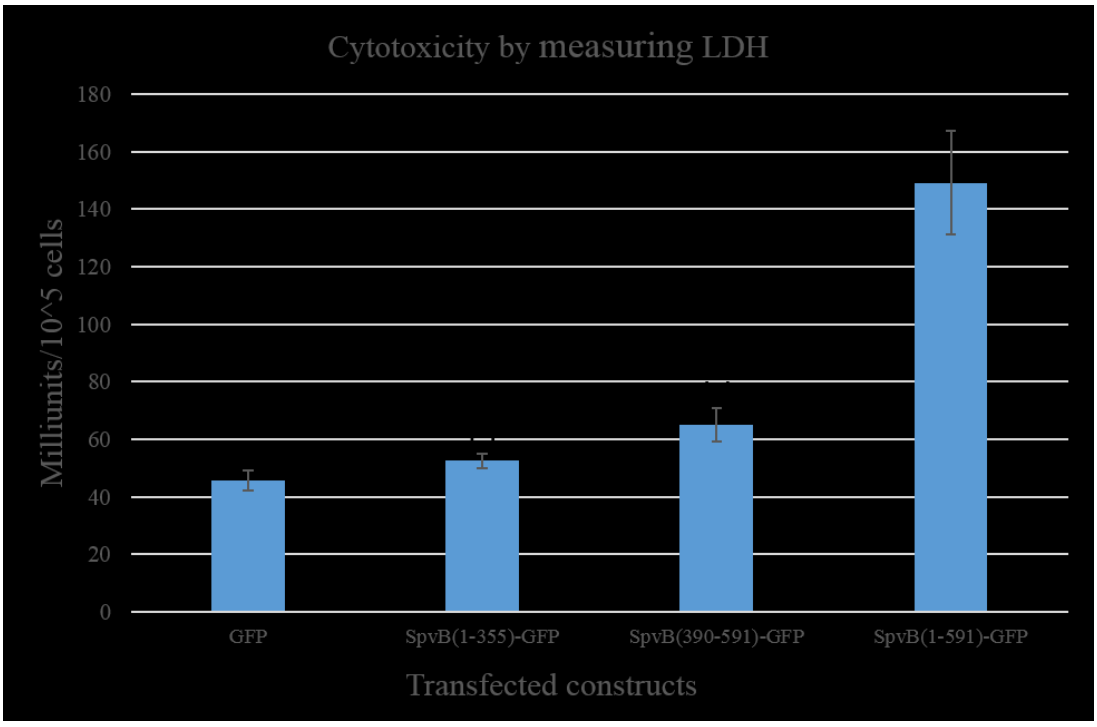

Fig. 3-24. Cytotoxicity measuring by lactate dehydrogenase (LDH). HeLa cells were transfected with empty vector pEGFP-N1 and *spv*B constructs. Values of cytotoxicity are the means of three independent determinations. P value were determined by Student's test, compared with the cell only overexpressing GFP. ** indicates $p<0.01$.

3.3.4 Secretion of SpvB-Flag in *Salmonella* strains

In order to test the secretion of SpvB in *Salmonella*, the Flag tag was fused to the C-terminus of $SpvB^{(1-591)}$ and this construct was expressed in *Salmonella* under several conditions: (1) in LB medium; (2) in LB supplemented with 0.3M NaCl to stimulate SPI-1 TTSS and (3) in low pH medium that stimulated the SPI-2 TTSS. After expression of $SpvB^{(1-591)}$-Flag, cells were spun down and the supernatant was analyzed by Western blot to detect $SpvB^{(1-591)}$-Flag. To detect possible cell leakage, the presence of a cytosolic DnaK chaperon was followed by anti-DnaK antibody. Anti-SopE2 serum was used to follow SopE2 (a known SPI-1 substrate), and anti-SseL serum followed anti-SseL (a known SPI-2 substrate).

It was found that $SpvB^{(1-591)}$-Flag and SopE, but not SseL were present in the supernatant from wild-type *Salmonella* grown in a SPI-1 stimulating condition (Fig. 3-25). However, DnaK was also detected, indicating some level of cell disruption. Therefore, it was not clear if SpvB was indeed secreted through SPI-1 TTSS. The same leakage problem occurred when bacteria were grown in the LB medium. When bacteria were grown in the SPI-2 stimulating condition, no DnaK was detected in the media. As expected, SseL was detected in the media, indicating that the SPI-2 TTSS was indeed functional (Fig. 3-25). However, no $SpvB^{(1-591)}$-Flag was detected in the supernatant, implying that this protein is not secreted by the SPI-2 TTSS.

The secretion assay was also done in *Salmonella* strains defective in secretion systems. *Salmonella* Δ*spi-1* strain was grown in a SPI-2 stimulating condition, Δ*spi-2 s*train in a SPI-1 stimulating condition, and Δ*spi-1&2* strains in LB medium. DnaK was present in the supernatant arising from bacteria grown in LB and SPI-1 stimulating media, but not in the SPI-2 stimulating medium. SseL was also detected in the supernatant of SPI-2 stimulating medium, but SpvB was not (Fig. 3-26). In conclusion, the secretion of SpvB though a functional SPI-2 TTSS was not observed. These results disagree with the previously published data showing secretion of SpvB by *Δspi-1* mutant strain (Δ*inv*A) and *Δspi-2* mutant strain (Δ*ssr*A) (Gotoh *et al.*, 2003).

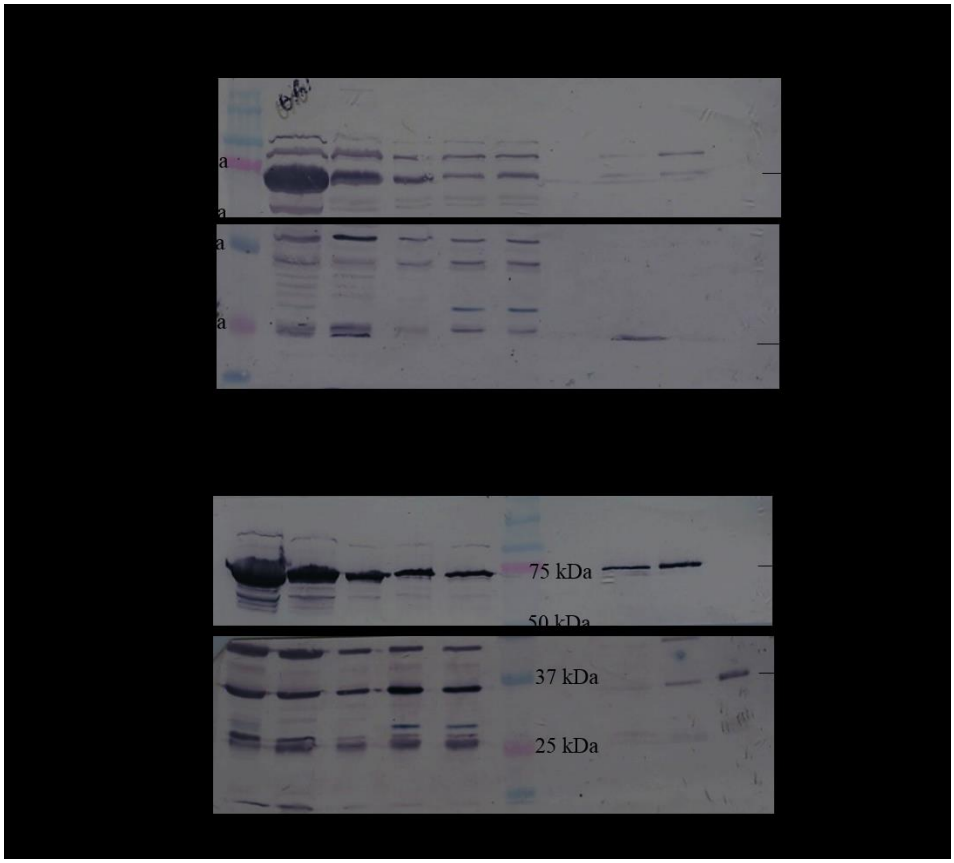

Fig. 3-25. Secretion of SpvB in the wild-type *Salmonella* strain. **A**. Western blot result when detecting with anti-Flag and anti-SopE2 antibodies. **B**. Western blot result when detecting with anti-DnaK and Anti-SseL antibodies. The primary antibodies used for detecting desired proteins were labelled on the left side of the Western blot. Samples loaded on A and B were identical. Protein markers was used on the left side on the first blot and in the middle on the second bolt. Lane 1: cell pellet of the starting overnight culture, 2: cell pellet grown in LB medium, 3: cell pellet grown in SPI-1 condition, 4: cell pellet grown in SPI-2 condition before IPTG induction, 5: cell pellet grown in SPI-2 condition after IPTG induction, 6: protein precipitated from the cell supernatant grown in LB medium, 7: protein precipitated from the cell supernatant grown in SPI-1 medium, 8: protein precipitated from the cell supernatant grown in SPI-2 medium.

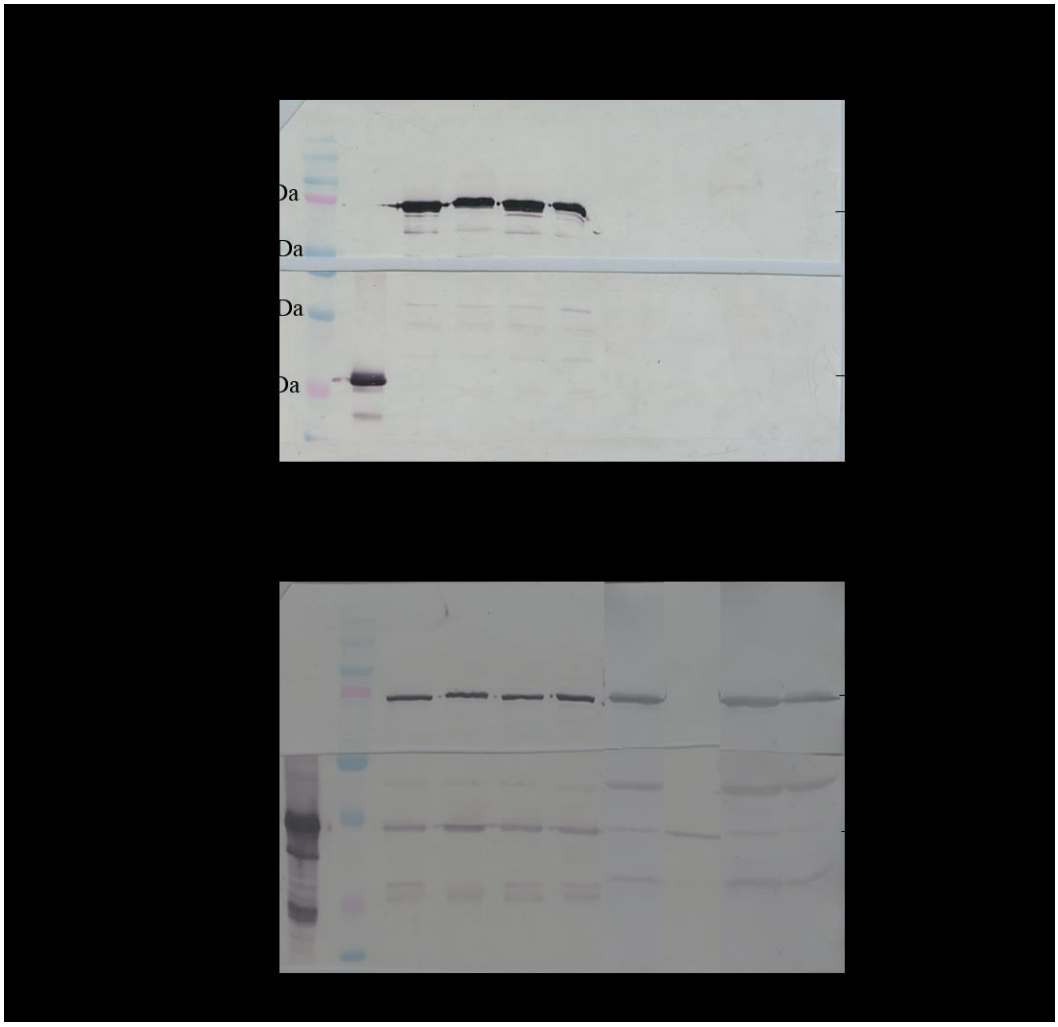

Fig. 3-26. Secretion of SpvB in the wild-type and mutant *Salmonella* strains. **A**. Western blot result when detecting with anti-Flag and anti-SopE2 antibodies. **B**. Western blot result when detecting with anti-DnaK and Anti-SseL antibodies. The primary antibodies used for detecting desired proteins were labelled on the left side of the Western blot. Samples loaded on A and B were identical. Protein markers was used on the left side on the first blot and in the middle on the second bolt. Lane 1: protein control (SopE2 in A and SseL in B), 2: cell pellet of wild-type strain, 3: cell pellet of Δ*spi-1*strain, 4: cell pellet of Δ*spi-2*strain, 5: cell pellet of Δ*spi-1&2* strain, 6: protein precipitated from supernatant of wild-type strain, 7: protein precipitated from supernatant of Δ*spi-1*strain, 8: protein precipitated from supernatant of Δ*spi-2* strain, 9: protein precipitated from supernatant of Δ*spi-1&2* strain.

4. Discussion

4.1 GtgE and Rab32

4.1.1 GtgE displays very low activity *in vitro* against GST-Rab32

GtgE is an effector present in *S.* Typhimurium strains but absent in *S.* Typhi strains. *S.* Typhimurium has a broad range of hosts, while *S.* Typhi is human-specific (Spanò and Galán, 2012). Expression of GtgE in *S.* Typhi helped this bacterium to overcome the host-specificity restriction as this engineered strain was able to invade mouse macrophages (Spanò and Galán, 2012). GtgE was identified as a cysteine protease that specifically cleaves Rab29, Rab32 and Rab38 but not other Rab proteins (Spanò and Galán, 2012).

To confirm the activity of recombinant GtgE toward Rab32, SDS-PAGE based analysis was performed. The cleavage results showed indeed a low level of $GtgE^{(2-228)}$ protease activity based on the appearance of a new lower molecular weight bands not observed in the control. However, Rab32 was only partially cleaved even after 2 h incubation with 1:2 molar ratio of GtgE:Rab32. The low protease activity of GtgE *in vitro* might be due to the extensive flexibility of the N-terminal segment of GtgE containing the active site Cys45. It was found that Rab29, the GtgE substrate, was recruited on the membrane of SCV of *S.* Typhi but not on the membrane of SCV of *S.* Typhimurium (Spano *et al.*, 2011). This indicates that GtgE is secreted to cleave Rabs near the SCV surface. The presence of a membrane or a protein anchored to the membrane might be a factor in the correct folding of GtgE.

GtgE truncations were also used to test their cleavage activity. It was found that the truncation construct $GtgE^{(14-214)}$ was still active, however $GtgE^{(31-214)}$ lost activity almost completely. This suggests that the N-terminal region is essential for the GtgE activity and the first 30 residues are needed to stabilize the GtgE active site.

GtgE constructs were efficiently expressed and purified. As indicated by dynamic light scattering, molecules in solution were monodispersed, which was promising for successful crystallization. However, despite screening several hundred crystallization conditions for each construct, no crystals were obtained for any of the investigated constructs. Unfortunately, the standard crystallization rescue strategies, such as chemical modification of surface accessible lysines or surface entropy reducing mutations, were not helpful in crystallizing this protein. Similarly, co-crystallization screening of a GtgE active site mutants with peptide substrate did not produce crystals. I conclude that the failure to crystallize GtgE stems from the

flexibility/disorder of its N-terminal ~80 residues. Indeed, limited proteolysis of GtgE$^{(43-214)}$ (Kohler *et al.*, 2014) showed the presence of a smaller 17 kDa fragment, which was identified by mass spectrometry as GtgE$^{(79-214)}$. The GtgE$^{(79-214)}$ was further degraded into a smaller fragment at 15 kDa, which was identified as GtgE$^{(79-200)}$ (Kohler *et al.*, 2014). Thus, the N-terminal first ~80 residues and the C-terminal ~28 residues are partially disordered. The fragment GtgE$^{(79-214)}$ was crystallized and its structure solved (Kohler *et al.*, 2014).

I have also used an NMR approach in this project to determine the structure of GtgE$^{(14-214)}$(C45S). The HSQC spectrum was used to evaluate the state of GtgE. In the well-ordered protein, the environment of individual NH group differs, leading to a wide distribution of the NH signals in the spectrum. The NH groups within the flexible regions are exposed to multiple environments, which average to a much more similar effect on their chemical shift and a narrower distribution of peaks in the spectrum. While the NH signals for GtgE were well dispersed, they were present for only ~75% of residues. The titration of GtgE$^{(14-214)}$(C45S) with a 5-fold excess of RATIGVDFLAK peptide introduced almost no changes in the spectrum. Such lack of changes indicates that there is at most only very weak binding of the peptide to GtgE. This could mean that the GtgE recognizes some three dimensional features of the substrate outside of the linear peptide containing the cleavage site.

4.1.2 N-terminal region makes GtgE unstable

The GtgE constructs behaved differently in nanopore analysis. From the histogram of current blockade, GtgE$^{(14-214)}$ showed less bumping events and had an additional translocation peak when compared with the profile with His-GtgE$^{(2-228)}$. This result indicates that the regions at the N- and C-termini affect the conformation of the protein. Since more bumping events were found in His-GtgE$^{(2-228)}$, it was likely that the N-terminal region interacts with the C-terminal region to make the protein more compact and reduces the conformational flexibility of the termini. Compared with GtgE$^{(14-214)}$, GtgE$^{(31-214)}$ was involved in fewer bumping events, more intercalation events but showed no translocation events. This suggests that GtgE$^{(14-214)}$ is less compact than GtgE$^{(31-214)}$ with the N-terminal segment being disordered. It is likely that the first 14 N terminal residues makes GtgE unstable.

4.1.3 Conclusion and perspectives

The purified GtgE showed low activity *in vitro* with its substrate. The possibility that the activity is stimulated by the presence of a membrane was investigated by following the reaction in the presence of lipid vesicles, however no increase in the activity was evident. This low protease activity *in vitro* (as well as lack of success in GtgE crystallization) is likely related to the flexibility of the protein, particularly of its first ~80 residues which contain the nucleophilic Cys45 of the catalytic triad. Further research will be required to study why GtgE shows low enzyme activity and what are the structural determinants of its substrate specificity.

4.2 SpvB and actin

4.2.1 Structure determination of the N-terminal domain of SpvB

SpvB is an essential effector for the virulence of *Salmonella*. It is known that the C-terminal domain of SpvB ADP-ribosylates actin and the modification results in a degradation of actin cytoskeleton (Margarit *et al.*, 2006). The structure and function of the N-terminal domain was unknown. In this project, the structure of $SpvB^{(26-355)}$ was determined at 2.4 Å resolution. Based on size exclusion chromatography and dynamic light scattering $SpvB^{(26-355)}$ was present in solution as a monomer. Although there are two molecules of $SpvB^{(26-355)}$ in the asymmetric unit of the crystal ($P4_32_12$ space group), the analysis of contacts in the crystal supports the notion that SpvB-N is monomeric.

4.2.2 Co-immunoprecipitation assay excluded strong interaction between SpvB and actin

The groove present on the surface of $SpvB^{(26-355)}$ suggests that the function of this domain might involve binding another moiety and the extent of the groove points toward an extended peptide moiety as a possible target. Considering that the C-terminal domain of SpvB modifies actin, it seemed plausible that the N-terminal domain of SpvB binds to actin to aid in the function of the C-terminal domain. The co-IP assay was performed to detect the interaction between various SpvB fragments ($SpvB^{(26-355)}$-HA, $SpvB^{(390-591)}$-HA, $SpvB^{(26-591)}$-HA and $SpvB^{(1-591)}$-HA) and actin. However, actin was not detected after precipitating SpvB constructs. It is known that the C-terminal domain of SpvB is able to modify actin and prevents the polymerization of actin *in vitro* (Margarit et al., 2006). This indicates that the C-terminal domain of SpvB has to contact actin. Since actin was not detected in the co-IP experiment, it was likely that the interaction between C-terminal domain of SpvB and actin was transient. This does not support the

hypothesis that the N-terminal of SpvB binds actin to promote the activity of the C-terminal domain.

4.2.3 SpvB$^{(390-591)}$ is sufficient to disrupt the host cytoskeleton and induce cell apoptosis

To validate the function of SpvB domains in causing the observed cell phenotype, SpvB constructs (SpvB$^{(1-355)}$-GFP, SpvB$^{(390-591)}$-GFP and SpvB$^{(1-591)}$-GFP) were transfected into HeLa cells. The expression of SpvB$^{(1-591)}$-GFP or SpvB$^{(390-591)}$-GFP caused cell deformation and detachment from the cover slides where the cells were plated, while no obvious phenotype was found when cells overexpressed SpvB$^{(1-355)}$-GFP. It is known that the expression of SpvB results in degradation of the actin cytoskeleton and induces cell cycle arrest and apoptosis (Paesold *et al.*, 2002; Mesa-Pereira *et al.*, 2013). Our transfections with truncated constructs showed that the C-terminal domain of SpvB led to the same phenotype as the full length SpvB.

Since expression of the full length SpvB as well as the C-terminal domain alone caused cell death, it was not possible to determine localization of these SpvB constructs. Therefore the active site mutation EAE536AAA was introduced in SpvB$^{(390-591)}$-GFP and SpvB$^{(1-591)}$-GFP to inactivate SpvB ADP-ribosyltransferase activity. These plasmids were used to transfect HeLa cells. The immunofluorescent assay to detect localization of the SpvB constructs showed that the N-terminal domain of SpvB predominantly localized to the nucleus in the same fashion as GFP alone expressed from the empty vector (control), while SpvB$^{(390-591)}$(EAE536AAA)-GFP and SpvB$^{(1-591)}$(EAE536AAA)-GFP were predominantly localized to the cytosol. The different localization of the SpvB$^{(1-355)}$ from the other two constructs indicated that the C-terminal domain of SpvB played a dominant role in SpvB localization to the cytosol in order to access and modify G-actin. The N-terminal domain of SpvB seems to play no role in the localization of SpvB in the host cells. In conclusion, the C-terminal domain was sufficient to cause cell deformation and detachment by directing the localization of SpvB to the cytosol and by modifying actin to interfere with actin cytoskeleton dynamics.

4.2.4 SpvB$^{(1-355)}$ has a marginal effect on the cytotoxicity inside the host cells

To test the function of SpvB$^{(1-355)}$ inside the host cells, a cytotoxicity assay was performed. HeLa cells were transfected with SpvB constructs and their cytotoxicity was evaluated by measuring LDH activity. Cells expressing SpvB$^{(1-355)}$-GFP had only 15% increasing compared with the levels of LDH in cells expressing only GFP. This indicated that SpvB$^{(1-355)}$ had a small

cytotoxic effect. Cells expressing SpvB$^{(390-591)}$-GFP showed a 43% increase in cytotoxicity and a 2.3-fold increase in cytotoxicity was observed for cells expressing SpvB$^{(1-591)}$-GFP. The effect of SpvB$^{(1-591)}$ was more than the sum of effects caused by the N-terminal and the C-terminal domains. This result suggests that these two domains of SpvB cooperate to some extent in inducing cytotoxicity.

4.2.5 SpvB appears not to be secreted through SPI-2 TTSS

The C-terminal domain of SpvB was sufficient to cause the abnormal phenotype and to modify actin, indicating that the N-terminal region of SpvB may have no function inside the host cells but rather in the bacterial cell. Considering that SpvB is an effector, the secretion path can be divided into three stages: from the ribosome to the secretion systems, from the secretion systems to the host cytosol and inside the host cytosol. Although the N-terminal domain of SpvB is homologous to the N-terminal region of TcB, absence of the rest of the toxin apparatus makes SpvB secreted in a different way to Tc toxin. It is therefore possible that the N-terminal domain of SpvB plays a role in secretion of SpvB.

The SpvB-Flag was expressed in *Salmonella* wild-type and mutant strains and the secretion assay was performed to detect the secretion of SpvB. No SpvB secretion was observed under the condition stimulating SPI-2 TTSS. SpvB is less likely secreted through SPI-1 TTSS, although our experiment was not conclusive due the cell leakage problem under SPI-1 stimulating conditions. However, it is known that the expression of SpvB is upregulated in the late endocytosis stage, while SPI-1 TTSS is downregulated as the bacterium resides in the SCV (Schlumberger and Hardt, 2006). On the time axis, the maximum expression of SpvB and the activity of the SPI-1 TTSS do not coincide, supporting the hypothesis that the secretion of SpvB may be independent of TTSS. Indeed, although we have seen SpvB in the medium in the SPI-1 stimulating condition, which could likely be attributed to the observed cell leakage, we did not see secretion of SpvB under SPI-2 stimulating condition, in agreement with Gotoh et al. (Gotoh *et al.*, 2003).

4.2.6 Conclusions and perspectives

In conclusion, the C-terminal domain of SpvB was sufficient to cause the abnormal host cell phenotype, while the function of the N-terminal domain of SpvB was most likely associated with the events inside the bacterial cell leading to SpvB secretion. The secretion assay indicated

that SpvB was likely not secreted through SPI-2 TTSS. Therefore, how SpvB is secreted remains an open question. Further experiments will be required to find out the secretion path of SpvB.

5. Reference

Adams, P.D., Afonine, P.V., Bunkóczi, G., Chen, V.B., Davis, I.W., Echols, N., Headd, J.J., Hung, L.-W., Kapral, G.J., and Grosse-Kunstleve, R.W. (2010). PHENIX: a comprehensive Python-based system for macromolecular structure solution. Acta Cryst. D *66*, 213-221.

Adams, P.D., Grosse-Kunstleve, R.W., Hung, L.-W., Ioerger, T.R., McCoy, A.J., Moriarty, N.W., Read, R.J., Sacchettini, J.C., Sauter, N.K., and Terwilliger, T.C. (2002). PHENIX: building new software for automated crystallographic structure determination. Acta Cryst. D *58*, 1948-1954.

Aktories, K., and Barbieri, J.T. (2005). Bacterial cytotoxins: targeting eukaryotic switches. Nat Rev Micro *3*, 397-410.

Aktories, K., and Barth, H. (2004a). The actin-ADP-ribosylating Clostridium botulinum C2 toxin. Anaerobe *10*, 101-105.

Aktories, K., and Barth, H. (2004b). Clostridium botulinum C2 toxin – New insights into the cellular up-take of the actin-ADP-ribosylating toxin. Int. J. Med. Microbiol. *293*, 557-564.

Aktories, K., Lang, A.E., Schwan, C., and Mannherz, H.G. (2011). Actin as target for modification by bacterial protein toxins. FEBS J. *278*, 4526-4543.

Bakowski, M.A., Braun, V., and Brumell, J.H. (2008). Salmonella-Containing Vacuoles: Directing Traffic and Nesting to Grow. Traffic *9*, 2022-2031.

Bakowski, M.A., Cirulis, J.T., Brown, N.F., Finlay, B.B., and Brumell, J.H. (2007). SopD acts cooperatively with SopB during Salmonella enterica serovar Typhimurium invasion. Cellular Microbiol. *9*, 2839-2855.

Barbieri, J.T., Riese, M.J., and Aktories, K. (2002). Bacterial Toxins that Modify the Actin Cytoskeleton. Annu. Rev. Cell Dev. Biol. *18*, 315-344.

Barta, M.L., Dickenson, N.E., Patil, M., Keightley, A., Wyckoff, G.J., Picking, W.D., Picking, W.L., and Geisbrecht, B.V. (2012). The Structures of Coiled-coil Domains from Type Three Secretion System Translocators Homology to Pore-Forming Toxins. . J. Mol. Biol. *417*, 395-405.

Barth, H., and Aktories, K. (2011). New insights into the mode of action of the actin ADP-ribosylating virulence factors Salmonella enterica SpvB and Clostridium botulinum C2 toxin. Eur. J. Cell Biol. *90*, 944-950.

Barth, H., and Stiles, B.G. (2008). Binary actin-ADP-ribosylating toxins and their use as molecular Trojan horses for drug delivery into eukaryotic cells. Curr. Med. Chem. *15*, 459-469.

Bergeron, J.R., Worrall, L.J., Sgourakis, N.G., DiMaio, F., Pfuetzner, R.A., Felise, H.B., Vuckovic, M., Angel, C.Y., Miller, S.I., and Baker, D. (2013). A refined model of the prototypical Salmonella SPI-1 T3SS basal body reveals the molecular basis for its assembly. PLoS Path. *9*, e1003307.

Boucrot, E., Henry, T., Borg, J.-P., Gorvel, J.-P., and Méresse, S. (2005). The Intracellular Fate of Salmonella Depends on the Recruitment of Kinesin. Science *308*, 1174-1178.

Bowe, F., Lipps, C.J., Tsolis, R.M., Groisman, E., Heffron, F., and Kusters, J.G. (1998). At Least Four Percent of the Salmonella typhimurium Genome Is Required for Fatal Infection of Mice. Infect. Immun. *66*, 3372-3377.

Browne, S.H., Hasegawa, P., Okamoto, S., Fierer, J., and Guiney, D.G. (2008). Identification of Salmonella SPI-2 secretion system components required for SpvB-mediated cytotoxicity in macrophages and virulence in mice. FEMS Immunol. Med. Microbiol. *52*, 194-201.

Brumell, J.H., Goosney, D.L., and Finlay, B.B. (2002). SifA, a Type III Secreted Effector of Salmonella typhimurium, Directs Salmonella-Induced Filament (Sif) Formation Along Microtubules. Traffic *3*, 407-415.

Brumell, J.H., and Grinstein, S. (2004). Salmonella redirects phagosomal maturation. Curr. Opin. Microbiol. *7*, 78-84.

Brumell, J.H., Kujat-Choy, S., Brown, N.F., Vallance, B.A., Knodler, L.A., and Finlay, B.B. (2003). SopD2 is a Novel Type III Secreted Effector of Salmonella typhimurium That Targets Late Endocytic Compartments Upon Delivery Into Host Cells. Traffic *4*, 36-48.

Buchwald, G., Friebel, A., Galán, J.E., Hardt, W.-D., Wittinghofer, A., and Scheffzek, K. (2002). Structural basis for the reversible activation of a Rho protein by the bacterial toxin SopE. EMBO J. *21*, 3286-3295.

Bujny, M.V., Ewels, P.A., Humphrey, S., Attar, N., Jepson, M.A., and Cullen, P.J. (2008). Sorting nexin-1 defines an early phase of Salmonella-containing vacuole-remodeling during Salmonella infection. J. Cell Sci. *121*, 2027-2036.

Bultema, J.J., Ambrosio, A.L., Burek, C.L., and Di Pietro, S.M. (2012). BLOC-2, AP-3, and AP-1 proteins function in concert with Rab38 and Rab32 proteins to mediate protein trafficking to lysosome-related organelles. J. Biol. Chem. *287*, 19550-19563.

Burkinshaw, B.J., Prehna, G., Worrall, L.J., and Strynadka, N.C. (2012). Structure of Salmonella effector protein SopB N-terminal domain in complex with host Rho GTPase Cdc42. J. Biol. Chem. *287*, 13348-13355.

Burkinshaw, B.J., and Strynadka, N.C. (2014). Assembly and structure of the T3SS. BBA-Mol. Cell Res. *1843*, 1649-1663.

Busby, J.N., Panjikar, S., Landsberg, M.J., Hurst, M.R., and Lott, J.S. (2013). The BC component of ABC toxins is an RHS-repeat-containing protein encapsulation device. Nature *501*, 547-550.

Cantalupo, G., Alifano, P., Roberti, V., Bruni, C.B., and Bucci, C. (2001). Rab‐interacting lysosomal protein (RILP): the Rab7 effector required for transport to lysosomes. EMBO J. *20*, 683-693.

Chen, C.Y., Eckmann, L., Libby, S.J., Fang, F.C., Okamoto, S., Kagnoff, M.F., Fierer, J., and Guiney, D.G. (1996). Expression of Salmonella typhimurium rpoS and rpoS-dependent genes in the intracellular environment of eukaryotic cells. Infect. Immun. *64*, 4739-4743.

Chen, L., Wang, H., Zhang, J., Gu, L., Huang, N., Zhou, J.-M., and Chai, J. (2008). Structural basis for the catalytic mechanism of phosphothreonine lyase. Nat. Struct. Mol. Biol. *15*, 101-102.

Collazo, C.M., and Galán, J.E. (1997). The invasion-associated type III system of Salmonella typhimurium directs the translocation of Sip proteins into the host cell. Mol. Microbiol. *24*, 747-756.

Criss, A.K., and Casanova, J.E. (2003). Coordinate Regulation of Salmonella enterica Serovar Typhimurium Invasion of Epithelial Cells by the Arp2/3 Complex and Rho GTPases. Infect. Immun. *71*, 2885-2891.

Crump, J.A., Luby, S.P., and Mintz, E.D. (2004). The global burden of typhoid fever. Bull. W.H.O. *82*, 346-353.

Crump, J.A., and Mintz, E.D. (2010). Global Trends in Typhoid and Paratyphoid Fever. Clin. Infect. Dis. *50*, 241-246.

De Groote, M.A., Ochsner, U.A., Shiloh, M.U., Nathan, C., McCord, J.M., Dinauer, M.C., Libby, S.J., Vazquez-Torres, A., Xu, Y., and Fang, F.C. (1997). Periplasmic superoxide dismutase

protects Salmonella from products of phagocyte NADPH-oxidase and nitric oxide synthase. Proc. Natl. Acad. Sci. U.S.A. *94*, 13997-14001.
DeLano, W.L. (2002). The PyMOL molecular graphics system.
Dell'Angelica, E.C. (2004). The building BLOC(k)s of lysosomes and related organelles. Curr. Opin. Cell Biol. *16*, 458-464.
Derewenda, Z.S. (2004). Rational Protein Crystallization by Mutational Surface Engineering. Structure *12*, 529-535.
Diao, J., Zhang, Y., Huibregtse, J.M., Zhou, D., and Chen, J. (2008). Crystal structure of SopA, a Salmonella effector protein mimicking a eukaryotic ubiquitin ligase. Nat. Struct. Mol. Biol. *15*, 65-70.
Diepold, A., and Wagner, S. (2014). Assembly of the bacterial type III secretion machinery. *38*, 802-822.
Du, F., and Galán, J.E. (2009). Selective inhibition of type III secretion activated signaling by the Salmonella effector AvrA. PLoS Path. *5*, e1000595.
Emsley, P., Lohkamp, B., Scott, W.G., and Cowtan, K. (2010a). Features and development of Coot. Acta Cryst. D *66*, 486-501.
Emsley, P., Lohkamp, B., Scott, W.G., and Cowtan, K. (2010b). Features and development of Coot. Acta Crystallographica Section D: Biological Crystallography *66*, 486-501.
Fang, F.C., Libby, S.J., Buchmeier, N.A., Loewen, P.C., Switala, J., Harwood, J., and Guiney, D.G. (1992). The alternative sigma factor katF (rpoS) regulates Salmonella virulence. Proc. Natl. Acad. Sci. U. S. A. *89*, 11978-11982.
Farrant, J.L., Sansone, A., Canvin, J.R., Pallen, M.J., Langford, P.R., Wallis, T.S., Dougan, G., and Kroll, J.S. (1997). Bacterial copper- and zinc-cofactored superoxide dismutase contributes to the pathogenesis of systemic salmonellosis. Mol. Microbiol. *25*, 785-796.
Faucher, S.P., Curtiss, R., and Daigle, F. (2005). Selective capture of Salmonella enterica serovar Typhi genes expressed in macrophages that are absent from the Salmonella enterica serovar Typhimurium genome. Infect. Immun. *73*, 5217-5221.
Favrin, S.J., Jassim, S.A., and Griffiths, M.W. (2003). Application of a novel immunomagnetic separation–bacteriophage assay for the detection of Salmonella enteritidis and Escherichia coli O157:H7 in food. Int. J. Food Microbiol. *85*, 63-71.
Ferré-D'Amaré, A.R., and Burley, S.K. (1994). Use of dynamic light scattering to assess crystallizability of macromolecules and macromolecular assemblies. Structure *2*, 357-359.
Fields, P.I., Swanson, R.V., Haidaris, C.G., and Heffron, F. (1986). Mutants of Salmonella typhimurium that cannot survive within the macrophage are avirulent. Proc. Natl. Acad. Sci. *83*, 5189-5193.
Fierer, J., Eckmann, L., Fang, F., Pfeifer, C., Finlay, B.B., and Guiney, D. (1993). Expression of the Salmonella virulence plasmid gene spvB in cultured macrophages and nonphagocytic cells. Infect. Immun. *61*, 5231-5236.
Fierer, J., Krause, M., Tauxe, R., and Guiney, D. (1992). Salmonella typhimurium Bacteremia: Association with the Virulence Plasmid. J. Infect. Dis. *166*, 639-642.
Figueira, R., and Holden, D.W. (2012). Functions of the Salmonella pathogenicity island 2 (SPI-2) type III secretion system effectors. Microbiology *158*, 1147-1161.
Figueroa‐Bossi, N., and Bossi, L. (1999). Inducible prophages contribute to Salmonella virulence in mice. Mol. Microbiol. *33*, 167-176.

Figueroa‐Bossi, N., Uzzau, S., Maloriol, D., and Bossi, L. (2001). Variable assortment of prophages provides a transferable repertoire of pathogenic determinants in Salmonella. Mol. Microbiol. *39*, 260-272.

Galán, J.E. (2001). *Salmonella* Interaction with Host Cells: Type III secretion at work. Annu. Rev. Cell. Dev. Biol. *17*, 53-86.

Galán, J.E., Lara-Tejero, M., Marlovits, T.C., and Wagner, S. (2014). Bacterial Type III Secretion Systems: Specialized Nanomachines for Protein Delivery into Target Cells. Annu. Rev. Microbiol. *68*, 415-438.

Galán, J.E., and Wolf-Watz, H. (2006). Protein delivery into eukaryotic cells by type III secretion machines. Nature *444*, 567-573.

Gotoh, H., Okada, N., Kim, Y.-G., Shiraishi, K., Hirami, N., Haneda, T., Kurita, A., Kikuchi, Y., and Danbara, H. (2003). Extracellular secretion of the virulence plasmid-encoded ADP-ribosyltransferase SpvB in Salmonella. Microb. Pathog. *34*, 227-238.

Grzonka, Z., Jankowska, E., Kasprzykowski, F., Kasprzykowska, R., Lankiewicz, L., Wiczk, W., Wieczerzak, E., Ciarkowski, J., Drabik, P., and Janowski, R. (2000). Structural studies of cysteine proteases and their inhibitors. Acta Biochim. Pol. *48*, 1-20.

Grzonka, Z., Jankowska, E., Kasprzykowski, F., Kasprzykowska, R., Lankiewicz, L., Wiczk, W., Wieczerzak, E., Ciarkowski, J., Drabik, P., Janowski, R., *et al.* (2001). Structural studies of cysteine proteases and their inhibitors. Acta Biochim. Pol. *48*, 1-20.

Guiney, D. (2005). The role of host cell death in Salmonella infections. In Role of Apoptosis in Infection (Springer), pp. 131-150.

Guiney, D.G., and Fierer, J. (2011). The Role of the spv Genes in Salmonella Pathogenesis. Frontiers in microbiology *2*, 129.

Guiney, D.G., and Lesnick, M. (2005). Targeting of the actin cytoskeleton during infection by Salmonella strains. Clin. Immunol. *114*, 248-255.

Haghjoo, E., and Galán, J.E. (2004). Salmonella typhiencodes a functional cytolethal distending toxin that is delivered into host cells by a bacterial-internalization pathway. Proc. Natl. Acad. Sci. U. S. A. *101*, 4614-4619.

Haneda, T., Ishii, Y., Shimizu, H., Ohshima, K., Iida, N., Danbara, H., and Okada, N. (2012). Salmonella type III effector SpvC, a phosphothreonine lyase, contributes to reduction in inflammatory response during intestinal phase of infection. Cell. Microbiol. *14*, 485-499.

Hansen-Wester, I., and Hensel, M. (2001). Salmonella pathogenicity islands encoding type III secretion systems. Microb. Infect. *3*, 549-559.

Haraga, A., and Miller, S.I. (2006). A Salmonella type III secretion effector interacts with the mammalian serine/threonine protein kinase PKN1. Cell. Microbiol. *8*, 837-846.

Hardt, W.-D., Chen, L.-M., Schuebel, K.E., Bustelo, X.R., and Galán, J.E. (1998). S. typhimurium encodes an activator of Rho GTPases that induces membrane ruffling and nuclear responses in host cells. Cell *93*, 815-826.

Hayward, R.D., and Koronakis, V. (1999). Direct nucleation and bundling of actin by the SipC protein of invasive Salmonella. EMBO J. *18*, 4926-4934.

Hayward, R.D., and Koronakiss, V. (2002). Direct modulation of the host cell cytoskeleton by Salmonella actin-binding proteins. Trends Cell Biol. *12*, 15-20.

Henry, T., Couillault, C., Rockenfeller, P., Boucrot, E., Dumont, A., Schroeder, N., Hermant, A., Knodler, L.A., Lecine, P., Steele-Mortimer, O., *et al.* (2006). The Salmonella effector protein PipB2 is a linker for kinesin-1. Proc. Natl. Acad. Sci. U. S. A. *103*, 13497-13502.

Higashide, W., and Zhou, D. (2006). The First 45 Amino Acids of SopA Are Necessary for InvB Binding and SPI-1 Secretion. J. Bacteriol. *188*, 2411-2420.

Ho, T.D., Figueroa-Bossi, N., Wang, M., Uzzau, S., Bossi, L., and Slauch, J.M. (2002). Identification of GtgE, a novel virulence factor encoded on the Gifsy-2 bacteriophage of Salmonella enterica serovar Typhimurium. J. Bacteriol. *184*, 5234-5239.

Hochmann, H., Pust, S., von Figura, G., Aktories, K., and Barth, H. (2006). Salmonella enterica SpvB ADP-Ribosylates Actin at Position Arginine-177 Characterization of the Catalytic Domain within the SpvB Protein and a Comparison to Binary Clostridial Actin-ADP-Ribosylating Toxins†. Biochemistry *45*, 1271-1277.

Hoiseth, S.K., and Stocker, B. (1981). Aromatic-dependent Salmonella typhimurium are non-virulent and effective as live vaccines. Nature *291*, 238-239.

Ishii, S., Yano, T., Ebihara, A., Okamoto, A., Manzoku, M., and Hayashi, H. (2010). Crystal Structure of the Peptidase Domain of Streptococcus ComA, a Bifunctional ATP-binding Cassette Transporter Involved in the Quorum-sensing Pathway. J. Biol. Chem. *285*, 10777-10785.

Ishola, O.O., and Holt, P.S. (2008). Salmonella Enteritidis experimental infection in chickens: Effects of challenge dose on serum immunoglobulin G antibody response. Afr. J. Biotechnol. *7*, 3783-3787.

Jantsch, J., Chikkaballi, D., and Hensel, M. (2011). Cellular aspects of immunity to intracellular Salmonella enterica. Immunol. Rev. *240*, 185-195.

Jepson, M.A., Kenny, B., and Leard, A.D. (2001). Role of sipA in the early stages of Salmonella typhimurium entry into epithelial cells. Cell. Microbiol. *3*, 417-426.

Jetha, N.N., Wiggin, M., and Marziali, A. (2009). Forming an α-Hemolysin Nanopore for Single-Molecule Analysis. In Micro and Nano Technologies in Bioanalysis (Springer), pp. 113-127.

Jiang, X., Rossanese, O.W., Brown, N.F., Kujat-Choy, S., Galán, J.E., Finlay, B.B., and Brumell, J.H. (2004). The related effector proteins SopD and SopD2 from Salmonella enterica serovar Typhimurium contribute to virulence during systemic infection of mice. Mol. Microbiol. *54*, 1186-1198.

Karplus, P.A., and Diederichs, K. (2012). Linking Crystallographic Model and Data Quality. Science *336*, 1030-1033.

Knodler, L.A., and Steele-Mortimer, O. (2003). Taking Possession: Biogenesis of the Salmonella-Containing Vacuole. Traffic *4*, 587-599.

Kohler, A.C., Spanò, S., Galán, J.E., and Stebbins, C.E. (2014). Structural and enzymatic characterization of a host-specificity determinant from Salmonella. Acta Cryst. D *70*, 384-391.

Kosarewicz, A., Königsmaier, L., and Marlovits, T.C. (2012). The Blueprint of the Type-3 Injectisome. Philos. Trans. R. Soc. Lond. B *367*, 1140-1154.

Kubori, T., Sukhan, A., Aizawa, S.-I., and Galán, J.E. (2000). Molecular characterization and assembly of the needle complex of the Salmonella typhimurium type III protein secretion system. Proc. Natl. Acad. Sci. U.S.A. *97*, 10225-10230.

Kuijl, C., Savage, N.D.L., Marsman, M., Tuin, A.W., Janssen, L., Egan, D.A., Ketema, M., van den Nieuwendijk, R., van den Eeden, S.J.F., Geluk, A., *et al.* (2007). Intracellular bacterial growth is controlled by a kinase network around PKB/AKT1. Nature *450*, 725-730.

Kwan, A.H., Mobli, M., Gooley, P.R., King, G.F., and Mackay, J.P. (2011). Macromolecular NMR spectroscopy for the non‐spectroscopist. FEBS J. *278*, 687-703.

Laskowski, R.A. (2009). PDBsum new things. Nucleic Acids Res. *37*, D355-D359.

Li, H., Xu, H., Zhou, Y., Zhang, J., Long, C., Li, S., Chen, S., Zhou, J.-M., and Shao, F. (2007). The Phosphothreonine Lyase Activity of a Bacterial Type III Effector Family. Science *315*, 1000-1003.

Libby, S.J., Adams, L.G., Ficht, T.A., Allen, C., Whitford, H.A., Buchmeier, N.A., Bossie, S., and Guiney, D.G. (1997). The spv genes on the Salmonella dublin virulence plasmid are required for severe enteritis and systemic infection in the natural host. Infect. Immun. *65*, 1786-1792.

Libby, S.J., Lesnick, M., Hasegawa, P., Kurth, M., Belcher, C., Fierer, J., and Guiney, D.G. (2002). Characterization of the spv Locus in Salmonella enterica Serovar Arizona. Infect. Immun. *70*, 3290-3294.

Lilic, M., Galkin, V.E., Orlova, A., VanLoock, M.S., Egelman, E.H., and Stebbins, C.E. (2003). Salmonella SipA Polymerizes Actin by Stapling Filaments with Nonglobular Protein Arms. Science *301*, 1918-1921.

Lodish, H. (2008). Molecular cell biology (Macmillan).

Majowicz, S.E., Musto, J., Scallan, E., Angulo, F.J., Kirk, M., O'Brien, S.J., Jones, T.F., Fazil, A., Hoekstra, R.M., and Studies, f.t.I.C.o.E.D.B.o.I. (2010). The Global Burden of Nontyphoidal Salmonella Gastroenteritis. Clin. Infect. Dis. *50*, 882-889.

Mallo, G.V., Espina, M., Smith, A.C., Terebiznik, M.R., Alemán, A., Finlay, B.B., Rameh, L.E., Grinstein, S., and Brumell, J.H. (2008). SopB promotes phosphatidylinositol 3-phosphate formation on Salmonella vacuoles by recruiting Rab5 and Vps34. J. Cell Biol. *182*, 741-752.

Marcus, S.L., Brumell, J.H., Pfeifer, C.G., and Finlay, B.B. (2000). Salmonella pathogenicity islands: big virulence in small packages. Microb. Infect. *2*, 145-156.

Margarit, S.M., Davidson, W., Frego, L., and Stebbins, C.E. (2006). A Steric Antagonism of Actin Polymerization by a Salmonella Virulence Protein. Structure *14*, 1219-1229.

Mazurkiewicz, P., Thomas, J., Thompson, J.A., Liu, M., Arbibe, L., Sansonetti, P., and Holden, D.W. (2008). SpvC is a Salmonella effector with phosphothreonine lyase activity on host mitogen-activated protein kinases. Mol. Microbiol. *67*, 1371-1383.

McCoy, A.J., Grosse-Kunstleve, R.W., Adams, P.D., Winn, M.D., Storoni, L.C., and Read, R.J. (2007). Phaser crystallographic software. J. Appl. Crystallogr. *40*, 658-674.

McGhie, E.J., Brawn, L.C., Hume, P.J., Humphreys, D., and Koronakis, V. (2009). Salmonella takes control: effector-driven manipulation of the host. Curr. Opin. Microbiol. *12*, 117-124.

Meller, A., and Branton, D. (2002). Single molecule measurements of DNA transport through a nanopore. Electrophoresis *23*, 2583-2591.

Meng, H., Detillieux, D., Baran, C., Krasniqi, B., Christensen, C., Madampage, C., Stefureac, R.I., and Lee, J.S. (2010). Nanopore analysis of tethered peptides. J. Pept. Sci. *16*, 701-708.

Mesa-Pereira, B., Medina, C., Camacho, E.M., Flores, A., and Santero, E. (2013). Novel tools to analyze the function of Salmonella effectors show that SvpB ectopic expression induces cell cycle arrest in tumor cells. PLoS One *8*, e78458.

Meusch, D., Gatsogiannis, C., Efremov, R.G., Lang, A.E., Hofnagel, O., Vetter, I.R., Aktories, K., and Raunser, S. (2014). Mechanism of Tc toxin action revealed in molecular detail. Nature *508*, 61-65.

Miao, E.A., Brittnacher, M., Haraga, A., Jeng, R.L., Welch, M.D., and Miller, S.I. (2003). Salmonella effectors translocated across the vacuolar membrane interact with the actin cytoskeleton. Mol. Microbiol. *48*, 401-415.

Millard, T.H., Sharp, S.J., and Machesky, L.M. (2004). Signalling to actin assembly via the WASP (Wiskott-Aldrich syndrome protein)-family proteins and the Arp2/3 complex. Biochem. J. *380*, 1-17.

Minor, W., Cymborowski, M., Otwinowski, Z., and Chruszcz, M. (2006). HKL-3000: the integration of data reduction and structure solution–from diffraction images to an initial model in minutes. Acta Cryst. D *62*, 859-866.

Moest, T.P., and Méresse, S. (2013). Salmonella T3SSs: successful mission of the secret(ion) agents. Curr. Opin. Microbiol. *16*, 38-44.

Nawabi, P., Catron, D.M., and Haldar, K. (2008). Esterification of cholesterol by a type III secretion effector during intracellular Salmonella infection. Mol. Microbiol. *68*, 173-185.

Ohlson, M.B., Fluhr, K., Birmingham, C.L., Brumell, J.H., and Miller, S.I. (2005). SseJ Deacylase Activity by Salmonella enterica Serovar Typhimurium Promotes Virulence in Mice. Infect. Immun. *73*, 6249-6259.

Ohlson, M.B., Huang, Z., Alto, N.M., Blanc, M.-P., Dixon, J.E., Chai, J., and Miller, S.I. (2008). Structure and function of SifA indicate that interactions with SKIP, SseJ, and RhoA family GTPases induce endosomal tubulation. Cell host & microbe *4*, 434-446.

Paesold, G., Guiney, D.G., Eckmann, L., and Kagnoff, M.F. (2002). Genes in the Salmonella pathogenicity island 2 and the Salmonella virulence plasmid are essential for Salmonella-induced apoptosis in intestinal epithelial cells. Cell. Microbiol. *4*, 771-781.

Pfeffer, S.R. (2013). Rab GTPase regulation of membrane identity. Curr. Opin. Cell Biol. *25*, 414-419.

Polgár, L., and Asbóth, B. (1986). The basic difference in catalyses by serine and cysteine proteinases resides in charge stabilization in the transition state. J. Theor. Biol. *121*, 323-326.

Pollitt, A.Y., and Insall, R.H. (2009). WASP and SCAR/WAVE proteins: the drivers of actin assembly. J. Cell Sci. *122*, 2575-2578.

Quezada, C.M., Hicks, S.W., Galán, J.E., and Stebbins, C.E. (2009). A family of Salmonella virulence factors functions as a distinct class of autoregulated E3 ubiquitin ligases. Proc. Natl. Acad. Sci. U. S. A. *106*, 4864-4869.

Ramsden, A.E., Holden, D.W., and Mota, L.J. (2007). Membrane dynamics and spatial distribution of Salmonella-containing vacuoles. Trends Microbiol. *15*, 516-524.

Rawlings, N.D., Waller, M., Barrett, A.J., and Bateman, A. (2013). MEROPS: the database of proteolytic enzymes, their substrates and inhibitors. Nucleic Acids Res., 503-509.

Reeves, M.W., Evins, G.M., Heiba, A.A., Plikaytis, B.D., and Farmer, J.J. (1989). Clonal nature of Salmonella typhi and its genetic relatedness to other salmonellae as shown by multilocus enzyme electrophoresis, and proposal of Salmonella bongori comb. nov. J. Clin. Microbiol. *27*, 313-320.

Ruiz-Albert, J., Yu, X.-J., Beuzón, C.R., Blakey, A.N., Galyov, E.E., and Holden, D.W. (2002). Complementary activities of SseJ and SifA regulate dynamics of the Salmonella typhimurium vacuolar membrane. Mol. Microbiol. *44*, 645-661.

Rytkönen, A., Poh, J., Garmendia, J., Boyle, C., Thompson, A., Liu, M., Freemont, P., Hinton, J.C.D., and Holden, D.W. (2007). SseL, a Salmonella deubiquitinase required for macrophage killing and virulence. Proc. Natl. Acad. Sci. U. S. A. *104*, 3502-3507.

Sabbagh, S.C., Forest, C.G., Lepage, C., Leclerc, J.-M., and Daigle, F. (2010). So similar, yet so different: uncovering distinctive features in the genomes of Salmonella enterica serovars Typhimurium and Typhi. FEMS Microbiol. Let. *305*, 1-13.

Scherer, C.A., Cooper, E., and Miller, S.I. (2000). The Salmonella type III secretion translocon protein SspC is inserted into the epithelial cell plasma membrane upon infection. Mol. Microbiol. *37*, 1133-1145.

Schleberger, C., Hochmann, H., Barth, H., Aktories, K., and Schulz, G.E. (2006). Structure and Action of the Binary C2 Toxin from Clostridium botulinum. J. Mol. Biol. *364*, 705-715.

Schlumberger, M.C., and Hardt, W.-D. (2006). Salmonella type III secretion effectors: pulling the host cell's strings. Curr. Opin. Microbiol. *9*, 46-54.

Schlumberger, M.C., Müller, A.J., Ehrbar, K., Winnen, B., Duss, I., Stecher, B., and Hardt, W.-D. (2005). Real-time imaging of type III secretion: Salmonella SipA injection into host cells. Proc. Natl. Acad. Sci. U. S. A. *102*, 12548-12553.

Sheehan, B.J., and Dorman, C.J. (1998). In vivo analysis of the interactions of the LysR-like regulator SpvR with the operator sequences of the spvA and spvR virulence genes of Salmonella typhimurium. Mol. Microbiol. *30*, 91-105.

Simon, N.C., Aktories, K., and Barbieri, J.T. (2014). Novel bacterial ADP-ribosylating toxins: structure and function. Nat Rev Micro *12*, 599-611.

Smith, A.C., Do Heo, W., Braun, V., Jiang, X., Macrae, C., Casanova, J.E., Scidmore, M.A., Grinstein, S., Meyer, T., and Brumell, J.H. (2007). A network of Rab GTPases controls phagosome maturation and is modulated by Salmonella enterica serovar Typhimurium. The Journal of cell biology *176*, 263-268.

Spanò, S., and Galán, J.E. (2012). A Rab32-dependent pathway contributes to Salmonella typhi host restriction. Science *338*, 960-963.

Spano, S., Liu, X., and Galan, J.E. (2011). Proteolytic targeting of Rab29 by an effector protein distinguishes the intracellular compartments of human-adapted and broad-host Salmonella. Proc. Natl. Acad. Sci. U. S. A. *108*, 18418-18423.

Spanò, S., Ugalde, J.E., and Galán, J.E. (2008). Delivery of a Salmonella Typhi exotoxin from a host intracellular compartment. Cell host & microbe *3*, 30-38.

Stebbins, C.E., and Galán, J.E. (2000). Modulation of Host Signaling by a Bacterial Mimic: Structure of the Salmonella Effector SptP Bound to Rac1. Mol. Cell *6*, 1449-1460.

Steele-Mortimer, O. (2008). The Salmonella-containing vacuole—Moving with the times. Curr. Opin. Microbiol. *11*, 38-45.

Stefureac, R., Long, Y.-t., Kraatz, H.-B., Howard, P., and Lee, J.S. (2006). Transport of α-Helical Peptides through α-Hemolysin and Aerolysin Pores†. Biochemistry *45*, 9172-9179.

Stenmark, H., and Olkkonen, V.M. (2001). The Rab GTPase family. Genome Biol. *2*, S3007.

Tezcan-Merdol, D., Engstrand, L., and Rhen, M. (2005). Salmonella enterica SpvB-mediated ADP-ribosylation as an activator for host cell actin degradation. Int. J. Med. Microbiol. *295*, 201-212.

Tezcan-Merdol, D., Nyman, T., Lindberg, U., Haag, F., Koch-Nolte, F., and Rhen, M. (2001). Actin is ADP-ribosylated by the Salmonella enterica virulence-associated protein SpvB. Mol. Microbiol. *39*, 606-619.

Touchot, N., Chardin, P., and Tavitian, A. (1987). Four additional members of the ras gene superfamily isolated by an oligonucleotide strategy: molecular cloning of YPT-related cDNAs from a rat brain library. Proceedings of the National Academy of Sciences *84*, 8210-8214.

Uchiya, K., Barbieri, M.A., Funato, K., Shah, A.H., Stahl, P.D., and Groisman, E.A. (1999). A Salmonella virulence protein that inhibits cellular trafficking. EMBO J. *18*, 3924-3933.

Williams, C., Galyov, E.E., and Bagby, S. (2004). Solution structure, backbone dynamics, and interaction with Cdc42 of Salmonella guanine nucleotide exchange factor SopE2. Biochemistry *43*, 11998-12008.

Wilson, B.A., Salyers, A.A., Whitt, D.D., and Winkler, M.E. (2011). Bacterial pathogenesis: a molecular approach (American Society for Microbiology (ASM)).

Wu, H., Jones, R.M., and Neish, A.S. (2012). The Salmonella effector AvrA mediates bacterial intracellular survival during infection in vivo. Cell. Microbiol. *14*, 28-39.

Wu, K.-H., and Tai, P.C. (2004). Cys32 and His105 Are the Critical Residues for the Calcium-dependent Cysteine Proteolytic Activity of CvaB, an ATP-binding Cassette Transporter. J. Biol. Chem. *279*, 901-909.

Wuthrich, K. (2001). The way to NMR structures of proteins. Nat. Struct. Mol. Biol. *8*, 923-925.

Zerial, M., and McBride, H. (2001). Rab proteins as membrane organizers. Nat. Rev. Mol. Cell Biol. *2*, 107-117.

Zhang, Y., Higashide, W.M., McCormick, B.A., Chen, J., and Zhou, D. (2006). The inflammation-associated Salmonella SopA is a HECT-like E3 ubiquitin ligase. Mol. Microbiol. *62*, 786-793.

Zhao, K.Q., Hartnett, J., and Slater, M.R. (2007). 15N Labeling of Proteins Overexpressed in the Escherichia coli Strain KRX. Promega Notes *96*, 24-26.

Zierler, M.K., and Galán, J.E. (1995). Contact with cultured epithelial cells stimulates secretion of Salmonella typhimurium invasion protein InvJ. Infect. Immun. *63*, 4024-4028.